The Effect of Variable Climate and Vegetation Cover on Catchment-Scale Erosion Rates

Dissertation

der Mathematisch-Naturwissenschaftlichen Fakultät

der Eberhard Karls Universität Tübingen

zur Erlangung des Grades eines

Doktors der Naturwissenschaften

(Dr. rer. nat.)

vorgelegt von

Hemanti Sharma

aus Mainpuri/Indien

Tübingen

2022

Gedruckt mit Genehmigung der Mathematisch-Naturwissenschaftlichen Fakultät der Eberhard Karls Universität Tübingen.

Tag der mündlichen Qualifikation:	20.10.2022
Dekan:	Prof. Dr. Thilo Stehle
1. Berichterstatter/-in:	Prof. Dr. Todd Ehlers
2. Berichterstatter/-in:	Prof. Dr. Christiane Zarfl

Abstract

The influence of variations in tectonics (rock uplift rates), climate, and associated vegetation cover (including other factors) on catchment processes has long been of interest to geomorphologists. However, the interactions of climate and vegetation with surface processes are relatively complex to understand. For example, an increase in precipitation supports vegetation growth and, at the same time, leads to high erosion rates. This study investigates the influence of different rock uplift rates and variations in precipitation and vegetation cover in catchment erosion at variable timescales (from millennial to daily timescales). The investigation is done through numerical simulations using a complex landscape evolution model (Landlab) modified to account for vegetation cover (and type) and remote sensing, and geographical information system (GIS). The model inputs were parameterized to four study areas with similar granodioritic lithology and distinct climate and ecological settings in Chilean Coastal Cordillera.

Three sets of numerical simulations were conducted using Landlab: (1) To evaluate the role of changing rock uplift rates over the periodicity of variations in climate and vegetation at Milankovitch timescales (i.e., 21 kyr, 41 kyr, and 100 kyr) on long term catchment processes. (2) To identify which factor, precipitation or vegetation change is vital in influencing catchment erosion at season timescale. (3) The role of vegetation cover and type in influencing erosion rates during extreme precipitation events in present-day climatic conditions.

The results indicate that at longer timescales, catchment processes are significantly influenced by Milankovitch timescale variations in climate and vegetation. These transient changes are superimposed upon tectonically driven rock uplift rates. At the seasonal timescale, precipitation variations pose a first-order control on catchment erosion, and the role of vegetation changes is secondary but still significant. However, at daily timescales, vegetation cover and type distribution play a more vital role (over precipitation variations) in controlling erosion rates during extreme precipitation events.

Overall, this thesis augments the understanding of the significance of each natural driver (i.e., tectonics, climate, and vegetation) over others, at different timescales, on catchment-scale surface processes in distinct climate and ecological settings.

Zusammenfassung

Der Einfluss von Schwankungen in der Tektonik (Gesteinshebungsraten), des Klimas und der damit verbundenen Vegetationsbedeckung (einschließlich anderer Faktoren) auf die Prozesse in Wassereinzugsgebieten ist für Geomorphologen schon lange von Interesse. Die Wechselwirkungen von Klima und Vegetation mit Oberflächenprozessen sind jedoch relativ komplex zu verstehen. So fördert beispielsweise eine Zunahme der Niederschläge das Wachstum der Vegetation und führt gleichzeitig zu hohen Erosionsraten. In dieser Studie wird der Einfluss verschiedener Felshebungsraten und Schwankungen der Niederschläge und der Vegetationsbedeckung auf die Erosion in Einzugsgebieten auf unterschiedlichen Zeitskalen (von Jahrtausenden bis zu täglichen Zeitskalen) untersucht. Die Untersuchung erfolgt durch numerische Simulationen unter Verwendung eines komplexen Landschaftsentwicklungsmodells (Landlab), das so modifiziert wurde, dass es die Vegetationsbedeckung (und -art) sowie Fernerkundungsdaten und ein geografisches Informationssystem (GIS) berücksichtigt. Die Modelleingaben wurden für vier Untersuchungsgebiete mit ähnlicher granodioritischer Lithologie und unterschiedlichen klimatischen und ökologischen Bedingungen in der chilenischen Küstenkordillere parametrisiert.

Mit Hilfe von Landlab wurden drei numerische Simulationen durchgeführt: (1) Bewertung der Rolle von sich ändernden Gesteinshebungsraten über die Periodizität von Klima- und Vegetationsvariationen auf Milankovitch-Zeitskalen (d.h. 21 kyr, 41 kyr und 100 kyr) auf langfristige Einzugsgebietsprozesse. (2) Es soll ermittelt werden, welcher Faktor - Niederschlag oder Vegetationsveränderung - für die Beeinflussung der Einzugsgebietserosion auf der Zeitskala der Jahreszeiten entscheidend ist. (3) Die Rolle der Vegetationsbedeckung und des Vegetationstyps bei der Beeinflussung der Erosionsraten während extremer Niederschlagsereignisse unter heutigen Klimabedingungen.

Die Ergebnisse deuten darauf hin, dass die Prozesse in den Einzugsgebieten auf längeren Zeitskalen erheblich von den Veränderungen des Klimas und der Vegetation auf der Milankovitch-Skala beeinflusst werden. Diese vorübergehenden Veränderungen werden von tektonisch bedingten Gesteinshebungsraten überlagert. Auf der saisonalen Zeitskala beeinflussen Niederschlagsschwankungen die Erosion von Einzugsgebieten in erster Linie, und Vegetationsveränderungen spielen eine untergeordnete, aber dennoch wichtige Rolle. Auf der täglichen Zeitskala spielen jedoch die Vegetationsbedeckung und die Verteilung der Vegetationstypen eine wichtigere Rolle (als die Niederschlagsschwankungen) bei der Kontrolle der Erosionsraten während extremer Niederschlagsereignisse.

Insgesamt trägt diese Arbeit zu einem besseren Verständnis der Bedeutung der einzelnen natürlichen Faktoren (d. h. Tektonik, Klima und Vegetation) im Vergleich zu anderen Faktoren auf

unterschiedlichen Zeitskalen bei Oberflächenprozessen in Einzugsgebieten in unterschiedlichen klimatischen und ökologischen Umgebungen bei.

Acknowledgments

First of all, I want to thank my supervisor Prof. Dr. Todd A. Ehlers, for putting trust in me and providing me with this research opportunity to continue working in the ESD workgroup. I would also like to thank Prof. Dr.-Ing. Olaf A. Cirpka and DFG for giving me a chance to work on this project in IRTG Hydrosystem Modelling. I would also like to thank my second supervisor, Dr. Christoph Glotzbach, for his detailed, constructive criticism, which helped me improve my work. I also thank the IRTG Hydromod (and DFG) for the beneficial Spring and Fall-schools and for providing me an opportunity to acquire international exposure during hydrogeology field school at the University of Waterloo, Canada, in Spring – 2019. And for my research stay at the University of Calgary, where I got the chance to work with my Canadian supervisor Dr. Yvonne Martin. I would also like to thank Dr. Yvonne Martin for being very supportive and carrying out detailed brainstorming sessions to shape one of my research objectives and let me attend her very informative lectures. I would also like to thank my ex-office mate, Dr. Manuel Schmid, for being very supportive during the initial phase of my Ph.D. by clearing even my silliest doubts related to Landlab. I would also like to thank Dr. Kirstin Übernickel and Dr. Mirjam Schaller for their generous data and knowledge sharing about EarthShape study areas. I would especially like to thank Willi for constantly providing IT support; without him, my life as a numerical modeler would have never been this easier. I would also like to acknowledge every (present and past) member of the ESD workgroup for their constant support in research or general guidance.

Secondly, I would like to thank my very cooperative colleagues at RTG, who made my Ph.D. life in Tübingen much easier. And not to forget Monika Jekelius in the Administration for providing valuable assistance at every step of my Ph.D., so I didn’t have to worry about so much paperwork.

Lastly, I would like to thank my family and friends for constantly supporting me. I would especially like to acknowledge the emotional support from my family during the ups and downs I faced during my Ph.D. journey.

Table of Contents

List of Figures (excluding manuscripts)

List of Tables (excluding manuscripts)

1 Introduction

Several decades of research have demonstrated the influence of tectonics, climate, and biota in shaping modern landscapes. In natural systems, the interactions of the above parameters with physical, chemical, and biological surface processes are highly complex. The first such study by Grove Karl Gilbert (1877) highlighted the importance of the coupled influence of the above parameters on catchment-scale weathering, erosion, and sedimentation processes.

Also, the significance of each natural driver in modifying the topography varies over different timescales. For example, the rock uplift rate is conventionally identified as the first-order driver of long-term mean erosion rates at millennial timescales. However, it is also widely documented that surface processes are significantly affected by mean annual precipitation (MAP) and vegetation cover (amongst other factors). In contrast, at shorter (e.g., seasonal or diurnal) timescales, the changes in rock uplift rates are statistically negligible. In that scenario, the significance of seasonality in precipitation over vegetation (or vice-versa) on erosion rates is still debated. The ambiguity in current knowledge on the topic raises a variety of open questions, a couple of which define the motivation of this thesis.

This thesis aims to enhance the knowledge on the topic by investigating the role of rock uplift rates, climate, and vegetation cover (also plant functional types) on catchment-scale erosion and sedimentation at variable timescales in distinct climate and ecological settings. The investigated timescales range from a millennial (Milankovitch) to seasonal and diurnal. The top-down approach (e.g., temporal downscaling) in the model formulation is adopted to capture the significance of each model driver (over others) on erosion rates at different timescales. For example, it is reported that rock uplift rates play a significant role in driving long-term erosion rates (over climate and vegetation change) at geologic timescales (e.g., millions of years). However, at shorter timescales (e.g., diurnal to seasonal), changes in tectonics are insignificant; hence, climate and vegetation cover variability are vital in driving erosion rates. However, it is unclear which parameter (climate or vegetation) poses a first-order control on surface processes at diurnal and (or) seasonal timescales. This is done by implementing a numerical landscape evolution model (LEM) modified to account for vegetation cover (and type) for the study areas in the Chilean Coastal Cordillera (section 1.4) with an abrupt climate and ecological gradient.

This thesis is divided into six chapters comprising the introduction, model description, scientific results, conclusions, and appendices. The first chapter (Introduction) includes the motivation, research questions (with underlying hypotheses), and a brief description of the study areas. The second chapter (Model Description) includes an overview of the numerical basis of the landscape evolution model and its components and modifications based on vegetation cover and plant functional types (PFT). It also includes the basics of the hydrological model (used in the third objective of this thesis). The third chapter (Scientific results) includes the research articles (one published and two latest drafts of the manuscripts)

aiming to address the respective research questions. The fourth chapter (Summary and Conclusions) includes an overall summary, concludes the previously stated research questions and underlying hypotheses, and provides a scientific outlook for future research.

1.1 Motivation

It has long been reported that tectonics, climate, and vegetation cover play a significant role in shaping modern landscapes. In this section, an overview of the influence of the driving parameters (e.g., tectonics, climate and biota) on surface processes are documented, motivating this study.

1.1.1 Influence of uplift rates on erosion rates

For decades, the direct influence of tectonics on mean elevation, erosion rates, and river channel profiles has been extensively demonstrated (e.g., Kirby and Whipple, 2001, 2012; Turowski et al., 2006). For example, in an ideal steady-state topography, mean catchment erosion rates are equal to the rock uplift rates, according to the law of continuity of mass (Tucker et al., 2001). Also, tectonically active mountain ranges experience a high frequency of erosional events (e.g., landslides) as the erosion rates adjust to the rock uplift rates (e.g., Burbank et al., 1996; Montgomery and Brandon, 2002). For example, a recent study by Adams et al. (2020) highlighted the non-linear relationship between erosion and precipitation in tectonically active mountain ranges (e.g., Himalayas). Also, the influence of tectonic uplift on erosion rates in the fluvial systems is found to be independent of bedrock lithology, provided the dominant drivers are saltation-abrasion of the river erosion (Egholm et al., 2013).

1.1.2 Influence of precipitation and vegetation on erosion rates

The coupled effects of climate and tectonics on erosion rates have been widely accepted in the scientific community. For example, climate change plays a crucial role in shaping the landscapes when the rock uplift rates are constant (Whipple et al., 1999). Also, the main controlling factors for bedrock erosivity are related to climate (apart from lithology) (Whipple and Tucker, 1999). The increase in catchment relief with decreasing precipitation has already been documented (e.g., Bonnet and Crave, 2003; Gabet et al., 2004). This implies that at a given rock uplift rate, erosion rates decrease with a decrease in precipitation and lead to higher topographic elevations.

Recently, the idea of control of vegetation cover on surface processes has widely flourished, as an increase in vegetation cover stabilizes the slopes and hence reduces erosion and sediment transport. A significant scientific contribution has been made to link landscape development with vegetation cover (e.g., Acosta et al., 2015; Amundson et al., 2015; Istanbulluoglu, 2005). The first numerical modeling study implementing a vegetation–erosion coupling was conducted by Collins et al. (2004). This study was followed by the work of Istanbulluoglu and Bras (2005), which quantified the effect of vegetation on landscape relief and drainage formation. Recent work by Schmid et al. (2018) quantified the

individual and coupled effects of precipitation and vegetation cover variations over millennial timescales. Several observational studies at shorter timescales demonstrated the impact of vegetation cover on erosion reduction. For example, Boix-Fayos et al. (2008) reported a reduction of sediment yield by 54%, linked with a three-fold increase in forest cover in SE Spain. Also, a plot-scale study by Meng et al. (2021) reported higher erosion rates in earth bank terraces than the slopes with hedgerows (shrubs). Large-scale vegetation restoration and afforestation play a significant role in reducing sediment transport (Wang et al., 2016) and rainfall to runoff conversion (Gao et al., 2015).

The natural systems are highly complex, and landscape development involves an interplay of tectonics, climate, and vegetation cover. Considering the constant rock uplift rates over timescales relevant in this study ($< 10^5$ years), the erosion rates are influenced by both precipitation and associated vegetation cover changes. However, it is challenging to quantify the individual effects of precipitation and vegetation cover on surface processes. For example, an increase in rainfall leads to higher surface runoff but, at the same time, facilitates vegetation growth. This is due to the increase in water availability for plant growth, including temperature, solar radiation, soil characteristics, etc. Previous regional studies have reported a positive relationship between precipitation and vegetation cover (e.g., Huxman et al., 2004; Sala et al., 1988; Zhang et al., 2016). The first observational study by Langbein and Schumm (1958) suggested the association of high MAP with denser vegetation to reduce erosion rates. Also, the catchment-scale erosion rates vary spatially and temporally (Wang et al., 2021) and depend on topography (slope), vegetation cover, and type (Zhang et al., 2011, 2014; Starke et al., 2020) and precipitation rates (Cerdà, 1998). However, the degree of influence of precipitation and vegetation cover may be different based on the timescales of topographical change. For example, Wei et al. (2015) documented that differences in vegetation cover may contribute to long-term erosion and sedimentation. However, seasonal variations in runoff and sediment yield are mainly contributed by intra-annual rainfall variations. An efficient method to explore the effects of variations (ranging from millennial to diurnal timescales) in precipitation and (or) vegetation cover on erosion rates is through numerical landscape evolution modeling (LEM). The LEM can be parameterized for variations in vegetation-dependent surface processes (e.g., hillslope, fluvial, infiltration, etc.) over various time scales.

1.2 Research Questions and Hypotheses

This section comprises a detailed description of the research questions and their underlying hypotheses addressed in this study. The models utilized in addressing the research questions are described in the second chapter of this thesis.

Research Question 1: How do the rock uplift rates and the periodicity of variations in climate and vegetation cover affect the erosion and sedimentation over millennial (i.e., Milankovitch cycles) timescales?

This study investigates the transient landscape response for mixed bedrock–alluvial systems. This is done for different rock uplift rates and periodic changes (Milankovitch cycles) in precipitation and vegetation. The focus is on the changes in erosion and sedimentation occurring over millennial to million-year timescales. The underlying hypotheses evaluated in this study are as follows:

(i) If vegetation cover and climate vary on Milankovitch timescales, then any increase or decrease in catchment erosion will be more pronounced over longer (e.g., 100 kyr) rather than shorter (e.g., 21 kyr) periodicities due to the longer duration of change imposed.

(ii) If increasing rates of tectonic uplift (e.g., 0.05 - 0.2 mm yr^{-1}) cause an increase in catchment erosion rates, then any periodic variations in climate and vegetation cover will be muted (or lower amplitude) at higher uplift rates, as the effect of rock uplift on erosion will outweigh climate and vegetation change effects.

The above hypotheses are investigated using a stepwise increase in model complexity through numerical landscape evolution modeling. The contributions of individual processes (i.e., climate, vegetation, or tectonics) are identified separately before looking into the fully coupled system and resulting interactions. A two-dimensional landscape evolution model (Hobley et al., 2017) is implemented, which couples fluvial (Shobe et al., 2017) and hillslope (Johnstone and Hilley, 2014) and weathering (Ahnert, 1976) processes. This study is primarily focused on documenting the predicted sensitivity of catchments to variations in tectonics, climate, and vegetation change. The mean catchment vegetation cover is considered in the study. The model setup is tuned to the climate and ecological conditions along the Chilean Coastal Cordillera (Fig. 1), which features a similar lithological and tectonic setting. This was done to provide realistic vegetation cover and precipitation parameterizations in different ecological settings.

Research Question 2: How do the seasonal variations in precipitation and vegetation cover affect catchment-scale erosion rates in different climate and ecological settings?

This study investigates the seasonal transients in catchment erosion rates due to variations in precipitation and vegetation cover for four locations in the extreme climate and ecological gradient (i.e.,

arid, semi-arid, Mediterranean, and humid temperate) of the Chilean Coastal Cordillera. The underlying hypotheses evaluated in this study are as follows:

(i) If precipitation is the first-order driver of seasonal erosion rates, then the influence of seasonal changes in vegetation cover would be of low significance.
(ii) In arid and semi-arid regions, the catchment-scale erosion rates are more sensitive to seasonality in precipitation and vegetation than in the Mediterranean and humid-temperate regions.

To test the above hypotheses, a sensitivity analysis of fluvial and hillslope erosion is investigated over four Chilean study areas (Fig. 1). This is done to investigate the individual effects of seasonal changes in vegetation cover and precipitation compared to simulations with coupled variations in precipitation and vegetation cover. A landscape evolution modeling approach is applied, similar to research question 1, with an addition of the consideration of infiltration and evapotranspiration and spatially variable vegetation cover.

Research Question 3: How do the extreme precipitation events affect catchment-scale erosion rates in regions with variable land use and land cover types?

This study investigates the influence of vegetation cover, PFT-dependent coupled hillslope and fluvial processes, soil-water infiltration, and evapotranspiration on catchment-scale erosion rates at daily time steps using a complex landscape evolution model. Emphasis is placed on the sensitivity of erosion to different land cover types and stochastic precipitation variations, including extreme events. The underlying hypotheses evaluated in this study are as follows:

(i) If land use and land cover (LULC) distribution pose first-order control on catchment erosion, then regions with less resilient vegetation cover (barren or grasses) would experience more erosion during extreme events, despite the prevalence of high magnitude precipitation in regions with more resilient vegetation cover (e.g., shrubs and trees).
(ii) If Landlab LEM (modified to account for PFTs) provides a reliable output at shorter time scales, its results should be comparable with that of a physically-based model.

The Landlab-SPACE LEM is simulated at daily time steps for ~4 decades to test the first hypothesis. The LEM couples PFT-dependent hillslope and fluvial processes and soil-water infiltration to compute catchment erosion for four study areas in the Chilean Coastal Cordillera. The surface water discharge rates (normalized by domain area) obtained from LEM (Landlab-SAPCE) (Hobley et al., 2017) and the hydrological model (Soil and Water Assessment Tool) (Winchell et al., 2013) are compared and correlated for validation of LEM results, to test the second hypothesis.

1.3 Study Areas

This section summarizes the geologic, climate, and vegetation settings of the four selected catchments in the Chilean Coastal Cordillera (Fig. 1) investigated in this thesis. These catchments are located in the Pan de Azúcar National Park (arid, ~26°S), Santa Gracia nature preserve (semi-arid, ~30°S), La Campana (mediterranean, ~33°S), and Nahuelbuta (temperate-humid, ~38°S) national parks. These study areas span ~1,300 km of the Chilean Coastal Cordillera. These study areas are selected for their steep climate and ecological gradient from North (arid environment with small shrubs) to South (humid-temperate environment with evergreen mixed forests) (Schaller et al., 2020). The study areas are part of the German-Chilean priority research program EarthShape (www.earthshape.net) and ongoing research efforts within these catchments.

The bedrock of the four study areas is composed of granitoid rocks, including granites, granodiorites, and tonalites in Pan de Azúcar, La Campana, and Nahuelbuta, respectively and gabbro and diorites in Santa Gracia (Oeser et al., 2018). The soil types in each catchment based on grain size distribution are defined as sandy loam in three northern catchments and sandy clay loam in Nahuelbuta (Bernhard et al., 2018). The western margin of Chile along the latitudes of the different study areas is characterized by a similar tectonic setting whereby an oceanic plate (currently the Nazca plate) has been subducting under the South American plate since the Palaeozoic. Despite this common tectonic setting along, slight differences in current rock uplift rates are documented in the regions surrounding the three northern catchments (i.e., < 0.1 mm yr^{-1} for ~ 26 °S to ~33 °S) (Melnick, 2016) and the southern catchment (i.e., 0.04 to > 0.2 mm yr^{-1} for ~38 °S over the last 4±1.2 Ma) (Glodny et al., 2008; Melnick et al., 2009). Over geologic (millennial) timescales, measured denudation rates in the region range between ~0.005 to ~0.6 mm yr^{-1} (Schaller et al., 2018).

The previous gradients in MAP and MAT and latitudinal variations in solar radiation result in a southward increase in vegetation density (Bernhard et al., 2018). The vegetation gradient evident from mean MODIS Normalized Difference Vegetation Index (NDVI) values range from ~0.1 in Pan de Azúcar (north) to ~0.8 in Nahuelbuta (south) (Didan, Kamel, 2015). This gradient in climate and vegetation cover from north to south in the Chilean Coastal Cordillera acts as a natural laboratory to study the effects of variations in precipitation and vegetation (in different environments) on catchment-scale erosion rates over variable timescales.

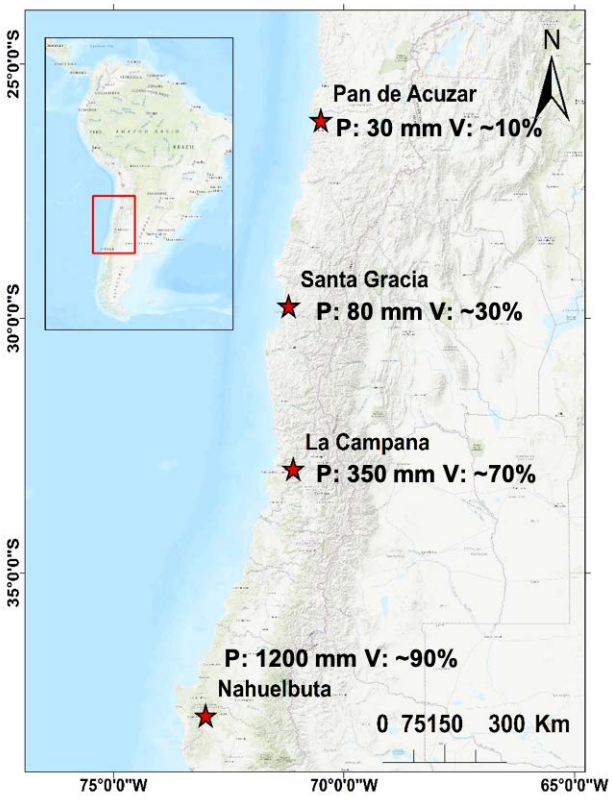

Figure 1. The representative study areas in the Chilean Coastal Cordillera were used for the model setup (ESRI 2019). These study areas are part of the German EarthShape priority research program (www.earthshape.net).

2 Model Description

This chapter describes the numerical landscape evolution and hydrological models used in this study. We also describe the landscape evolution model components simulating the surface processes in the subsequent sections. The description of selected components (e.g., fluvial, hillslope, soil-water infiltration, etc.) also includes the modification of underlying governing equations based on vegetation cover.

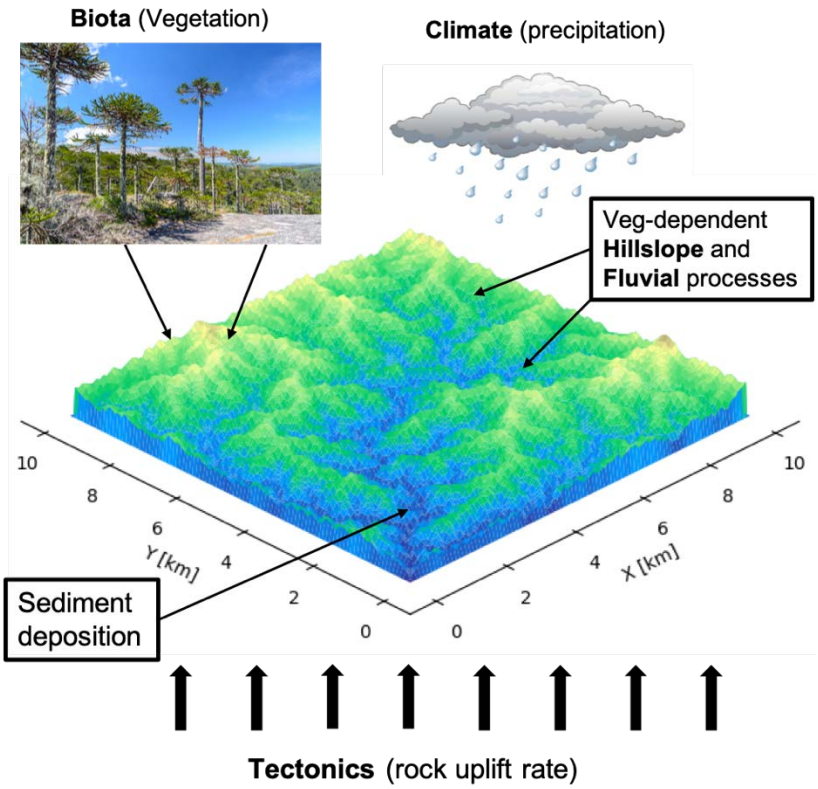

Figure 2. An example of a landscape evolution model domain to investigate the coupled effects of tectonics, climate, and biota on erosion and sedimentation over a synthetic steady-state topography generated using Landlab.

The numerical models offer an excellent tool for investigating the complex interplay of tectonics, climate, and vegetation on various surface processes, which play a significant role in shaping the landscapes over various timescales (e.g., Horritt and Bates, 2002; Tucker and Hancock, 2010). These timescales range from hours to a day (e.g., simulation of flood events) to millions of years (e.g., the evolution of topography). These models include the mathematical representation of the theory behind each process and their interactions in landscape development (Coulthard, 2001; Hobley et al., 2017; Willgoose, 2005; Tucker and Hancock, 2010). A simplified representation of a landscape evolution model domain of a synthetic low relief catchment evolved as a result of coupled forcings in tectonics (rock uplift rates), climate (precipitation), and biota (vegetation) is shown in Fig. 2.

2.1 Landscape Evolution Model

This thesis utilizes a flexible, open-source python-based Landlab modeling toolkit (with plug and play functionality). Landlab allows for the coupling of various process-based models (or components) simulating, for example, fluvial and hillslope processes, weathering, hydrology, geodynamics, etc., over large temporal and spatial scales in a single grid (Hobley et al., 2017). It also allows for the formulation of numerical model setups (e.g., application-specific equations in combination with pre-defined Landlab components) over a two-dimensional simulation grid with user-defined size, shape, and boundary conditions. The two-dimensional model grids are especially essential for storing spatially variable model parameters. The gridding engine of Landlab supports multiple grid shapes, for example, rectangular (or raster), hexagonal, and Voronoi-Delaunay mesh grids (Hobley et al., 2017). The composition of Landlab grids involves nodes (points in space [x, y]), cells (polygons surrounding the non-boundary nodes), and links (directional connections between adjacent pairs of nodes). The number of links per node depends on the grid shape; for example, rectangular grids have four links, and hexagonal grids have six links per node.

In this study, for simplicity, we utilized the rectangular (raster) grid, which is supported by most of the Landlab components and also compatible with raster-based model input (e.g., DEM, satellite-derived NDVI, and land cover maps). The core nodes (non-boundary) are enclosed by cells and active links. The boundary (or parameter) nodes may be categorized as a fixed value (Dirichlet), fixed gradient (Neumann), looped or closed. Similarly, links at boundary nodes are defined as active (allowing flux between nodes), fixed (allowing fixed flux), or inactive (allowing no flux). The Landlab components (and their functionality) used in this study are described in section 1.3.1.

2.2 Landscape evolution model components

As mentioned in the previous section, Landlab offers a variety of physically-based models in the form of model components and allows for user-defined models. The models used in this study include the simulations of the fluvial (Shobe et al., 2017) and hillslope (Johnstone and Hilley, 2014) processes, weathering and soil production (Ahnert, 1976; Barnhart et al., 2019), hydrology (Barnhart et al., 2020), and soil-water infiltration (Green and Ampt, 1911; Julien et al., 1995; Rengers et al., 2016). A detailed description of the model components (and governing equations), including the modification based on vegetation (e.g., fluvial and hillslope processes and infiltration), is presented in this section.

Fluvial Processes

The simulation of fluvial processes involves the SPACE 1.0 component of the Landlab. SPACE is an acronym for Stream Power with Alluvium Conservation and Entrainment. It is an extension of the work of Davy and Lague (2009), Lague (2010), and Zhang et al. (Zhang et al., 2015) that treats bedrock

and sediment layers separately (Shobe et al., 2017). The SPACE is a type of erosion-deposition model in terms of sediment dynamics (e.g., sediment is conserved in the river bed and the water column). The bedrock erosion is calculated progressively with the thinning of the sediment layer, allowing for simultaneous bedrock erosion and sediment entrainment. The model also allows the transition between detachment- and transport-limited fluvial processes over large spatial and temporal scales. The conceptual representation of the SPACE model is depicted in Fig. 3. The major processes (in the form of equations) are described in subsequent paragraphs; for detailed explanations of processes (not included here), please refer to Shobe et al. (2017).

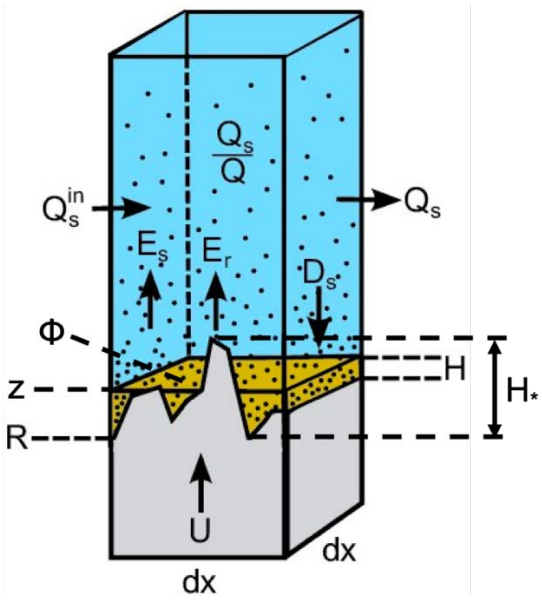

Figure 3. Conceptual representation of fluvial processes in a single model cell in SPACE. The major elements are; z: topographic elevation, R: bedrock elevation, H: sediment depth, H*: bedrock roughness, U: uplift rate, and ϕ: sediment porosity (adapted from Shobe et al., 2017).

The model computes the rate of change in topography based on the conservation of mass. Such that the change in channel bed elevation (z) at a time interval of dt is equal to the change in bedrock elevation (R) and sediment depth (H),

$$\frac{dz}{dt} = \frac{dR}{dt} + \frac{dH}{dt}, \quad (1)$$

Following Davy and Lague (2009), the change in sediment depth is calculated based on the conservation of sediment in the channel bed as,

$$\frac{dH}{dt} = \frac{D_s - E_s}{1-\phi}, \quad (2)$$

where D_s is the sediment deposition flux per unit bed area [L T^{-1}] on the river bed, E_s is the sediment entrainment flux per unit bed area [L T^{-1}] in the water column, and ϕ is the sediment porosity. Similarly, the rate of change in bedrock elevation is calculated as follows,

$$\frac{dR}{dt} = U - E_r, \tag{3}$$

where U is the rate of rock uplift and E_r is the bedrock erosion flux per unit bed area [L T^{-1}]. For simplicity, the porosity of bedrock is assumed as zero. The bedrock erosion, sediment entrainment, and deposition fluxes (per unit bed area) are calculated as,

$$E_r = (K_r Q^m S^n - \omega_{cr})\, e^{-H/H_*}, \tag{4}$$

$$E_s = (K_s Q^m S^n - \omega_{cs}) \left(1 - e^{-\frac{H}{H_*}}\right), \tag{5}$$

$$D_s = \frac{Q_s}{Q}, \tag{6}$$

where, K_s [m^{-1}] and K_r [m^{-1}] are the sediment erodibility and bedrock erodibility parameters, respectively. The above equations denote the threshold stream power for sediment entrainment and bedrock erosion as ω_{cs} [m yr^{-1}] and ω_{cr} [m yr^{-1}]. Bedrock roughness is denoted as H_* [m], and the term e^{-H/H_*} corresponds to the soil production from bedrock. With higher bedrock roughness magnitudes, more sediment would be produced.

The parameters, K_s and K_r, were modified in the model using the approach of Istanbulluoglu (2005) and Schmid et al. (2018) by introducing the effect of Manning's roughness to quantify the effect of vegetation cover on bed shear stress,

$$\tau_v = \rho_w g (n_s + n_v)^{6/10} q^m S^n F_t, \tag{7}$$

where ρ_w [kg m^{-3}] and g [m s^{-2}] are the density of water and acceleration due to gravity, respectively. Manning's numbers for bare soil and vegetated surface are denoted as n_s and n_v. F_t represents the shear stress partitioning ratio. Manning's number for vegetation cover and F_t are calculated as follows,

$$n_v = n_{vr} \left(\frac{V}{V_r}\right)^w, \tag{8}$$

$$F_t = \left(\frac{n_s}{n_s + n_v}\right)^{\frac{3}{2}}, \tag{9}$$

where n_{vr} is Manning's number for the reference vegetation. Here, V_r is reference vegetation cover (V=100 %), V is local vegetation cover in a model cell, and w is an empirical scaling factor.

By combining the stream power equation (Tucker et al., 1999; Howard, 1994; Whipple and Tucker, 1999) and the above concept of the effect of vegetation on shear stress, we follow the approach of

Schmid et al. (2018) to define new sediment and bedrock erodibility parameters influenced by the surface vegetation cover on fluvial erosion, as follows,

$$K_{vs} = K_s \rho_w g (n_s + n_v)^{6/10} F_t, \quad (10)$$

$$K_{vr} = K_r \rho_w g (n_s + n_v)^{6/10} F_t, \quad (11)$$

where K_{vs} [m^{-1}] and K_{vr} [m^{-1}] are modified sediment erodibility and bedrock erodibility, respectively. These are influenced by fractional vegetation cover V. Hence, K_s and K_r in Eqs. 4 and 5 are replaced by K_{vs} and K_{vr} to include an effect of vegetation cover on fluvial processes in the model.

For the inclusion of the effect of PFTs in fluvial processes, the Manning's number for vegetated surfaces (n_v, in a model cell) is replaced by the Manning's number for grasses (n_g), shrubs (n_{sh}), or trees (n_t) in Eqs. 10 and 11, based on the approach of Kalyanapu et al. (2010).

Hillslope Processes

The simulation of hillslope processes involves the DepthDependentDiffuser component of the Landlab. This component applies a linear diffusion rule, with dependency on sediment depth and topographic slope in the style of Johnstone and Hiley (2014). The schematic diagram for a simple hillslope diffusion model is shown in Fig. 4.

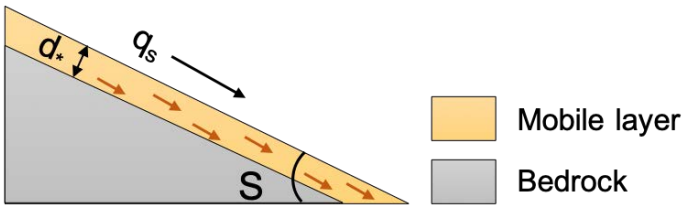

Figure 4. Conceptual representation of hillslope processes in DepthDependentDiffuser. The major elements are S: topographic slope, qs: sediment flux along the slope, and d*: sediment transport decay depth.

The rate of change in topography due to hillslope diffusion (Fernandes and Dietrich, 1997; Martin, 2000) is defined as follows:

$$\frac{dz}{dt} = \nabla q_s, \quad (12)$$

where q_s is sediment flux along the slope S. We applied the slope- and depth-dependent linear diffusion rule following the approach of Johnstone and Hilley (2014) such that,

$$q_s = K_d S d_* (1 - e^{-H/d_*}), \quad (13)$$

where K_d is the diffusion coefficient [$L^2\ T^{-1}$], d_* is sediment transport decay depth [m], and H denotes sediment thickness.

The diffusion coefficient is defined as a function of vegetation cover present on hillslopes, which is estimated following the approach of Istanbulluoglu and Bras (2005), Dunne et al. (2010), and Schmid et al. (2018) as follows,

$$K_d = K_b e^{-(\alpha V)}, \quad (14)$$

where K_d is defined as a function of vegetation cover V, an exponential decay coefficient α, and linear diffusivity K_b for bare soil.

Weathering and soil production

The simulation of weathering and soil production involves the ExponentialWeatherer component of the Landlab. This component is based on the exponential weathering (mixture of chemical, biological, and physical) of bedrock on the hillslopes, which leads to the thickening of the sediment layer. It applies the soil production function in the style of Ahnert (1976) to calculate the rate of weathering, such that:

$$W = W_o \cdot e^{-\frac{H}{d_*}}, \quad (15)$$

where W is the weathering (or soil production rate) [LT^{-1}], W_o is the maximum rate of weathering [LT^{-1}], d_* is sediment transport decay depth [m], and H is the sediment thickness.

Hydrology

The simulation of precipitation-induced surface runoff involves the FlowAccumulator component of the Landlab. The FlowAccumulator component accumulates the channel flow and calculates the drainage area by implementing different methods for directing the flow in Landlab (Barnhart et al., 2020). The d8 flow routing scheme is implemented in this study, where the flux (through an active link) is directed to the neighboring node with the steepest slope. This runoff rate is calculated as a product of drainage area and precipitation input.

Soil water infiltration and vegetation modification

The simulation of weathering and soil production involves the SoilInfiltrationGreenAmpt component of the Landlab. The soil-water infiltration rate is estimated by applying the Green-Ampt equation (Green and Ampt, 1911; Julien et al., 1995),

$$f(t) = K_e \left(1 + \frac{\psi \cdot \Delta\theta}{F}\right), \quad (16)$$

where f(t) is the infiltration rate [m s^{-1}] at time t, K_e is the effective hydraulic conductivity [m s^{-1}], F is cumulative infiltration [m], Ψ is suction at the wetting front [m], and $\Delta\theta$ is the difference between saturated and initial volumetric moisture content [m^3 m^{-3}].

Following the approach of Istanbulluoglu and Bras (2006) for loamy soils, the soil-water infiltration is modified to account for variable vegetation cover in each grid cell, as follows:

$$I_c(t) = f(t)(1 - V(t)) + 4f(t)(V(t)), \quad (17)$$

$$I_a(t) = Min[P(t), I_c(t)], \quad (18)$$

where I_c is the infiltration capacity and V is the vegetation cover (between 0 and 1) in a model grid cell at time-step *t*.

2.3 Hydrological model

A hydrological model represents the components and physical processes (e.g., precipitation, evapotranspiration, infiltration, etc.) of the water cycle and is based on water balance in the watershed. While addressing the third research question in this thesis (see section 1.3), the output (i.e., runoff rates) of the landscape evolution model is cross-checked with the hydrological model to validate the results. Hence, a brief description of the model is presented in this sub-section.

2.3.1 Soil and Water Assessment Tool

This study (in section 3.3) utilizes ArcSWAT-2012, an ArcView extension of the Soil and Water Assessment Tool (SWAT) hydrological model. This section includes a generalized description of the SWAT model's functionality, inputs, and methodology.

SWAT is a physically-based, semi-distributed hydrological model based on the water balance concept. Catchment processes, including runoff, evapotranspiration, sediment, nutrient transport, and crop growth, are simulated based on topographical, meteorological, soil, and land cover data (Winchell et al., 2013). The model is developed to predict the impact of land management practices on water, sediment, and agricultural sediment yields in large and complex watersheds with varying soil and land cover over long periods (Arnold et al., 1998). It is implemented due to its capability to account for the spatial distribution of land use and land cover in the watershed. It is a computationally efficient model enabling the study of long-term impacts (e.g., from days to decades). However, it is a continuous-time model and is not designed to simulate detailed, single event flood routing. A schematic diagram for the water balance concept implemented in SWAT is represented in Fig. 5.

For a better physical description and to enhance the accuracy of the water balance, a watershed is discretized into several sub-basins. The topographic slopes are extracted from the watershed and stored as a separate raster layer. Input information for each sub-basin is grouped into different categories, i.e., climate, hydrologic response units (HRUs), and main channel (reach) draining the sub-basin. Each HRU combines land cover, soil type, and topographic slope. Surface water discharge is predicted for each HRU and routed to obtain total surface runoff for the watershed. A flowchart representing the simple methodology of ArcSWAT-2012 is shown in Fig. 6.

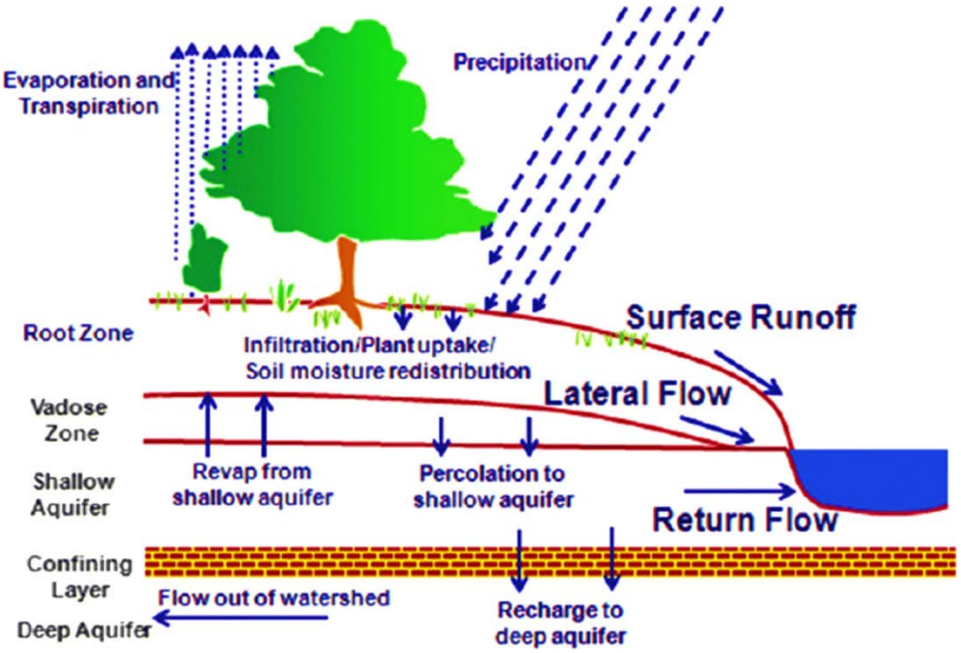

Figure 5. Schematic diagram of water balance concept in SWAT model (adapted from Neitsch et al., 2011).

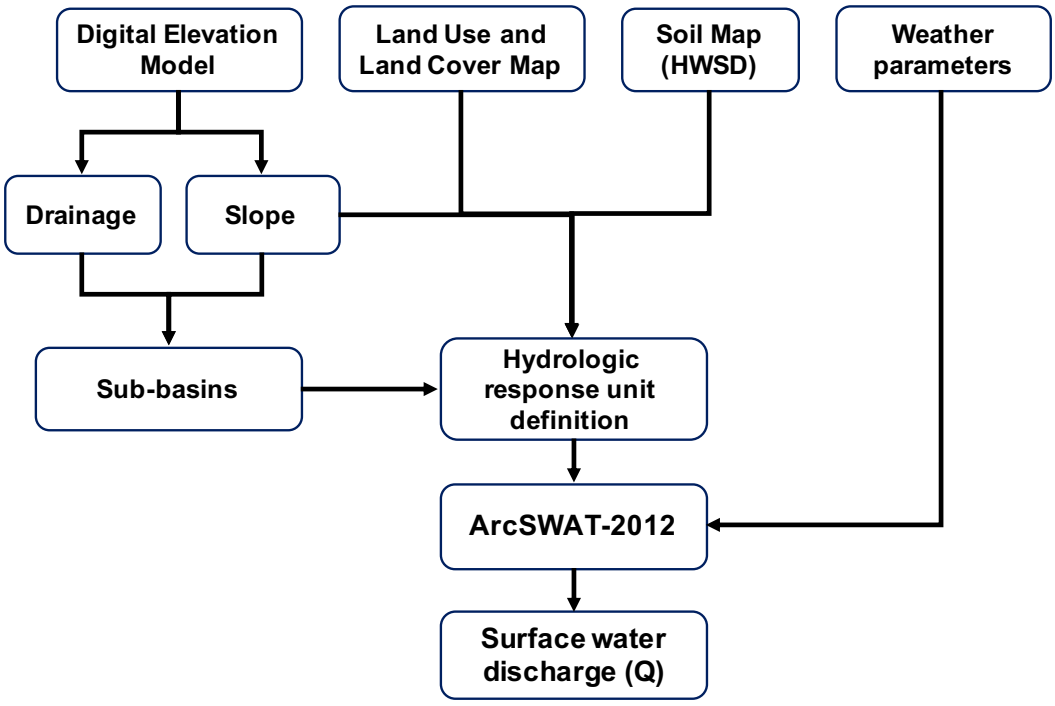

Figure 6. A simplified representation of the methodology of ArcSWAT-2012 in the estimation of surface water discharge rates at the catchment outlet. The input files include a DEM, LULC, soil map (obtained from Harmonized World Soil Database), and weather parameters. The weather parameters include precipitation, solar radiation, wind speed, and temperature from weather stations or stochastically generated.

3 Scientific Results

This section comprises the manuscripts addressing the research questions and testing their underlying hypotheses. This section is divided into three manuscripts, out of which one is already published in a journal, and the other two are the latest versions of the manuscripts and are soon to be submitted for publication.

3.1 Effect rock uplift and the periodicity of variations in climate and vegetation cover on catchment erosion at millennial timescales

3.1.1 Declarations of contribution to the joint publication

This section of the dissertation was published and is available online through open access under *https://doi.org/10.5194/esurf-9-1045-2021*. The full citation of the publication is as follows:

Sharma, H., Ehlers, T. A., Glotzbach, C., Schmid, M., and Tielbörger, K.: Effect of rock uplift and Milankovitch timescale variations in precipitation and vegetation cover on catchment erosion rates, Earth Surf. Dyn., 9, 1045–1072, https://doi.org/10.5194/esurf-9-1045-2021, 2021.

The manuscript was prepared and contributed by five authors, namely Hemanti Sharma (HS), Todd A. Ehlers (TAE), Christoph Glotzbach (CG), Manuel Schmid (MS), and Katja Tielbörger (KT). Todd Ehlers formulated the initial research framework with feedback from Christoph Glotzbach and Katja Tielbörger. The initial model setup was prepared by Hemanti Sharma with the help of Manuel Schmid. All the co-authors jointly contributed in analysis and interpretation of results. The manuscript was prepared by Hemanti Sharma and Todd Ehlers with the feedback from Christoph Glotzbach and Katja Tielbörger. The detailed contributions of each author for the above publication are presented in Table 1.

Table 1. Contribution of authors (in percentage) in the manuscript with the title *"Effect of rock uplift and Milankovitch timescale variations in precipitation and vegetation cover on catchment erosion rates"*. The article was published on 26.08.2021.

Author	Author position	Scientific ideas [%]	Data generation [%]	Analysis & interpretation [%]	Paper writing [%]
HS	1	35	60	50	55
TAE	2	35	10	30	20
CG	3	10	0	5	10
MS	4	10	30	10	0
KT	5	10	0	5	15

3.1.2 Effect of rock uplift and Milankovitch timescale variations in precipitation and vegetation cover on catchment erosion rates

Earth Surf. Dynam., 9, 1045–1072, 2021
https://doi.org/10.5194/esurf-9-1045-2021
© Author(s) 2021. This work is distributed under
the Creative Commons Attribution 4.0 License.

Earth Surface Dynamics
Open Access
EGU

Effect of rock uplift and Milankovitch timescale variations in precipitation and vegetation cover on catchment erosion rates

Hemanti Sharma[1], Todd A. Ehlers[1], Christoph Glotzbach[1], Manuel Schmid[1], and Katja Tielbörger[2]

[1]Department of Geosciences, University of Tübingen, 72076 Tübingen, Germany
[2]Department of Biology, Plant Ecology Group, University of Tübingen,
Auf der Morgenstelle 5, 72076 Tübingen, Germany

Correspondence: Todd A. Ehlers (todd.ehlers@uni-tuebingen.de)

Received: 1 March 2021 – Discussion started: 13 April 2021
Revised: 19 July 2021 – Accepted: 30 July 2021 – Published: 26 August 2021

Abstract. Catchment erosion and sedimentation are influenced by variations in the rates of rock uplift (tectonics) and periodic fluctuations in climate and vegetation cover. This study focuses on quantifying the effects of changing climate and vegetation on erosion and sedimentation over distinct climate–vegetation settings by applying the Landlab–SPACE landscape evolution model. As catchment evolution is subjected to tectonic and climate forcings at millennial to million-year timescales, the simulations are performed for different tectonic scenarios and periodicities in climate–vegetation change. We present a series of generalized experiments that explore the sensitivity of catchment hillslope and fluvial erosion as well as sedimentation for different rock uplift rates (0.05, 0.1, 0.2 mm a^{-1}) and Milankovitch climate periodicities (23, 41, and 100 kyr). Model inputs were parameterized for two different climate and vegetation conditions at two sites in the Chilean Coastal Cordillera at $\sim$ 26° S (arid and sparsely vegetated) and $\sim$ 33° S (Mediterranean). For each setting, steady-state topographies were produced for each uplift rate before introducing periodic variations in precipitation and vegetation cover. Following this, the sensitivity of these landscapes was analyzed for 3 Myr in a transient state. Results suggest that regardless of the uplift rate, transients in precipitation and vegetation cover resulted in transients in erosion rates in the direction of change in precipitation and vegetation. The transients in sedimentation were observed to be in the opposite direction of change in the precipitation and vegetation cover, with phase lags of $\sim$ 1.5–2.5 kyr. These phase lags can be attributed to the changes in plant functional type (PFT) distribution induced by the changes in climate and the regolith production rate. These effects are most pronounced over longer-period changes (100 kyr) and higher rock uplift rates (0.2 mm yr^{-1}). This holds true for both the vegetation and climate settings considered. Furthermore, transient changes in catchment erosion due to varying vegetation and precipitation were between $\sim$ 35 % and 110 % of the background (rock uplift) rate and would be measurable with commonly used techniques (e.g., sediment flux histories, cosmogenic nuclides). Taken together, we find that vegetation-dependent erosion and sedimentation are influenced by Milankovitch timescale changes in climate but that these transient changes are superimposed upon tectonically driven rates of rock uplift.

Published by Copernicus Publications on behalf of the European Geosciences Union.

1 Introduction

The pioneering work of Grove Karl Gilbert (Gilbert, 1877) highlighted the fact that surface uplift, climate, and biota (amongst other things) jointly influence catchment-scale rates of weathering and erosion. In recent decades a wide range of studies have built upon these concepts and quantified different ways in which climate, tectonics, or vegetation cover influence rates of erosion and sedimentation. For example, recent work highlights the fact that denser vegetation and lower precipitation both decrease erosion (Alonso et al., 2006; Bonnet and Crave, 2003; Huntley et al., 2013; McPhillips et al., 2013; Miller et al., 2013; Perron, 2017; Schaller et al., 2018; Starke et al., 2020; Tucker, 2004). In addition, periodic changes in climate (such as changes driven by Milankovitch timescale orbital variations) have also been recognized as influencing rates of catchment erosion and sedimentation (Braun et al., 2015; Hancock and Anderson, 2002; Hyun et al., 2005; Schaller et al., 2004), although our ability to measure orbital-timescale-induced erosional changes can be challenging (e.g., Schaller and Ehlers, 2006; Whipple, 2009). Several studies have also documented how the combined effects of either climate and vegetation change or variable rates of rock uplift and climate change (including glaciation) impact catchment-scale processes (Herman et al., 2010; Mishra et al., 2019; Schmid et al., 2018; Tucker, 2004; Yanites and Ehlers, 2012). Taken together, previous studies have found that the long-term development of topography (such as over million-year timescales) is in many situations sensitive to the tectonic, climate, and vegetation history of the region and that competing effects of different coeval processes (e.g., climate change and tectonics) exist but are not well understood.

Quantification of climate, vegetation, and tectonic effects on catchment erosion is challenging because these processes are confounded and can, if coupled, have opposing effects on erosion and/or sedimentation. For example, precipitation has both direct (positive) and indirect effects on erosion that operate via vegetation cover. Namely, plants require water to grow and survive, and vegetation cover is usually positively affected by precipitation both on a global scale (i.e., when comparing biomes across latitudinal gradients) and on a regional or local scale (e.g., Huxman et al., 2004; Sala et al., 1988; Zhang et al., 2016). Though vegetation cover is also influenced by temperature, seasonality, and many other abiotic factors such as soil type and thickness, the positive relationship of biomass and cover with water availability is rather general. For example, in dry ecosystems such as hot deserts and Mediterranean systems, vegetation cover is primarily limited by water availability and is therefore very low. As precipitation increases, vegetation cover increases rapidly, although water availability can still be the limiting factor in addition to other factors (Breckle, 2002). In temperate systems, wherein water is abundant and soils are well developed, plant growth is primarily limited by low winter temperatures. Overall, the relationship between precipitation and vegetation cover follows a saturation curve with large sensitivity (e.g., measured as rain use efficiency – RUE) to precipitation in arid to Mediterranean systems and low sensitivity in temperate or tropical systems (Gerten et al., 2008; Huxman et al., 2004; Yang et al., 2008; Knapp et al., 2017).

Previous modeling and observational studies have made significant progress in understanding the interactions between surface processes and either climate (Dixon et al., 2009; Routschek et al., 2014; Seybold et al., 2017; Slater and Singer, 2013), vegetation (Acosta et al., 2015; Amundson et al., 2015; Istanbulluoglu and Bras, 2005), or coupled climate–vegetation dynamics (Dosseto et al., 2010; Jeffery et al., 2014; Mishra et al., 2019; Schmid et al., 2018). Over geologic (millennial to million-year) timescales, observational studies of these interactions are impossible (or require proxy data) and numerical modeling approaches provide a means to explore interactions between climate, vegetation, tectonics, and topography. The first observational study of this kind suggested that high MAP (mean annual precipitation) is associated with denser vegetation, hence resulting in lower erosion rates (Davy and Lague, 2009). One of the first numerical modeling studies implementing a vegetation–erosion coupling was conducted by Collins et al. (2004). This study was followed by work from Istanbulluoglu and Bras (2006), which quantified the effect of vegetation on landscape relief and drainage formation. More recently, work by Schmid et al. (2018) included the effects of transient climate and vegetation coupled with a landscape evolution model to predict topographic and erosional variations over millennial to million-year timescales. However, Schmid et al. (2018) presented a simplified approach to consider hillslope and detachment-limited fluvial erosion and only considered a homogeneous substrate. Other studies have documented the fact that sediment or bedrock erosion by rivers is not dominated purely by detachment-limited (Howard, 1994) or transport-limited fluvial erosion (Willgoose et al., 1991). Rather, it often involves a combination of or transition between the two conditions (e.g., Pelletier, 2012). Given this, treatment of bedrock erosion and sediment transport for mixed bedrock–alluvial streambeds provides a more realistic framework for understanding the influence of climate, vegetation, and tectonic processes on topographic development. Recent work (Shobe et al., 2017) presented an additional component (SPACE) to the Landlab surface process model. SPACE allows for the simulation of mixed detachment–transport-limited fluvial processes, including separate layers for bedrock and loose sediment. Finally, the sensitivity of topography to different rock uplift rates in variable climate–vegetation settings has not yet been investigated. The combined interactions of tectonics (rock uplift) and variable climate and vegetation warrant investigation given the significant influence of rock uplift on mean elevation, erosion rates and river channel profiles (Kirby and Whipple, 2012; Turowski et al., 2006), and hillslopes.

In this study, we complement previous work and investigate the transient landscape response for mixed bedrock–alluvial systems. We do this for different rates of rock uplift and periodic changes (Milankovitch cycles) in precipitation and vegetation. Our focus is on erosion and sedimentation changes occurring over millennial to million-year timescales. Sub-annual to decadal-scale changes are beyond the scope of this study. More specifically, this study evaluates the following two hypotheses: first, if vegetation cover and climate vary on Milankovitch timescales, then any increases or decreases in catchment erosion will be more pronounced over longer (e.g., 100 kyr) rather than shorter (e.g., 21 kyr) periodicities due to the longer duration of change imposed. Second, if increasing rates of tectonic uplift cause increases in catchment erosion rates, then any periodic variations in climate and vegetation cover will be muted (lower amplitude) at higher uplift rates because the effect of rock uplift on erosion will outweigh climate and vegetation change effects. Given the complexity of this problem, we investigate these hypotheses through numerical landscape evolution modeling using a stepwise increase in model complexity whereby the contributions of individual processes (i.e., climate, vegetation, or tectonics) are identified separately before looking into the fully coupled system and resulting interactions. We apply a two-dimensional coupled detachment–transport-limited landscape evolution model for fluvial processes. In addition, hillslope diffusion (Johnstone and Hilley, 2014) and weathering and soil production (Ahnert, 1977) processes are considered. Although this study is primarily focused on documenting the predicted sensitivity of catchments to variations in tectonics, climate, and vegetation change, we have tuned our model setup to the conditions along the Chilean Coastal Cordillera (Fig. 1), which features a similar tectonic setting but an extreme climate and ecological gradient. This was done to provide realistic parameterizations for vegetation cover and precipitation in different ecological settings. This area is also part of the German–Chilean priority research program, EarthShape: Earth Surface Shaping by Biota (https://esdynamics.geo.uni-tuebingen.de/earthshape/index.php?id=129, last access: 15 January 2021), for which extensive research is ongoing.

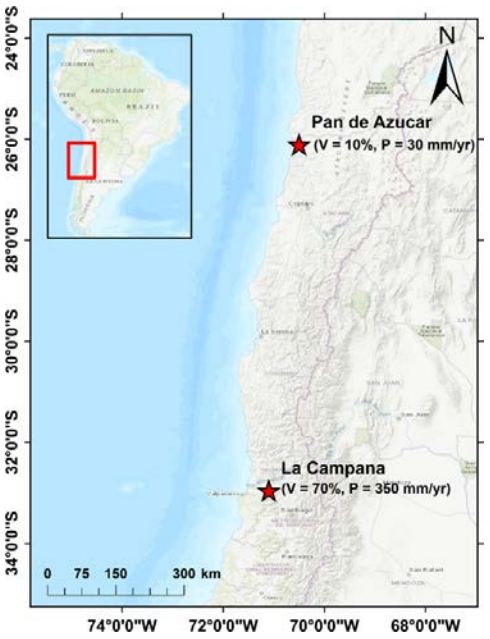

Figure 1. The representative study areas in the Chilean Coastal Cordillera used for the model setup. The model parameters were loosely tuned to the climate and vegetation conditions in these areas (Schmid et al., 2018). The Pan de Azucar area in the north neighbors the Atacama Desert and has sparse vegetation cover (10 %) and an arid climate (30 mm yr^{-1}). The La Campana area in south has a Mediterranean climate and ecosystem with more abundant vegetation (70 %) and precipitation (350 mm yr^{-1}). These two study areas are part of the German EarthShape priority research program (https://esdynamics.geo.uni-tuebingen.de/earthshape/index.php?id=129, last access: 15 January 2021).

2 Methods

We apply the landscape evolution model, Landlab (Hobley et al., 2017), using the SPACE 1.0 module of Shobe et al. (2017) for detachment- vs. transport-limited fluvial processes. The Landlab–SPACE programs were modified for vegetation-dependent hillslope and fluvial erosion using the approach of Schmid et al. (2018). In general, the geomorphic processes considered involve weathering and regolith production calibrated to the Chilean Coastal Cordillera observations of Schaller et al. (2018), vegetation-dependent coupled detachment–transport-limited fluvial erosion, and depth-dependent hillslope diffusion. The model parameters (i.e., bedrock and sediment erodibility and diffusion coefficient) in the simulations are based on those of Schmid et al. (2018). A detailed explanation of the weathering, erosion, sediment transport, and deposition processes is provided in Appendix A, and a summary of model parameters used is given in Table A1.

2.1 Model setup and scenarios considered

The model consists of a 10 km by 10 km rectangular grid with 100 m node spacing (Fig. 2a), with a total domain area of 100 km^2. We conducted generalized simulations that are loosely tuned to the climate and vegetation conditions in two areas in the Chilean Coastal Cordillera (Fig. 1), which have

predominantly granitoid lithology (van Dongen et al., 2019; Kojima et al., 2017; Oeser et al., 2018; Rossel et al., 2018). These areas exhibit a large climate and vegetation gradient ranging from an arid climate (MAP: 30 mm) and sparse vegetation (10 %) in Pan de Azucar National Park to a wetter Mediterranean climate (MAP: 35 cm) with more abundant vegetation (70 %) in La Campana National Park.

Bedrock elevation and sediment cover thickness are considered to be separate layers to quantify simultaneous bedrock erosion and sediment entrainment across the model domain. Simulations were conducted for 15 Myr to generate a steady-state topography with the mean values of precipitation and vegetation cover for the two study areas. The rates of rock uplift are kept constant during the steady-state simulations and subsequently in the transient stage with oscillating vegetation cover and precipitation. After the development of a steady-state topography, transient forcings in vegetation cover and mean annual precipitation (MAP) (Fig. 2b) were introduced for 3 Myr. Vegetation cover varied by ± 10 % around the mean value used to develop the steady-state topography. The 10 % vegetation cover variation is based on the dynamic vegetation modeling results of Werner et al. (2018) for the Chilean Coastal Cordillera. They found that from the Last Glacial Maximum to the present, vegetation cover in the region varied by ~ 10 %. The periodicity of vegetation change varied between simulations (Table A1).

Changes in vegetation cover are driven by climatic variations; MAP has been shown to be much more influential than temperature changes, especially in relatively dry regions (e.g., Mowll et al., 2015) and in grasslands (e.g., Sala et al., 1988). Many previous studies have shown that annual primary production (ANPP) and associated vegetation cover increase linearly (Mowll et al., 2015; Xia et al., 2014) or in an asymptotic manner with MAP (Huxman et al., 2004; Smith et al., 2017; Yang et al., 2008; Zhang et al., 2016; Knapp et al., 2017). These findings are also highly consistent among different approaches such as global (Gerten et al., 2008) and regional (Zhang et al., 2016) models, field and remotely sensed observations across biomes and among years (Huxman et al., 2004; Xia et al., 2014; Yang et al., 2008), and rapid vegetation responses to rainfall manipulation experiments (Smith et al., 2017). An asymptotic relationship appears to be the more common case, especially when looking at warm and dry ecosystems, i.e., regions up to approximately 600 mm MAP (Huxman et al., 2004; Mowll et al., 2015). Here, it has been demonstrated that the sensitivity of ANPP to MAP decreases from more water-limited systems such as deserts to Mediterranean and temperate regions (Huxman et al., 2004; Yang et al., 2008). Namely, the same increase in MAP will yield a much larger increase in vegetation cover in dry regions than in wetter ones. To implement these effects, we use an empirical approach based on vegetation–precipitation relationships observed in the Chilean Coastal Cordillera (see Schmid et al., 2018, for details) to estimate what mean annual precipitation rates are associated with different vegetation cover amounts (Fig. 2b and c).

The effects of vegetation cover on hillslope and fluvial processes are modified from the approach of Schmid et al. (2018); see also the Appendix and Table A1. Briefly, we applied a slope- and depth-dependent linear diffusion rule following the approach of Johnstone and Hilley (2014). The diffusion coefficient (K_d) is defined as a function of the bare soil diffusivity (K_b) and exponentially varies with vegetation cover following the approach of Istanbulluoglu and Bras (2005) and Dunne et al. (2010). Fluvial erosion is estimated for a two-layer topography (i.e., bedrock and sediment are treated explicitly) in the coupled detachment–transport-limited model. Bedrock erosion and sediment entrainment are calculated simultaneously in the model following the approach of Shobe et al. (2017). The effects of vegetation cover on fluvial erosion were implemented using the approach of Istanbulluoglu and Bras (2005) and Schmid et al. (2018) and by introducing the effect of a vegetation-dependent Manning roughness. The sediment and bedrock erodibility (K_vs and K_vr, respectively) are influenced by the fraction of vegetation cover V (see the Appendix for governing equations). Figure 3 shows the range of resulting diffusion coefficients (K_d) and sediment and bedrock erodibility (K_vs and K_vb, respectively) values considered in this study. The exponential and power-law relationships producing these values, respectively, are a source of nonlinearity manifested in the results discussed in subsequent sections.

As the study areas exhibit similar granitoid lithology, the erosional parameters (Table A1) are kept uniform for both the study areas. However, parameters based on climate conditions, namely soil production rate (Schaller et al., 2018), MAP, and vegetation cover (Schmid et al., 2018), are different for these areas. The vegetation cover and precipitation rate are kept uniform across the model domain due to low to moderate relief in target catchments (~ 750 m for Pan de Azucar and ~ 1500 m in La Campana).

The model scenarios considered were designed to provide a stepwise increase in model complexity to identify how variations in precipitation, vegetation cover, or rock uplift rate influence erosion and sedimentation. The model scenarios include the following.

1. Influence of oscillating precipitation and constant vegetation cover on erosion and sedimentation (Figs. 4a and 5, Sect. 3.1)

2. Influence of constant precipitation and oscillating vegetation cover on erosion and sedimentation (Figs. 4b and 6, Sect. 3.2)

3. Influence of coupled oscillations in precipitation and vegetation cover on erosion and sedimentation (Figs. 4c and 7, Sect. 3.3)

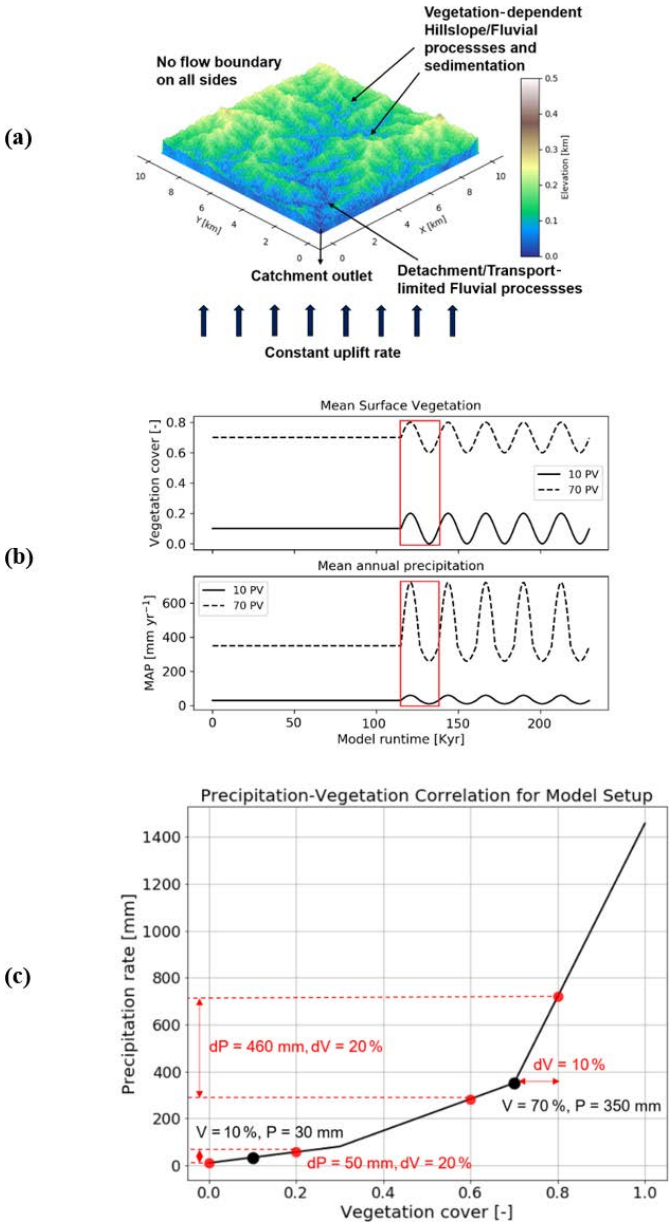

Figure 2. Model geometry as well as climate and vegetation forcings used in this study. **(a)** A simple representation of the model setup with a square grid, and catchment outlet in the lower left corner. **(b)** Graphical representation of the magnitude and pattern of fluctuations imposed on vegetation (top) and precipitation (bottom) during the transient state of the model. Red rectangles represent one cycle, whose effects are discussed in detail. **(c)** Graphical representation of precipitation and vegetation cover correlation from the Chilean study areas used as the empirical basis for how precipitation rates vary for $\pm 10\,\%$ changes in vegetation cover (Schmid et al., 2018).

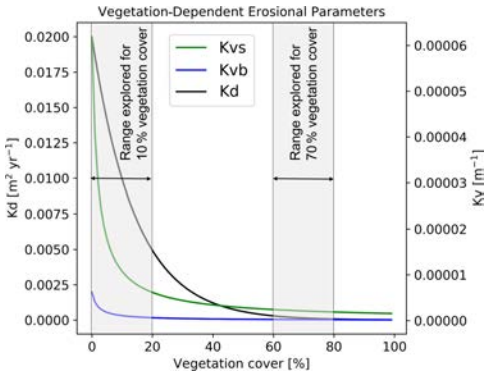

Figure 3. Graphical representation of the range of vegetation-dependent diffusion coefficient (K_d, left y axis), sediment erodibility (K_{vs}), and bedrock erodibility (K_{vb}) values considered in this study (see the Appendix for governing equations). The combined erodibility is referred to as K_v (right y axis).

4. Influence of different periodicities of precipitation–vegetation change on erosion and sedimentation (Fig. 8, Sect. 3.4)

5. Influence of rock uplift rate and oscillating precipitation–vegetation on erosion sedimentation (Fig. 9, Sect. 3.5)

The porosity (0.2) used in this study is lower than the usual range for soil (0.3–0.4), as sediment produced as a result of weathering in the study areas is a mixture of fine- and coarse-grained regolith (Schaller et al., 2020). Manning's numbers for bare soil and reference vegetation cover are the same as used by Schmid et al. (2018). The rate of rock uplift is kept temporally and spatially constant ($0.05\,\mathrm{mm\,a^{-1}}$) for both study areas for the simulations in scenarios 1–4. This is done in order to minimize the effect of tectonics on topography to isolate the sensitivity of geomorphic processes to changing precipitation and vegetation cover. In scenario 5, the effect of different rock uplift rates (i.e., 0.05, 0.1, and $0.2\,\mathrm{mm\,a^{-1}}$) is studied in combination with the coupled oscillations in precipitation and vegetation cover. The rock uplift rate used in scenarios 1–4 is estimated from the findings of Melnick (2016) and Avdievitch et al. (2018), which suggests modern and paleo-uplift and exhumation rates of $< 0.1\,\mathrm{mm\,a^{-1}}$ for the study areas and northern Coastal Cordillera in general. Similarly, the periodicity of oscillations for precipitation and vegetation cover is kept constant (23 kyr) for model scenarios 1, 2, 3, and 5. In scenario 4, the effect of different periodicities (i.e., 23, 41, and 100 kyr) is studied in combination with coupled oscillations in precipitation and vegetation cover. The periodicities of oscillations are based on Milankovitch cycles (Ashkenazy et al., 2010; Hyun et al., 2005). In the simulations with variations in either vegetation cover or climate, a perfect sinusoidal function is used to demonstrate the oscillations in precipitation rates for both catchments (Fig. 4a and b). However, in the case of coupled oscillations in vegetation cover and climate, an asymmetric sinusoidal function is used for precipitation rates (Fig. 4c). This is done due to the observed nonlinear relationships between changing vegetation cover and precipitation in Fig. 2. The nonlinearity stems from the fact that in high-vegetation-cover settings (e.g., 70 %; Fig. 2) a large increase in precipitation is needed to increase vegetation cover by 10 % compared to a smaller decrease in precipitation required to reduce vegetation cover by 10 %.

2.2 Boundary and initial conditions

An initial low-relief (< 1 m) random-noise topography was applied to the model grid at the start of the simulations. The initial topographies had a slight initial topographic slope of $\approx 1.4 \times 10^{-5}$ (Fig. 2a). The boundaries on all sides of the domain were closed (no flow) except the southwest corner node, which was an outlet node. From these conditions, the steady-state topography was calculated over 15 Myr model time, and the resulting bedrock elevation and sediment thickness were used as input for the transient scenarios described in Sect. 2.1.

3 Results

In the following sections, we focus our analysis on the mean catchment sediment thickness (i.e., the combined thickness of soil and regolith) over the entire domain, mean bedrock erosion rates (excluding sediment erosion), mean sediment entrainment rates, and mean catchment erosion rates. The mean catchment erosion rates are the sum of bedrock erosion and sediment entrainment rates. To simplify the presentation, results are shown only for the first cycle of transient climate and vegetation change. Results from the first cycle were representative of subsequent cycles (not shown), and no longer-term variations or trends in erosion–sedimentation were identified or warrant discussion.

3.1 Influence of oscillating precipitation and constant vegetation cover on erosion and sedimentation (scenario 1)

In this scenario, with a rock uplift rate of $0.05\,\mathrm{mm\,a^{-1}}$ and 23 kyr periodicity in precipitation, the mean catchment sediment entrainment rates follow the pattern of change in precipitation (Fig. 5a and b), but with an offset (phase lag) between the maxima and minima of entrainment and precipitation. A higher variation in the range of sediment entrainment rates (i.e., -0.036 to $0.043\,\mathrm{mm\,yr^{-1}}$; Fig. 5b) is observed for simulations with 10 % vegetation cover. Negative values in sediment entrainment rates correspond to sediment

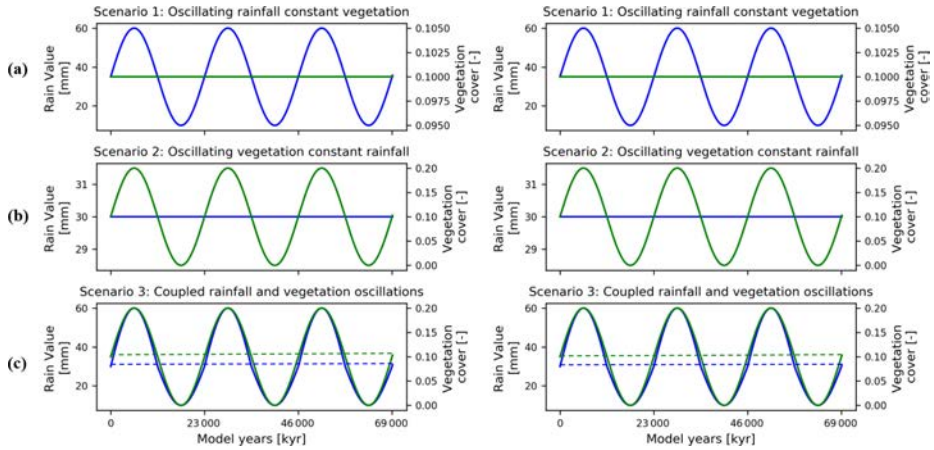

Figure 4. Graphical representation of the different precipitation and vegetation forcings applied to the model scenarios described in the text. Forcings for sparse vegetation (10 %) cover are shown on the left and dense vegetation (70 %) cover on the right. Scenarios explored include **(a)** oscillating precipitation and constant vegetation cover, **(b)** oscillating vegetation and constant precipitation, and **(c)** coupled oscillations in precipitation and vegetation cover.

deposition rates during drier periods. The peak in sediment entrainment rates (e.g., 0.043 mm yr^{-1} for 10 % veg., and $\sim$ 0.038 mm yr^{-1} for 70 % veg.; Fig. 5b) is observed with a time lag of ~ -2 kyr before the peak in maximum precipitation in both the 10 % and 70 % vegetation cover simulations. This result suggests that as precipitation increases sediment is readily entrained where available in the catchment until bedrock is locally exposed. The changes in mean catchment sediment thickness (Fig. 5c) are influenced by changes in the sediment entrainment and precipitation rates, but with a lag time between the maximum in precipitation and the minimum in sediment thickness. The lowest mean catchment sediment thickness (e.g., $\sim$ 0.97 m for 10 % veg., and $\sim$ 1.9 m for 70 % veg.; Fig. 5c) also occurs with a time lag of ($\sim$ 3 kyr) after the peak in precipitation rates for both the 10 % and 70 % vegetation cover simulations. The same time lag $\sim$ 3 kyr is observed in the peak in mean catchment bedrock erosion (e.g., $\sim$ 0.087 mm yr^{-1} for 10 % veg. and $\sim$ 0.1 mm yr^{-1} for 70 % veg.; Fig. 5d) and coincides with when the minimum sediment cover is present and more bedrock is exposed for erosion. As we use the total change in bedrock elevation to estimate bedrock erosion rates, the loss in bedrock due to weathering (exponential) is also accounted for. The phase lag in bedrock erosion and sediment thickness can be attributed to exponential weathering, which is discussed in detail in Sect. 4.2. Finally, the mean catchment erosion rates follow the pattern of change in precipitation rates (Fig. 5a and e) without a phase lag. The maximum erosion rates are similar in range for both the 10 % and 70 % vegetation cover simulations (e.g., $\sim$ 0.12 mm yr^{-1}; Fig. 5e). However, in the 10 % vegetation cover simulation, the minimum in the mean catchment erosion rate decreases more (e.g., to $\sim$ 0.01 mm yr^{-1}; Fig. 5e) relative to the higher-vegetation-cover scenario. The different decreases in the minimum erosion rate between the two vegetation cover amounts correspond to the differences in precipitation rates (Figs. 4a and 5a).

The absence of a phase lag between the mean catchment erosion and precipitation rates reflects the fact that the combined sediment entrainment and bedrock erosion rates when added together track the overall trend in precipitation rate changes, but the individual components (sediment vs. bedrock) respond differently.

3.2 Influence of constant precipitation and oscillating vegetation cover on erosion and sedimentation (scenario 2)

Results from this scenario with constant mean annual precipitation (at the mean value of the previous scenario) and oscillating vegetation cover (Figs. 4b and 6a) show a starkly different catchment response from scenario 1 (Sect. 3.1). The sediment entrainment rates for both simulations (Fig. 6b) show a small decrease in entrainment as vegetation cover increases (e.g., ~ -0.05 mm yr^{-1} for 10 % veg., and ~ -0.01 mm yr^{-1} for 70 % veg.; Fig. 6b. As vegetation cover decreases later in the cycle, entrainment rates increase (e.g., to $\sim$ 0.13 mm yr^{-1} for 10 % veg., and to 0.01 mm yr^{-1} for 70 % veg.; Fig. 6b). The larger magnitude of increase in entrainment for the 10 % vegetation cover case corre-

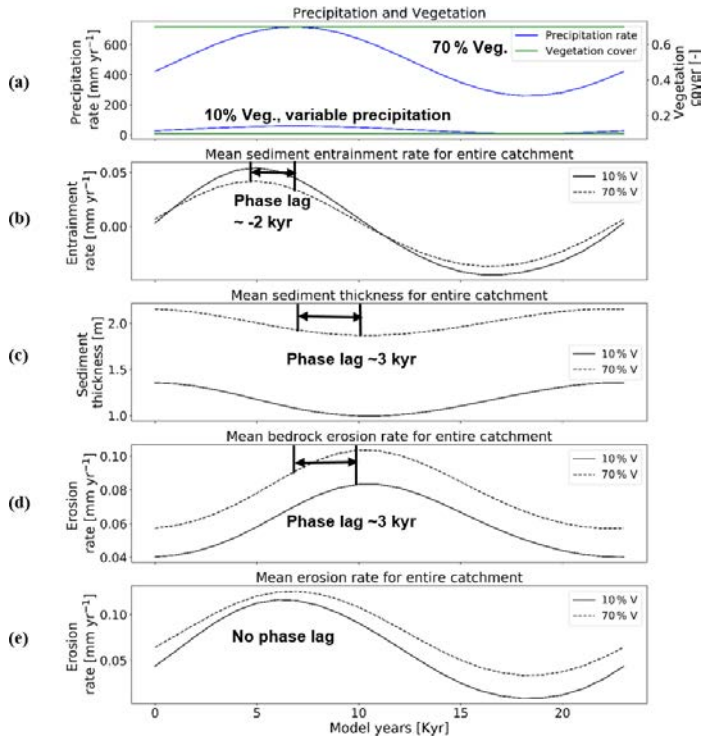

Figure 5. Temporal evolution of catchment-averaged predictions for scenario 1 described in the text (Sect. 3.1). Graphical representation of mean catchment sedimentation and erosion to **(a)** oscillating precipitation [mm yr^{-1}] and constant vegetation cover [–] in terms of **(b)** sediment entrainment [mm yr^{-1}], **(c)** sediment thickness [m], **(d)** bedrock erosion [mm yr^{-1}], and **(e)** mean erosion rates [mm yr^{-1}] for the entire catchment. The periodicity of climate and vegetation oscillations is 23 kyr with a rock uplift rate of 0.5 mm yr^{-1}.

sponds to the minimum (0 %) vegetation cover for which the potential for erosion is the highest. In the 10 % vegetation cover simulation, the lowest mean catchment sediment thickness was observed ∼ 1.5 kyr after the minimum in vegetation cover (Fig. 6c).

The range of mean catchment sediment thickness varies significantly in the simulations (e.g., ∼ 0.72–1.38 m for 10 % veg., and ∼ 2.2–∼ 2.3 m for 70 % veg.; Fig. 6c). The same time lag (∼ 1.5 kyr) is observed between the peak in mean catchment bedrock erosion rates (Fig. 6d) and the minimum in vegetation cover. This is most likely due to the maximum exposure of bedrock for erosion when catchment average sediment thicknesses are at their minimum. Also, the first phase of the cycle is mainly depositional while bedrock erosion (including weathering) is observed, which happens partly in places where there is no deposition. Finally, mean catchment erosion rates (Fig. 6e) are significantly affected (∼ +0.25 mm yr^{-1}) by oscillating vegetation cover in simulations with a mean 10 % vegetation. For the 70 % vegetation cover simulation, a similar maximum in erosion also occurs during the minimum in vegetation but is far less dramatic, presumably due to the still somewhat large (60 %) amount of vegetation cover present. Although the relief and slopes are lower in sparsely vegetated catchment (10 % V), significantly higher erosion rates are observed as precipitation is kept constant at 30 mm yr^{-1}, while the vegetation cover was reduced to 0 %. This can be attributed to low (bedrock–sediment) stream power thresholds.

3.3 Influence of coupled oscillations of precipitation and vegetation cover on erosion and sedimentation (scenario 3)

The catchment response to coupled oscillations in precipitation rate and vegetation cover (Fig. 4c) for erosion and sedimentation represents a composite of the effects discussed

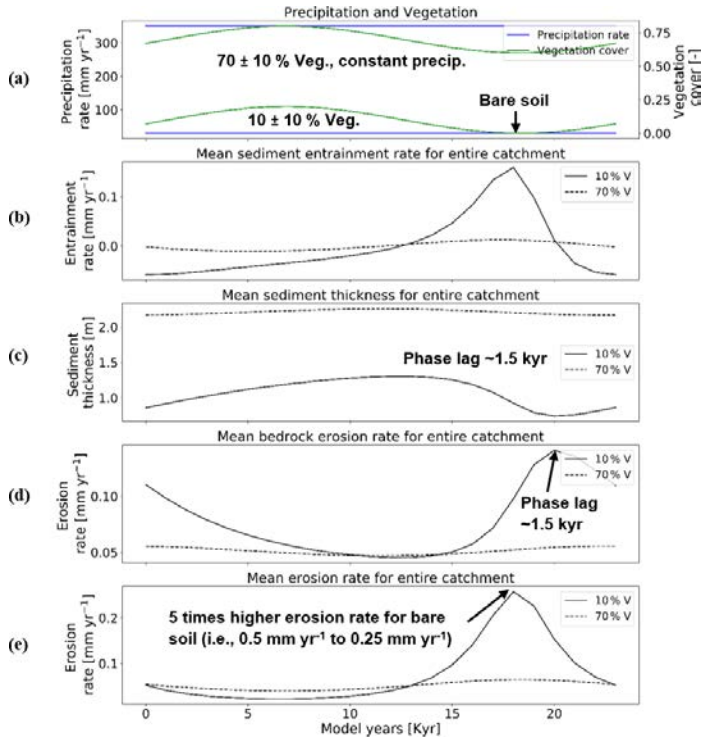

Figure 6. Temporal evolution of catchment-averaged predictions for scenario 2 described in the text (Sect. 3.2). Graphical representation of mean catchment sedimentation and erosion to **(a)** constant precipitation [mm yr^{-1}] and oscillating vegetation cover [–] in terms of **(b)** sediment entrainment [mm yr^{-1}], **(c)** sediment thickness [m], **(d)** bedrock erosion [mm yr^{-1}], and **(e)** mean erosion rates [mm yr^{-1}] for the entire catchment. The periodicity of climate and vegetation oscillations is 23 kyr with a rock uplift rate of 0.5 mm yr^{-1}.

in the previous two sections (Fig. 7). For example, the mean catchment sediment entrainment rates have a peak in entrainment rates ($\sim$ 1.5 kyr) prior to the peak in climate–vegetation values. A similar effect was noted for scenario 1 (Fig. 5, Sect. 3.1). As the precipitation rates and vegetation cover decrease later in the cycle (Fig. 7a), the sediment entrainment rates increase. In more detail, the 70 % vegetation cover simulations show a modest increase similar to that observed in scenario 1 (Fig. 5b), whereas the 10 % vegetation cover shows a sharp peak in the sediment entrainment rates when 0 % vegetation cover is present. This latter observation is similar to what is observed for scenario 2 (Fig. 6b, Sect. 3.2). Thus, in the case of covarying precipitation rates and vegetation cover, the response observed in terms of sediment entrainment is not predicted to be the same for all degrees of vegetation cover and depends heavily on the initial vegetation cover of the system around which variations occur.

Mean catchment sediment thicknesses in the 10 % vegetation cover simulation show a modest response and vary between 1.16 and 1.24 m (Fig. 7c), with a time lag of $\sim$ 2.5 kyr between the peak in precipitation–vegetation and minimum sediment thickness. This lag is also observed in the case of the 70 % vegetation cover simulation, but with a higher amplitude of change in sediment thickness (e.g., 2–2.22 m; Fig. 7c). A similar trend in time lags between the peaks in climate–vegetation and bedrock erosion (Fig. 6d) is also present. These observations for variations in sediment thickness again represent the combined effects of the results discussed in Sect. 3.1 and 3.2 (Figs. 5c and 6c).

The amplitude of change in bedrock erosion is 0.05–0.06 mm yr^{-1} for 10 % veg. and 0.05–0.08 mm yr^{-1} for 70 % veg. (Fig. 7d). The bedrock erosion response for both simulations represents a composite of the effects shown in the previous two scenarios (Sect. 3.1 and 3.2). Here the increase in time lag in the maximum in erosion rates (most notable

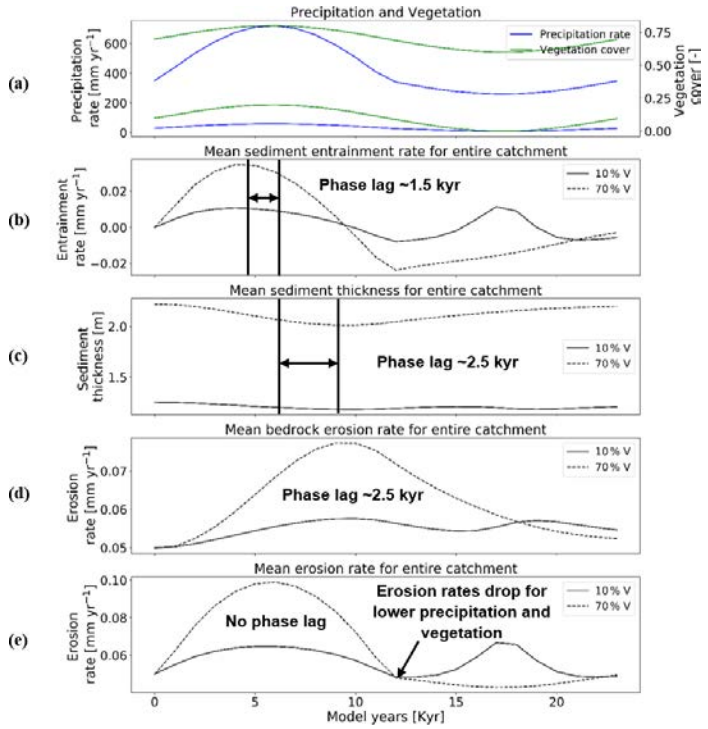

Figure 7. Temporal evolution of catchment-averaged predictions for scenario 3 described in the text (Sect. 3.3). Graphical representation of mean catchment sedimentation and erosion to **(a)** coupled oscillations in precipitation [mm yr^{-1}] and vegetation cover [–] in terms of **(b)** sediment entrainment [mm yr^{-1}], **(c)** sediment thickness [m], **(d)** bedrock erosion [mm yr^{-1}], and **(e)** mean erosion rates [mm yr^{-1}] for the entire catchment. The periodicity of climate and vegetation oscillations is 23 kyr with a rock uplift rate of 0.5 mm yr^{-1}.

for the 70 % vegetation cover simulation) resembles the effect of a large increase in precipitation rates (compared to Fig. 5d) for the first part of the cycle. Whereas the second peak in bedrock erosion visible in the 10 % vegetation cover scenario more closely resembles the effects shown in Fig. 6d when the vegetation cover goes to 0 %, the landscape is increasingly sensitive to erosion with whatever runoff (albeit little) is available.

Finally, the mean catchment erosion rates (Fig. 7e) again show the combined effects of the sediment entrainment rate and bedrock erosion histories previously discussed (Fig. 7b and d). In the simulation with 70 % initial vegetation cover, the mean catchment erosion rates follow the pattern of changes in precipitation rates (e.g., ranging from 0.04 to 0.1 mm yr^{-1}; Fig. 7e, see also Fig. 5e). A similar trend is present in the first half of the cycle in the simulation with 10 % vegetation cover, but with much lower magnitudes (i.e., 0.05 to 0.06 mm yr^{-1}; Fig. 7e). However, during the second half of the cycle, the erosion rates increase up to $\sim$ 0.06 mm yr^{-1} and have a second peak at $\sim$ 17–18 kyr for the 10 % vegetation simulation when the vegetation cover is at 0 %. The previous result is, however, in contradiction to the detachment-limited results shown in Fig. 17 of Schmid et al. (2018), who found that erosion rates decreased to 0 mm yr^{-1} for the period of no vegetation cover and a minimum precipitation rate of $\sim$ 10 mm yr^{-1}. This contradiction is related to the increase in sediment entrainment at this time (Fig. 7b), which heavily influences the mean erosion. The detachment-limited approach of Schmid et al. (2018) could not account for this and will be discussed in detail in Sect. 4.2. To summarize, as discussed previously the locations of the maximums and minimums in the mean erosion rate and the shape of the curves (Fig. 7e) can be linked to different times in the climate and vegetation history when either the effects of variable precipitation rate or vegetation cover dominate the mean catchment erosional response.

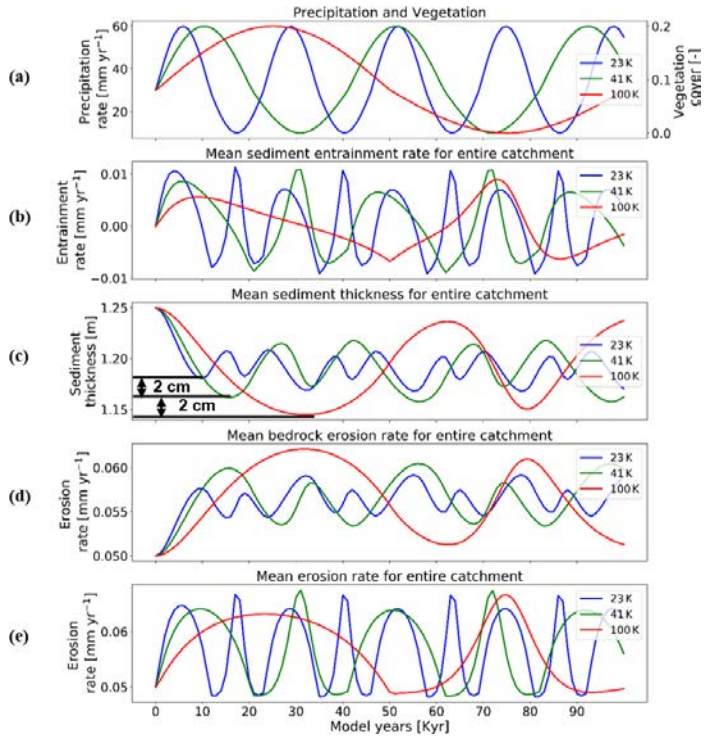

Figure 8. Temporal evolution of catchment-averaged predictions for scenario 4 described in the text (Sect. 3.4). Graphical representation of mean catchment sedimentation and erosion to **(a)** different periodicities of coupled oscillations in precipitation [mm yr^{-1}] and vegetation cover [–] in terms of **(b)** sediment entrainment [mm yr^{-1}], **(c)** sediment thickness [m], **(d)** bedrock erosion [mm yr^{-1}], and **(e)** mean erosion rates [mm yr^{-1}] for the entire catchment. The rate of rock uplift is kept constant at 0.5 mm yr^{-1}. The simulations represent 10 % initial vegetation cover.

3.4 Influence of the periodicity of precipitation–vegetation variations on erosion and sedimentation (scenario 4)

Here we show the influence of different periodicities (23, 41, and 100 kyr) in precipitation and vegetation change on catchment erosion and sedimentation for the cases of a 10 % mean vegetation cover (Fig. 8) and 70 % vegetation cover (Fig. 9). We find higher variations in mean sediment entrainment rates (Figs. 8b and 9b) for both the 10 % and 70 % vegetation cover simulations for the shorter periodicities (23 and 41 kyr). However, the phase lag in the peaks of sediment entrainment and precipitation rates was higher for longer periodicities (e.g., ∼ 9 %, ∼ 16.2 %, ∼ 19 % in 23, 43, and 100 kyr, respectively) for the 10 % vegetation cover case (Fig. 8b). These phase lags are, however, dampened in the highly vegetated landscapes (70 %) at longer periods (i.e., ∼ 9 %, ∼ 9.5 %, ∼ 14 % in 23, 43, and 100 kyr, respectively; Fig. 9b). In a landscape with 10 % vegetation cover, the simulation with longer periodicity (100 kyr) shows higher variations in mean catchment sediment thickness (e.g., 1.14–1.25 cm; Fig. 8c). This is mimicked in the landscape with 70 % vegetation cover, with the range of sediment thickness between 1.95 and 2.27 cm (Fig. 9c). A similar trend with a higher amplitude of change is also observed for bedrock erosion rates in the sparsely vegetated landscape (10 %) with values ranging from 0.05 to 0.062 mm yr^{-1} (Fig. 8d) for longer periodicity (100 kyr). The same pattern is observed in highly vegetated landscapes (70 %), with the values of bedrock erosion rates ranging from 0.045 to 0.094 mm yr^{-1} (Fig. 9d) for the longer periodicity (100 kyr).

Overall variations in mean catchment erosion rates (Figs. 8e and 9e) were not observed to be significant ($<$ 0.0001 mm yr^{-1}) as the period of precipitation and vegetation change increases.

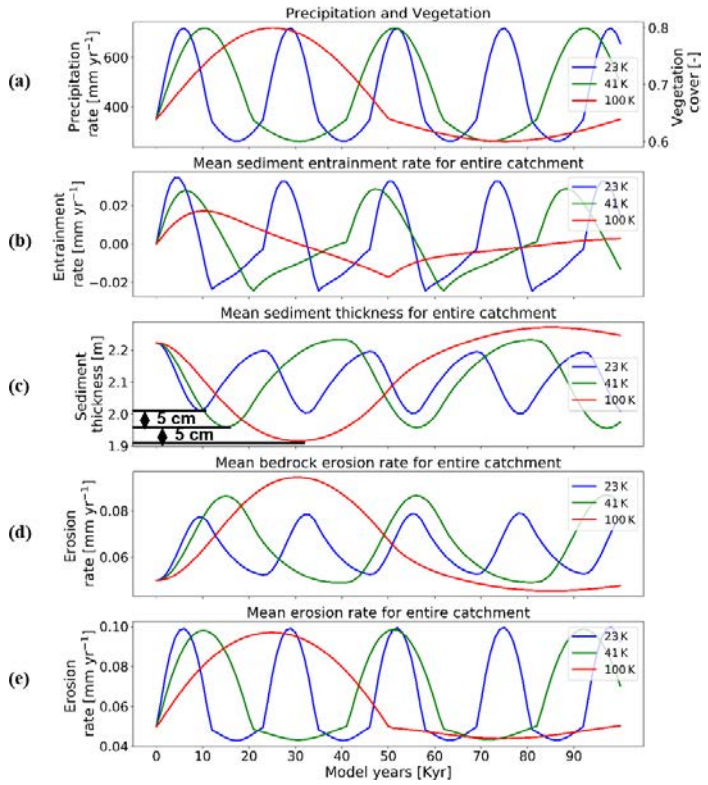

Figure 9. Temporal evolution of catchment-averaged predictions for scenario 4 described in the text (Sect. 3.4). Graphical representation of mean catchment sedimentation and erosion to **(a)** different periodicities of coupled oscillations in precipitation [mm yr^{-1}] and vegetation cover [–] in terms of **(b)** sediment entrainment [mm yr^{-1}], **(c)** sediment thickness [m], **(d)** bedrock erosion [mm yr^{-1}], and **(e)** mean erosion rates [mm yr^{-1}] for the entire catchment. The rate of rock uplift is kept constant at 0.5 mm yr^{-1}. The simulations represent 70 % initial vegetation cover.

3.5 Influence of rock uplift rate and oscillating precipitation–vegetation on erosion sedimentation (scenario 5)

Here we investigate the response of mean catchment erosion and sedimentation for different rates of rock uplift (i.e., 0.05, 0.1, 0.2 mm yr^{-1}) for the 10 % vegetation cover (Fig. 10) and 70 % vegetation cover (Fig. 11) scenarios. To simplify the presentation and comparison of results, the periodicity of precipitation and vegetation change is kept the same as in Sect. 3.3 (i.e., 23 kyr). In general, the results discussed below demonstrate the fact that the transient catchment response to coupled oscillations in precipitation rate and vegetation cover are similar in shape regardless of the rock uplift rate. The magnitude of change in mean catchment erosion associated with precipitation and vegetation changes increases with increasing uplift rate, despite an identical amount of vegetation and precipitation change imposed (Figs. 10a and 11a) on each rock uplift rate simulation.

In more detail, the temporal pattern of changes in sediment entrainment rates (Figs. 10b and 11b) is similar for all uplift rates considered, but the amplitude of change increases as the uplift rate increases. In addition, the phase lag between the peaks in sediment entrainment rates and maximum precipitation rates in the 10 % vegetation simulation (Fig. 10b) varies with the rock uplift rate. For example, the peaks in sediment entrainment rates have a phase lag of ~ -4kyr, -2.5, and -2 kyr for rock uplift rates of 0.2, 0.1, and 0.05 mm a^{-1}, respectively (Fig. 10b), in first half of the vegetation–precipitation oscillation. However, the phase lags are overall shorter in highly vegetated landscapes (70 %)

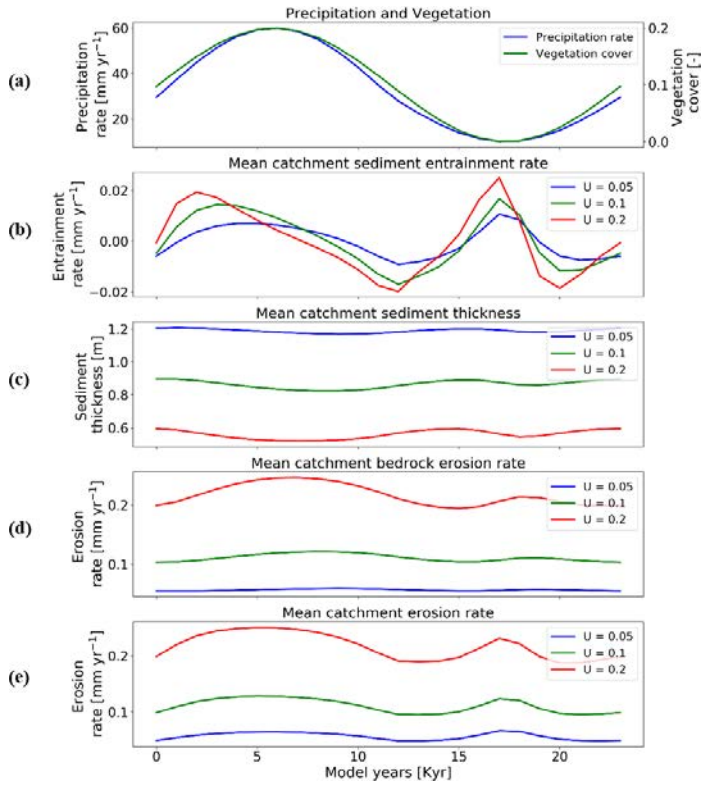

Figure 10. Temporal evolution of catchment-averaged predictions for scenario 5 described in the text (Sect. 3.5). Graphical representation of mean catchment sedimentation and erosion with different rates of rock uplift [mm a^{-1}] to **(a)** coupled oscillations in precipitation [mm yr^{-1}] and vegetation cover [–] in terms of **(b)** sediment entrainment [mm yr^{-1}], **(c)** sediment thickness [m], **(d)** bedrock erosion [mm yr^{-1}], and **(e)** mean erosion rates [mm yr^{-1}] for the entire catchment. The periodicity of climate and vegetation oscillations is 23 kyr. The simulations represent 10 % initial vegetation cover.

(e.g., ~ -3, -2, -1 kyr) before the maximum in precipitation for rock uplift rates of 0.2, 0.1, and 0.05 mm a^{-1}, respectively (Fig. 11b).

For the landscape with 10 % vegetation cover, the simulation with the highest rates of rock uplift (0.02 mm a^{-1}) showed lower mean catchment sediment thickness (e.g., $\sim$ 0.5–$\sim$ 0.6 m; Fig. 10c). In contrast, the slowest rock uplift simulation (0.05 mm a^{-1}) had thicker sediment of $\sim$ 1.16–$\sim$ 1.24 m (Fig. 10c). The same pattern was observed in the catchment with 70 % vegetation cover: the higher sediment thicknesses occur for the lower rates of rock uplift (e.g., $\sim$ 2–$\sim$ 2.2 m; Fig. 11c). These results for sediment thickness variations reflect the fact that higher rock uplift rates result in steeper slopes (not shown) and higher mean catchment erosion rates (Figs. 10e and 11e) such that regolith production rates are outpaced by erosion and therefore result in thinner sediment. Also, the thicker sediment for lower uplift rates could be an integrated result of slightly lower erosion rates compared to sediment production rates over the whole 15 Myr model runtime (steady state). This result is akin to the observational results from Heimsath et al. (1997).

Temporal variations in bedrock and mean catchment erosion rates are similar to those described in Sect. 3.3 (Fig. 7) for the sparsely and more heavily vegetated conditions. The primary difference is that at high rock uplift rates the amplitude of bedrock or mean catchment erosion increases (Figs. 10d, e and 11d, e). To summarize, these results highlight the fact that regardless of the rock uplift rate, similar temporal changes are observed in sediment entrainment or thickness and in bedrock and catchment erosion for oscil-

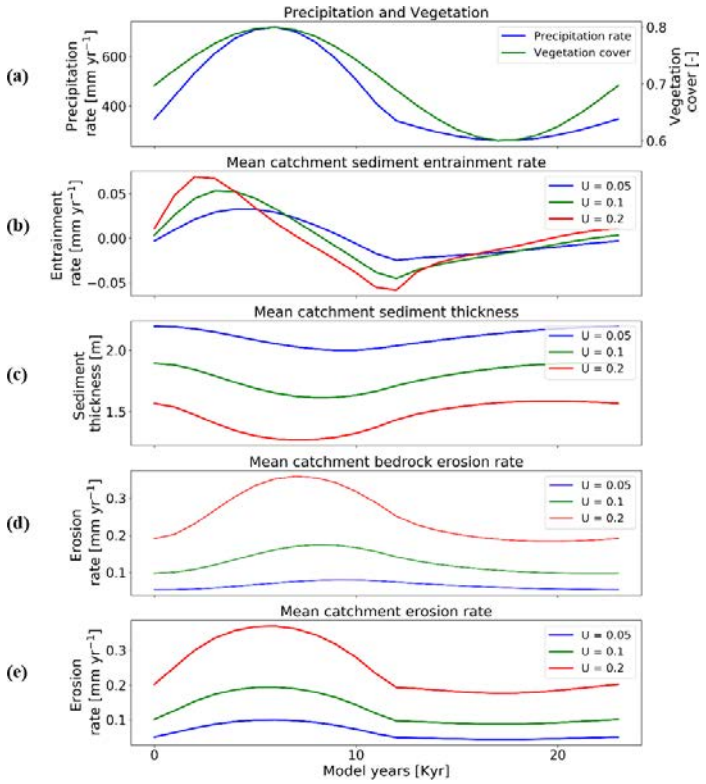

Figure 11. Temporal evolution of catchment-averaged predictions for scenario 5 described in the text (Sect. 3.5). Graphical representation of mean catchment sedimentation and erosion with different rates of rock uplift [mm a^{-1}] to **(a)** coupled oscillations in precipitation [mm yr^{-1}] and vegetation cover [–] in terms of **(b)** sediment entrainment [mm yr^{-1}], **(c)** sediment thickness [m], **(d)** bedrock erosion [mm yr^{-1}], **(e)** mean erosion rates [mm yr^{-1}] for entire catchment. The periodicity of climate and vegetation oscillations is 23 kyr. The simulations represent 70 % initial vegetation cover.

lating precipitation rates and vegetation cover. However, the amplitude of change (or absolute change) in entrainment and erosion rates increases with increases in rock uplift rate. This will be discussed in detail in Sect. 4.4.

4 Discussion

In this section, we synthesize the results from previous sections (scenarios 1–5) in detail. We further investigate the effects of coupled climate and vegetation oscillations (scenario 3) on the occurrence of erosion and sedimentation on a spatial scale.

4.1 Differences in effects between oscillating vegetation or precipitation

Here the sensitivity of erosion and sedimentation to variable precipitation and/or vegetation cover is analyzed. In the scenario with oscillating precipitation and constant vegetation cover, sparsely vegetated landscapes (10 %) erode slowly during periods of lower precipitation. This might be attributed to the dependency of the bedrock erosion and sediment entrainment on the amount of water available through precipitation, which in turn affects the erosion rates. The mean erosion in this scenario is dominated by bedrock erosion with a significant contribution from sediment entrainment. Also, the mean erosion rates over one climate oscillation cycle are observed to be slightly higher ($\sim$ 20 %) than mean erosion rates at steady state for sparsely vegetated land-

scape (10 % V). For densely vegetated landscape (70 % V), this difference is significant (i.e., 50 % higher mean erosion rates during a transient cycle in comparison to steady state). This implies the nonlinearity of the erosion response to changes in MAP, which is significantly higher in a densely vegetated landscape where the amplitude of change in MAP (e.g., 260–720 mm) is much higher than drier landscapes (e.g., 10–60 mm).

Similarly, in a scenario with constant precipitation and variable vegetation cover, sparsely vegetated landscapes (10 %) are observed to be much more sensitive in terms of erosion rates during periods of no vegetation cover. The amplitude of erosional change was 10 times higher than that of densely vegetated landscapes. The mean erosion in sparsely vegetated landscapes is dominated equally by bedrock erosion (Fig. 6d) and sediment entrainment due to the higher availability of bare soil. This justifies the argument of a higher sensitivity of sparsely vegetated landscapes to erosion and sedimentation. This result confirms the findings of Yetemen et al. (2015) (see Fig. 2g), which suggests that shear stress (erosion) decreases significantly (1 to 0.1) as the total grass cover (vegetation) is increased from 0 % (bare soil) to 20 %. Also, a small change in vegetation cover in densely vegetated landscapes would not result in significant differences in erosional processes. Unlike the previous scenario (oscillating precipitation and constant vegetation cover), we do not observe nonlinearity in erosion response to the changes in vegetation cover (i.e., mean erosion rates over one transient cycle are equal to steady-state mean erosion rates).

In general, mean catchment sediment thickness is observed to be inversely proportional to precipitation owing to higher stream power. This in turn translates to a higher sediment flux during wetter periods. The influence of oscillating precipitation and constant vegetation cover on sediment thickness is slightly higher in simulations with sparse vegetation cover. In simulations with constant precipitation and oscillating vegetation cover, the sensitivity of sediment thickness is much higher in landscapes with sparse vegetation. This can be attributed to an absence of vegetation cover. A decreased impact of oscillating vegetation cover on sediment thickness occurs in landscapes with denser vegetation cover and demonstrates that surface processes in these settings are not highly dependent on changes in vegetation density. This has been explained by Huxman et al. (2004), who found that vegetation cover responds to MAP variations in wet and dry systems during dry years.

4.2 Synthesis of coupled oscillations of precipitation and vegetation cover simulations

The sensitivity of erosion and sedimentation to coupled oscillations in precipitation and vegetation cover (scenario 3, Sect. 3.3) indicates that mean catchment erosion rates (Fig. 7e) are correlated with precipitation for densely vegetated landscapes (70 %). This is due to the dominating effect of mean annual precipitation changes (from 26 to 72 cm yr^{-1}) on erosion over vegetation cover change (from 60 % to 80 %; Fig. 7a) in these landscapes. This can be attributed to the higher amplitude of precipitation oscillations in these simulations required to change vegetation cover by $\pm$10 % (Fig. 2b). In the case of a sparsely vegetated landscape (10 %), mean erosion rates (Fig. 7e) are also correlated with precipitation, but only for the first half of the cycle when vegetation cover is present. However, mean erosion rates increase rapidly in the second half of the cycle when MAP decreases (from 60 to 10 mm yr^{-1}; Fig. 7a) and vegetation cover magnitudes decrease (from 20 % to 0 %; Fig. 7a). This inverse correlation between precipitation and erosion can be attributed to increasing susceptibility of the surface to sediment entrainment as vegetation cover decreases to bare soil, even with very low precipitation rates. The nonlinearity of erosion response to changes in MAP is reduced by half (in comparison to changing climate and constant vegetation) in coupled simulations.

Thus, the temporal evolution of mean erosion rates between heavily (70 %) and sparsely (10 %) vegetated landscapes varies depending on the initial vegetation state of the catchment. As a result, correlated and anticorrelated relationships between precipitation, vegetation cover, and erosion are predicted and are the result of precipitation or vegetation exerting a dominant or subsidiary influence on catchment erosion at different times in the catchment history and for different catchment precipitation and vegetation cover conditions. This prediction is consistent with observed correlations of vegetation cover and catchment average erosion rates recently documented along the western Andean margin by Starke et al. (2020).

The lag behavior observed in sediment entrainment, thickness, and bedrock erosion is explained in additional simulations we conducted (results not shown for brevity) wherein the weathering (regolith production) function was turned off in the model simulations (see Fig. A1). In these simulations, we did not observe any significant phase lags in maximum and minimum erosion rates, sediment thickness, or vegetation cover–precipitation. Also, the erosion rates for sparsely vegetated catchment (10 % V) drop to a minimum during the phase of bare soil and minimum precipitation (10 mm yr^{-1}). Hence, sediment supply through weathering can be attributed to double peaks observed in mean catchment sediment entrainment rates (Fig. 7b) and erosion rates (Fig. 7e). When there is no explicit weathering–regolith production involved in the model simulations, sediment supply for entrainment is significantly reduced. As a result, entrainment rates are observed to be 2 orders of magnitude lower than bedrock erosion; hence, entrainment rates are not shown in Fig. A1. This implies that weathering plays a major role in leading to the phase lags observed in the above results.

4.3 Differences between the periodicities of climate and vegetation cover oscillations

The periodicity of change in climate will mainly affect vegetation via the lag time it takes for the vegetation to respond; i.e., if the vegetation structure does not change (e.g., grasslands or forests), then grasslands are very flexible (Bellard et al., 2012; Kelly and Goulden, 2008; Smith et al., 2017). Grasslands can plastically respond from year to year, while forests may die off and be replaced by grasslands when it becomes drier and vice versa. This change in vegetation type might lead to the fluctuations in sedimentation and erosion rates due to periodicity of change in climate and vegetation cover.

4.4 The effect of rock uplift rate on signals of varying precipitation and vegetation cover

No difference in erosion rates was identified between the two different vegetation–precipitation simulations for a given uplift rate when the erosion rate is averaged over the full period of vegetation–precipitation change. In a steady-state landscape, erosion rates are equal to the rock uplift rates according to the law of continuity of mass (e.g., Tucker et al., 2001). This means that steady-state landscapes experience higher erosion rates with higher uplift rates. However, the mean catchment erosion rates shown in Figs. 10e and 11e show temporal variations in the erosion rate driven by oscillations in the precipitation rate and vegetation. When average erosion rates are calculated over a complete cycle of the oscillation, the mean erosion rates are slightly higher than rock uplift rates owing to the nonlinearity of erosion response to changes in MAP. This result indicates that any climate- or vegetation-driven changes in erosion will not be evident when observed over too long a period of time, but they might introduce shorter-term transients (high or low) depending on the climate–vegetation cycle of change. This finding is significant for observational studies seeking to measure the predictions shown in this study. More specifically, thermochronometer dating approaches used to quantify denudation rates over million-year timescales will be hard-pressed to measure any signal of how climate or vegetation change on Milankovitch timescales influences denudation. Rather, the rate of tectonic rock uplift or exhumation (in the case of erosion rates equalling the rock uplift rate) will be measured. In contrast, observational techniques sensitive to decadal (e.g., sediment fluxes) or millennial (e.g., cosmogenic radionuclides measured from river terraces) processes can be sensitive to timescales less than the period of oscillation and are more likely to record transient catchment erosion rates influenced by variations in precipitation or vegetation cover.

The vegetation- and precipitation-driven transients in mean catchment erosion rates predicted by this study were large enough to be measured by some observational techniques. For example, in sparsely vegetated landscapes the half-amplitude of change in erosion rates (from steady-state values) slightly decreases as the uplift rate increases. A higher magnitude of change in transient erosion rates (from steady-state values) is found in densely vegetated landscapes and is again slightly decreased as the uplift rate increases. Previous work by Schaller and Ehlers (2006) investigated the ability of denudation rates calculated from cosmogenic radionuclides measured in a sequence of fluvial terraces to record periodic (Milankovitch timescale) variations in denudation rates. The magnitude of change in predicted transient erosion rates described above is above the detection limit reported by Schaller and Ehlers (2006), particularly when the mean catchment denudation rate is $\sim 0.1\,\mathrm{mm\,yr^{-1}}$ or higher. Thus, the predictions suggested in this study are testable in field-based studies, and other methods such as basin sedimentation rate histories (e.g., determined from magneto-stratigraphy, optically stimulated luminescence, or other methods) also hold potential.

4.5 Spatial changes in where erosion and sedimentation changes occur

In the previous sections, our analysis focused on the spatially averaged response of the catchment in terms of changes in sedimentation and erosion. Here, we discuss the same model results as previously presented for but show two examples (for two different vegetation covers) of the spatial variations of erosion and sediment thickness within the catchments. This provides a basis for understanding where in the catchment changes are occurring.

Spatial variations in the pattern of erosion and sedimentation in the simulations with 23 kyr coupled precipitation and vegetation oscillations, as well as a rock uplift rate of $0.05\,\mathrm{mm\,a^{-1}}$, are shown in the topographic elevation, sediment thickness, and erosion rate changes for both the maximum and minimum in precipitation and vegetation cover. In the simulations with sparse vegetation cover (10 %) (Fig. 12) at the maximum in precipitation and vegetation cover, erosion rate changes from steady state are $\sim 0.03\,\mathrm{mm\,yr^{-1}}$ in valleys and $\sim 0.01\,\mathrm{mm\,yr^{-1}}$ on hillslopes. At the minimum in precipitation and vegetation cover, erosion rate changes from steady state are higher in valleys than hillslopes. This may be attributed to an absence of vegetation during this period, when the surface (bedrock or sediment) is readily available for erosion even with lower precipitation rates. The sediment thickness is observed to be slightly higher in the streambeds and valleys for streams with larger accumulation area. However, the smaller streams have lower sediment thickness compared to connected hillslopes. For example, higher sediment thickness (~ 1.24 m) is observed near the catchment outlet in the lower left corner of the domain. At the maximum in the precipitation and vegetation cover cycle, the landscape experiences a slightly higher contrast in sediment thickness compared to the steady-state condition,

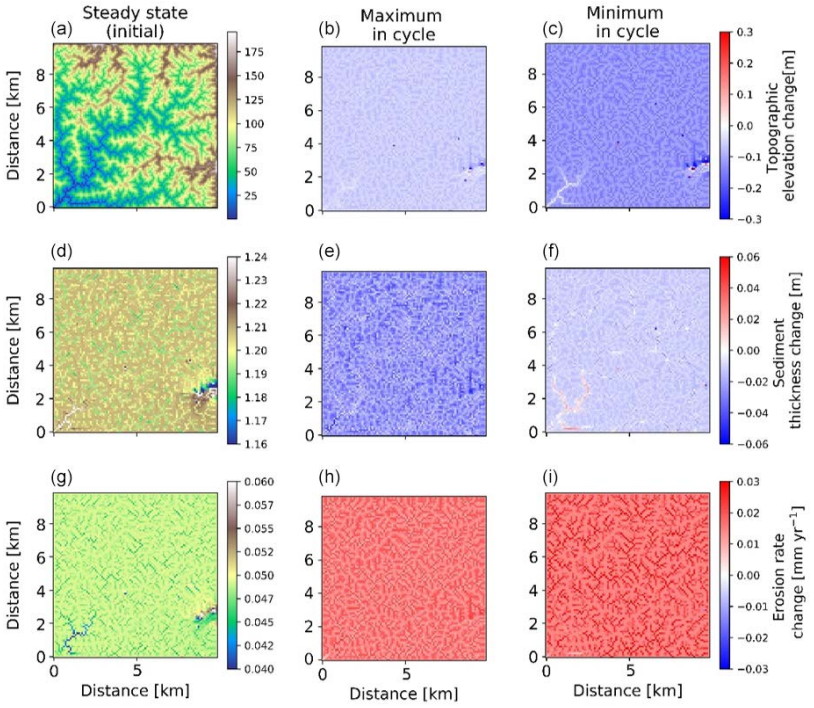

Figure 12. Two-dimensional map-view representation of changes in topographic elevations [m] **(a–c)**, sediment thickness [m] **(d–f)**, and erosion rates [mm yr^{-1}] **(g–i)**. These changes are represented with respect to steady-state conditions **(a, d, g)** for maximum **(b, e, h)** and minimum **(c, f, i)** values of precipitation and vegetation in an oscillation cycle. The simulations represent 10 % initial vegetation cover.

whereby a net lowering of the sediment layer is observed of approximately 2 to 5 cm on the hillslopes and ~ 6 cm near the catchment outlet. This can be attributed to higher sediment fluxes during this period. At the minimum in the precipitation and vegetation cover cycle, the landscape experiences a slight difference from the steady-state sediment thickness (~ 2 cm lowering) except for deposition in higher-order streams (up to ~ 2 cm) near the catchment outlet.

In the simulations with dense vegetation cover (70 %) (Fig. 13), erosion rate changes from steady-state conditions are higher during the maximum in the precipitation and vegetation cover cycle with higher magnitudes (~ 0.08 mm yr^{-1} in valleys and up to ~ 0.02 mm yr^{-1} on hillslopes and ridges) due to the higher precipitation rates. At minimum precipitation and vegetation cover magnitudes ($P = 26$ cm; $V = 60$ %), erosion rate changes are reduced (up to -0.03 mm yr^{-1}) in valleys and (up to -0.01 mm yr^{-1}) on hillslopes in comparison to the erosion rates at steady state. Sediment thickness is observed to be relatively higher in the streambeds and valleys (~ 2.25 m) than the hillslopes. It is contrastingly higher in the lowlands than the areas at higher elevations. At maximum precipitation and vegetation cover (maximum in the cycle) sediment thickness is ~ 10 cm lower on hillslopes and up to ~ 30 cm lower in valleys. The same trend with lower amplitude is evident for the minimum in the precipitation and vegetation cover cycle. This implies that at higher vegetation cover, sediment thickness is significantly reduced as a result of higher sediment flux during the peak in precipitation rates. This in turn signifies the dominance of precipitation changes over vegetation cover change in highly vegetated landscapes.

4.6 Comparison to previous studies

Results presented in this study document a higher sensitivity of catchment erosion and sedimentation of sparsely vegetation landscapes (10 %) to changes in vegetation cover, whereas densely vegetated (70%) landscapes are more responsive to changes in precipitation than vegetation changes. This confirms the broad findings of Schmid et al. (2018) and

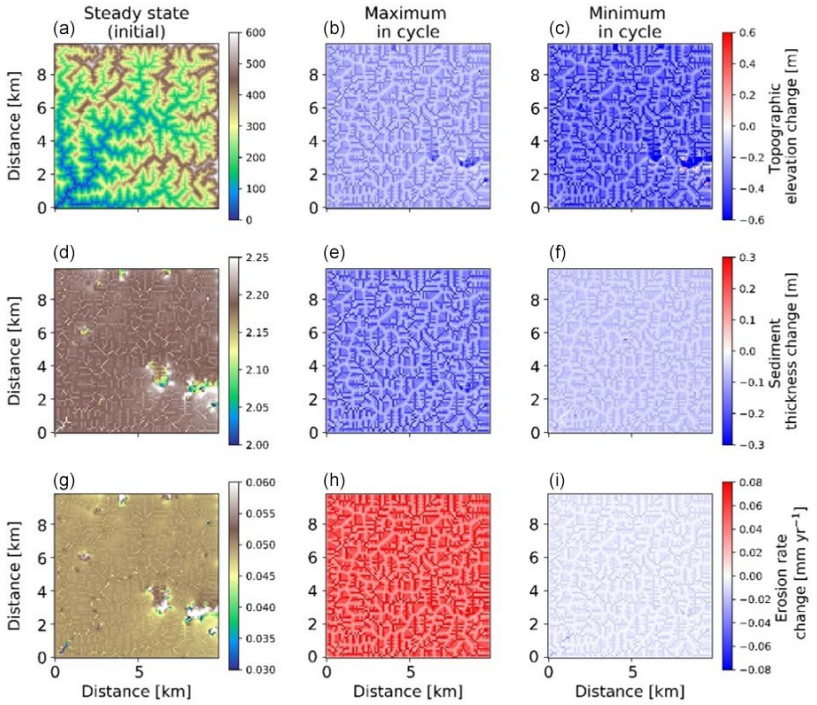

Figure 13. Two-dimensional map-view representation of changes in topographic elevations [m] **(a–c)**, sediment thickness [m] **(d–f)**, and erosion rates [mm yr^{-1}] **(g–i)**. These changes are represented with respect to steady-state conditions **(a, d, g)** for maximum **(b, e, h)** and minimum **(c, f, i)** values of precipitation and vegetation in an oscillation cycle. The simulations represent 70 % initial vegetation cover.

Yetemen et al. (2019), which suggest vulnerability of erosion rates in sparsely vegetated landscapes to changes in vegetation cover and, for densely vegetated landscapes, sensitivity to the changes in MAP. However, there are differences between the results of Schmid et al. (2018) and this study, particularly for the temporal changes in erosion rates we observe for the sparse-vegetation-cover (10 %) scenario with coupled precipitation–vegetation cover oscillations. More specifically, previous results from the detachment-limited model shown in Fig. 17 of Schmid et al. (2018) show that catchment erosion rates in sparsely vegetated landscapes decrease as the precipitation and vegetation cover increases in the first part of a cycle. In the second part of the cycle when precipitation and vegetation decrease to their minimum Schmid et al. (2018) predict erosion rates of $\sim 0\,\mathrm{mm\,yr^{-1}}$. However, in the coupled detachment–transport fluvial erosion model presented here (SPACE), we observe a different behavior and erosion rates slightly increase as precipitation and vegetation cover increase (from 0.05 to 0.065 mm yr^{-1}; Fig. 7e), rather than decrease. This difference is due to the higher sediment entrainment rates we predict during the period of no vegetation and low precipitation ($10\,\mathrm{mm\,yr^{-1}}$), which is a result of higher vulnerability of bare soil to erosion, even with very low precipitation rates. Therefore, the application of a detachment-limited vs. coupled detachment–transport-limited modeling approach has bearing on the predicted response, and when comparing results to natural systems care should be taken in which approach is used.

Previous geochemistry-related observational studies from the Chilean Coastal Cordillera (EarthShape study areas, https://esdynamics.geo.uni-tuebingen.de/earthshape/index.php?id=129, last access: 15 January 2021) are also available for comparison to this study. For example, the steady-state sediment thicknesses in our simulations for 10 % and 70 % initial vegetation cover are predicted to be higher than the field observations reported by Schaller et al. (2018) and Oeser et al. (2018), who reported a ~ 20 and ~ 60 cm depth of mobile sediment layers on hillslopes in the Pan de Azucar and La Campana study areas, respectively. Also, the natural topography is steeper with higher relief, and rock uplift rates

might be different. Spatial variations in vegetation also occur (e.g., in La Campana), with higher vegetation density along valleys, which might lead to the discrepancies between the observed and predicted sediment thickness. However, the trend in our results (higher sediment thickness for densely vegetated – 70 % – landscapes) follows the findings of Oeser et al. (2018), who document sediment increase with increasing mean annual precipitation and vegetation in the Chilean Coastal Cordillera.

In addition, previous field studies (Oeser et al., 2018; Owen et al., 2011; Schaller et al., 2018) applied cosmogenic nuclides to estimate the denudation and soil production rates in the Chilean Coastal Cordillera. They suggest an increase in soil production rates from arid zones in the north to wet tropical zones in the south of the Chilean Coastal Cordillera. These findings are consistent with the predicted increase in sediment depths (e.g., 1.24 m for $V = 10\,\%$ and 2.22 m for $V = 70\,\%$; Fig. 7b) in our study. Finally, the effects of rock uplift and precipitation rates on topography and erosion rates, as documented by Bonnet and Crave (2003) and Lague et al. (2003), show a linear relationship between mean topographic elevation and rock uplift rate for steady-state conditions.

4.7 Model limitations

The model setup used in this study was intended to quantify the sensitivity of hillslope and fluvial erosion as well as sediment transport and depositional processes for different climates with variations in precipitation rates and vegetation cover over Milankovitch timescales. This study was designed as an incremental step forward from previous modeling studies (Collins et al., 2004; Istanbulluoglu and Bras, 2005, 2006; Schmid et al., 2018).

There are several simplifying assumptions made in our modeling approach that warrant discussion and potential investigation in future studies. For example, this study assumed uniform vegetation cover and lithology for the entire catchment. The assumption of uniform vegetation cover in the catchment is likely reasonable given the relatively small ($10 \times 10\,\mathrm{km}^2$) size of catchments investigated and the modest topographic relief produced (between $\sim$ 75–600 m; Fig. 10a). Although temperature and precipitation (and therefore vegetation cover) can vary with elevation, the generally low relief of the catchments in this study does not make this a major concern. Due to the long (geologic) timescales considered in this study and computational considerations, mean annual precipitation rates were applied and stochastic distributions of precipitation could not be considered. While our approach is common for landscape evolution modeling studies conducted on geologic timescales, we recognize that in some settings (such as the arid region of this study; Fig. 1) precipitation events are rare, stochastic in nature, and might have an influence on the results presented here. This is a caveat that warrants future investigation.

The vegetation–erosion parameterization considered in this study follows from that of Istanbulluoglu and Bras (2006) and Schmid et al. (2018). In this parameterization the total vegetation cover of the catchment is considered only, rather than the distribution of vegetation cover by individual plant functional types (e.g., grass, shrubs, trees) that would have different Manning's coefficients associated with them. The "total vegetation cover" approach used in our (and previous) work is a reasonable starting point for understanding landscape evolution over large spatial and temporal scales because (a) more detailed observations about the changes in the distribution of plant functional types over Milankovitch timescales is not available and would be poorly constrained, and (b) empirical relationships between total vegetation cover and precipitation are available and easily implemented (e.g., Fig. 2b). However, future work should focus on exploring how the temporal and spatial distribution of different plant functional types during changing climate impacts catchment erosion given that recent work (Mishra et al., 2019; Starke et al., 2020) has identified this as important. This limitation can be handled in future studies with the full coupling of dynamic vegetation models, such as LPJ-GUESS (Smith et al., 2014; Werner et al., 2018), to a landscape evolution model for the explicit treatment of how different vegetation types change temporally and spatially within a catchment and influence catchment erosion. Also, the total vegetation cover in the model is not disturbed by flow and entrainment, which were observed to have a large impact on the results of Collins et al. (2004) and Istanbulluoglu and Bras (2005). If the vegetation cover was spatiotemporally influenced by the above processes in our simulations, the resulting erosion and sedimentation would have been hybrid between sparse ($10\,\%\ V$) and densely vegetated ($70\,\%\ V$) catchments, with vegetation losses in channels. The timescale for the current study was based on Milankovitch cycles to address the effects of periodicity on erosion and sedimentation. However, the effects of seasonal (sub-annual) variations in precipitation (Istanbulluoglu and Bras, 2006; Yetemen et al., 2015) and satellite-derived vegetation cover (with catchment-variable plant function type distributions) also warrant future investigation to determine if coupled seasonal variations in vegetation cover and precipitation influence catchment erosion.

Finally, the results of this study rely upon the vegetation–erosion parameterizations described in Sect. 2 and the Appendix (see also Fig. 3). While there is an observational basis for these relationships (see Sect. A1 and A2), there are, frankly, a sparse number of field studies available robustly constraining how different vegetation types and amounts influence hillslope and surface water erosional processes. Thus, we consider the erosional parameterizations used here to be hypotheses (rather than robust geomorphic transport laws) that warrant investigation in future field or flume studies.

5 Summary and conclusions

In this study, we investigate the effects of variable vegetation cover and climate over Milankovitch timescales on catchment-scale erosion and sedimentation. Simulations were presented to document if these transients are muted (lower amplitude) at higher rock uplift rates. The approach used here complements previous studies by using a coupled fluvial detachment–transport-limited and hillslope diffusion landscape evolution model, and it also investigates the degree to which transient effects of vegetation cover and precipitation are measurable in observational studies. The main conclusions deduced from this study are the following.

i. The stepwise increase in complexity of the model simulations was essential for identifying temporal changes in catchment erosion and sediment thickness. A nonlinear response in erosion and sediment thickness to varying precipitation and vegetation cover was observed, and results were dependent on the initial vegetation and precipitation state of the catchment. The sources of nonlinearity stem from (a) a nonlinear relationship between precipitation changes required to cause a $\pm 10\,\%$ change in vegetation cover (Fig. 2) and (b) exponential and power-law relationships in the prescribed vegetation-dependent hillslope and fluvial, respectively, geomorphic transport laws (Fig. 3, see also the Appendix).

ii. Analysis of results for covarying precipitation and vegetation cover indicates that erosion and sedimentation in densely vegetated landscapes ($V = 70\,\%$) are more heavily influenced by changes in precipitation than changes in vegetation cover. This is due to the higher amplitude of precipitation change needed to cause variations in vegetation cover in densely vegetated settings (Figs. 5a and 7e).

iii. Analysis of results for covarying precipitation and vegetation cover indicates that erosion and sedimentation in sparsely vegetated landscapes ($V = 10\,\%$) are more sensitive to variable vegetation cover with constant precipitation rates (Figs. 6 and 7e), particularly when precipitation rates decrease and vegetation cover approaches $0\,\%$.

iv. Concerning the first hypotheses stated in the Introduction, we found that the effect of Milankovitch periodicity variations on the amplitude of change in sediment thickness and bedrock erosion is more pronounced for longer climate and vegetation oscillations (100 kyr) in both climate and vegetation settings. This finding confirms the hypothesis. Furthermore, periodicity effects on erosion and sediment thickness are larger in densely ($70\,\%$) vegetated landscapes than sparsely ($10\,\%$) vegetated landscapes, thereby indicating a sensitivity of the response to the biogeographic zone the changes are imposed on.

v. With respect to our second hypothesis, all transient forcings in precipitation and vegetation cover explored in this study resulted in variations in erosion and sediment thickness around the mean erosion rate, which is determined by the rock uplift rate. As rock uplift rates increased from 0.05 to $0.2\,\mathrm{mm\,a^{-1}}$, the effects of periodic changes in precipitation and vegetation cover on erosion rates became more pronounced and were between about $35\,\%$ and $110\,\%$, respectively, of the background rock uplift rate. This finding negates the hypothesis and suggests that regardless of the tectonic setting considered (within the range of rock uplift rates explored here) erosional transients from varying precipitation and vegetation cover occur, but the detection of these changes requires measurement of erosion rates integrating over short timescales such that the average (tectonically driven) mean erosion rate is not recovered.

vi. Finally, in comparison to previous studies, the $35\,\%$ to $110\,\%$ transient changes in erosion rate documented here are at, or above, the detection limit for measurement cosmogenic radionuclides in river sediments preserved in fluvial terraces, but they would be undetectable with bedrock thermochronometer dating techniques that average erosion rates over longer timescales. The potential to measure vegetation-related transient changes in erosion rates with cosmogenic nuclides is highest in settings with higher rock uplift rates (e.g., 0.1 and $0.2\,\mathrm{mm\,a^{-1}}$) and at longer (41 to 100 kyr) periodicities.

Appendix A: Effect of vegetation and precipitation on hillslope and fluvial erosion

The approach in our study follows the law of continuity of mass (e.g., Tucker et al., 2001). It states that the rate of change in topographic elevation (z) is defined as follows:

$$\frac{\partial z}{\partial t} = U - \frac{\partial z}{\partial t}(\text{fluvial}) + \frac{\partial z}{\partial t}(\text{hillslope}), \tag{A1}$$

where U is uplift rate [m yr^{-1}] and t is time [yr]. The second and third terms on the right-hand side refer to the rate change in topographic elevation due to fluvial and hillslope processes, respectively.

A1 Vegetation-dependent hillslope processes

The rate of change in topography due to hillslope diffusion (Fernandes and Dietrich, 1997; Martin, 2000) is defined as follows:

$$\frac{\partial z}{\partial t}(\text{hillslope}) = \nabla q_\text{s}, \tag{A2}$$

where q_s is sediment flux along the slope S. We applied the slope- and depth-dependent linear diffusion rule following the approach of Johnstone and Hilley (2014) such that

$$q_\text{s} = K_\text{d} S d_* \left(1 - e^{-\frac{H}{d_*}}\right), \tag{A3}$$

where K_d is the diffusion coefficient [m^2 yr^{-1}], d_* is sediment transport decay depth [m], and H denotes sediment thickness.

The diffusion coefficient is defined as a function of vegetation cover present on hillslopes, which is estimated following the approach of Istanbulluoglu and Bras (2005), Dunne et al. (2010), and Schmid et al. (2018) as follows:

$$K_\text{d} = K_\text{b} e^{-(\alpha V)}, \tag{A4}$$

where K_d is defined as a function of vegetation cover V, an exponential decay coefficient α, and linear diffusivity K_b for bare soil.

A2 Vegetation-dependent fluvial processes

The fluvial erosion is estimated for a two-layer topography (i.e., bedrock and sediment are treated explicitly) in the coupled detachment–transport-limited model, SPACE 1.0 (Shobe et al., 2017). Bedrock erosion and sediment entrainment are calculated simultaneously in the model. Total fluvial erosion is defined as

$$\frac{\partial z}{\partial t}(\text{fluvial}) = \frac{\partial R}{\partial t} + \frac{\partial H}{\partial t}, \tag{A5}$$

where the left-hand side denotes the total fluvial erosion rate. The first and second terms on the right-hand side denote the bedrock erosion rate and sediment entrainment rate, respectively.

The rate of change in the height of bedrock R per unit time [m yr^{-1}] is defined as

$$\frac{\partial R}{\partial t} = U - E_\text{r}, \tag{A6}$$

where E_r [m yr^{-1}] is the volumetric erosion flux of bedrock per unit bed area.

The change in sediment thickness H [m] per unit time [yr] was calculated following Davy and Lague (2009) and Shobe et al. (2017). It is defined as a fraction net deposition rate and solid fraction sediments, as follows:

$$\frac{\partial H}{\partial t} = \frac{D_\text{s} - E_\text{s}}{1 - \varnothing}, \tag{A7}$$

where D_s [m yr^{-1}] is the deposition flux of sediment, E_s [m yr^{-1}] is volumetric sediment entrainment flux per unit bed area, and φ is the sediment porosity.

Following the approach of Shobe et al. (2017), E_s and E_r are given by

$$E_\text{s} = \left(K_\text{s} q^m S^n - \omega_\text{cs}\right)\left(1 - e^{-\frac{H}{H_*}}\right), \tag{A8}$$

$$E_\text{r} = \left(K_\text{r} q^m S^n - \omega_\text{cr}\right) e^{-H/H_*}, \tag{A9}$$

where K_s [m^{-1}] and K_r [m^{-1}] are the sediment erodibility and bedrock erodibility parameters, respectively. The threshold stream power for sediment entrainment and bedrock erosion are denoted as ω_cs [m yr^{-1}] and ω_cr [m yr^{-1}] in the above equations. Bedrock roughness is denoted as H_* [m], and the term e^{-H/H_*} corresponds to the soil production from bedrock. With higher bedrock roughness magnitudes, more sediment would be produced.

K_s and K_r were modified in the model using the approach of Istanbulluoglu (2005) and Schmid et al. (2018) by introducing the effect of Manning's roughness to quantify the effect of vegetation cover on bed shear stress:

$$\tau_\text{v} = \rho_\text{w} g (n_\text{s} + n_\text{v})^{6/10} q^m S^n F_t, \tag{A10}$$

where ρ_w [kg m^{-3}] and g [m s^{-2}] are the density of water and acceleration due to gravity, respectively. Manning's numbers for bare soil and vegetated surface are denoted as n_s and n_v. F_t represents the shear stress partitioning ratio. Manning's number for vegetation cover and F_t are calculated as follows:

$$n_\text{v} = n_\text{vr}\left(\frac{V}{V_\text{r}}\right)^w, \tag{A11}$$

$$F_t = \left(\frac{n_\text{s}}{n_\text{s} + n_\text{v}}\right)^{\frac{3}{2}}, \tag{A12}$$

where n_vr is Manning's number for the reference vegetation. Here, V_r is reference vegetation cover ($V = 100\,\%$), V is local vegetation cover in a model cell, and w is an empirical scaling factor.

By combining the stream power equation (Tucker et al., 1999; Howard, 1994; Whipple and Tucker, 1999) and the above concept of the effect of vegetation on shear stress, we follow the approach of Schmid et al. (2018) to define new sediment and bedrock erodibility parameters influenced by the surface vegetation cover on fluvial erosion, as follows:

$$K_{\mathrm{vs}} = K_{\mathrm{s}} \rho_{\mathrm{w}} g (n_{\mathrm{s}} + n_{\mathrm{v}})^{6/10} F_t, \tag{A13}$$

$$K_{\mathrm{vr}} = K_{\mathrm{r}} \rho_{\mathrm{w}} g (n_{\mathrm{s}} + n_{\mathrm{v}})^{6/10} F_t, \tag{A14}$$

where K_{vs} [m^{-1}] and K_{vr} [m^{-1}] are modified sediment erodibility and bedrock erodibility, respectively. These are influenced by fractional vegetation cover V. Hence, K_{s} and K_{r} in Eqs. (A8) and (A9) are replaced by K_{vs} and K_{vr} to include an effect of vegetation cover on fluvial processes in the model. The trends of K_{d}, K_{vs}, and K_{vr} are illustrated in Fig. 3.

A3 Influence of coupled oscillations of precipitation and vegetation cover on erosion and sedimentation (scenario 3) without weathering function

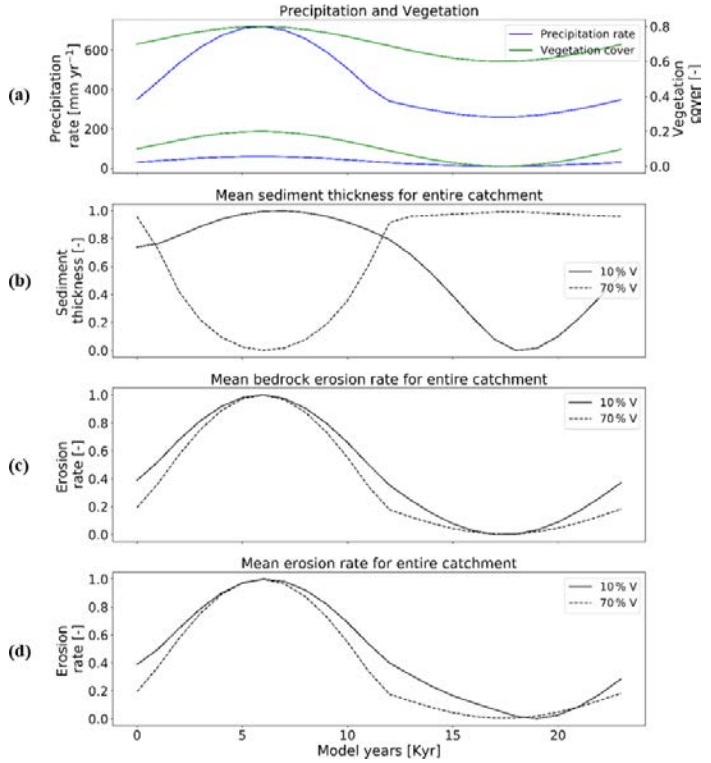

Figure A1. Temporal evolution of catchment-averaged predictions for scenario 3 (with no weathering) described in the text (Sect. 3.3). Graphical representation of normalized mean catchment sedimentation and erosion to **(a)** coupled oscillations in precipitation [mm yr^{-1}] and vegetation cover [–] in terms of **(b)** sediment thickness [–], **(c)** bedrock erosion [–], and **(d)** mean erosion rate [–] for the entire catchment. The periodicity of climate and vegetation oscillations is 23 kyr with a rock uplift rate of 0.5 mm yr^{-1}.

Table A1. Landscape evolution model input parameters used and corresponding units.

Model parameters	Values
Grid size	10 [km] × 10 [km], dx: 100 [m]
Model runtime (totalTime)	Steady state: 15 [Ma], transient state: 3 [Ma]
Rock uplift rates (U)	0.05, 0.1, 0.2 [mm a^{-1}]
Periodicities (sinePeriod)	23, 41, 100 [kyr] (Milankovitch cycles)
Initial sediment thickness (H_initial)	0 [m]
Bedrock erodibility (K_r)	2×10^{-9} [m^{-1}]
Sediment erodibility (K_s)	2×10^{-8} [m^{-1}]
Soil production decay depth (h^*)	0.5 [m]
Reach-scale bedrock roughness (H^*)	1 [m]
Porosity (φ)	0.2 [–]
Fraction of fine sediments (F_f)	0.2 [–]
Effective terminal settling velocity (V_s)	10 [m a^{-1}]
m, n	0.6, 1 [–]
Bedrock erosion threshold stream power (ω_cr)	5×10^{-4} [m a^{-1}]
Sed. entr. threshold stream power (ω_cs)	5×10^{-5} [m a^{-1}]
Maximum sediment production rate (W_o)	9.7×10^{-6} [m yr^{-1}] (10 % veg. cover, 1.3×10^{-4} [m yr^{-1}] (70 % veg. cover)
Mean annual precipitation (P)	0.03 [m yr^{-1}] (10 % veg. cover), 0.35 [m yr^{-1}] (70 % veg. cover)
Bare soil diffusivity (K_b)	0.01 [m^2 yr^{-1}]
Exponential decay coefficient (α)	0.3 [–]
Critical channel formation area (A_crit)	1×10^6 [m^2]
Reference vegetation cover (V_r)	1 (100 %)
Manning's number for bare soil (n_s)	0.01 [–]
Manning's number for ref. vegetation (n_v)	0.6 [–]
Scaling factor for vegetation influence (w)	1 [–]

Code and data availability. The code and data used in this study are freely available upon request.

Author contributions. HS and TAE designed the initial model setup and simulation programs. HS and TAE conducted model modifications, simulation runs, and analysis. MS provided assistance in program modification. KT provided insight into plant ecology in Chilean study areas and vegetation–climate change relationships. HS and TAE prepared the paper with contributions from CG, KT, and MS.

Competing interests. The authors declare that they have no conflict of interest.

Disclaimer. Publisher's note: Copernicus Publications remains neutral with regard to jurisdictional claims in published maps and institutional affiliations.

Acknowledgements. Hemanti Sharma and Todd A. Ehlers acknowledge support from the Open Access Publishing Fund of the University of Tübingen. We also acknowledge support from the Research Training Group 1829 Integrated Hydrosystem Modelling, funded by the German Research Foundation (DFG). In addition, Todd A. Ehlers, Katja Tielbörger, and Manuel Schmid acknowledge support from the German priority research program (SPP-1803; grants EH329/14-1 and EH329/14-2 to Todd A. Ehlers; TI 338/14-1 and TI338/14-2 to Katja Tielbörger). We thank Erkan Istanbulluoglu and Omer Yetemen for their constructive reviews.

Financial support. This research has been supported by the Deutsche Forschungsgemeinschaft (Research Training Group 1829 Integrated Hydrosystem Modelling, grant nos. SPP-1803, EH329/14-1, EH329/14-2, TI 338/14-1, and TI338/14-2).

This open-access publication was funded
by the University of Tübingen.

Review statement. This paper was edited by Greg Hancock and reviewed by Erkan Istanbulluoglu and Omer Yetemen.

References

Acosta, V. T., Schildgen, T. F., Clarke, B. A., Scherler, D., Bookhagen, B., Wittmann, H., von Blanckenburg, F., and Strecker, M. R.: Effect of vegetation cover on millennial-scale landscape denudation rates in East Africa, Lithosphere, 7, 408–420, https://doi.org/10.1130/l402.1, 2015.

Ahnert, F.: Some comments on the quantitative formulation of geomorphological processes in a theoretical model, Earth Surf. Process., 2, 191–201, https://doi.org/10.1002/esp.3290020211, 1977.

Alonso, R. N., Bookhagen, B., Carrapa, B., Coutand, I., Haschke, M., Hilley, G. E., Schoenbohm, L., Sobel, E. R., Strecker, M. R., Trauth, M. H., and Villanueva, A.: Tectonics, Climate, and Landscape Evolution of the Southern Central Andes: the Argentine Puna Plateau and Adjacent Regions between 22 and 30° S, in: The Andes: Active Subduction Orogeny, edited by: Oncken, O., Chong, G., Franz, G., Giese, P., Götze, H.-J., Ramos, V. A., Strecker, M. R., and Wigger, P., Springer, Berlin, Heidelberg, 265–283, 2006.

Amundson, R., Heimsath, A., Owen, J., Yoo, K., and Dietrich, W. E.: Hillslope soils and vegetation, Geomorphology, 234, 122–132, https://doi.org/10.1016/j.geomorph.2014.12.031, 2015.

Ashkenazy, Y., Eisenman, I., Gildor, H., and Tziperman, E.: The Effect of Milankovitch Variations in Insolation on Equatorial Seasonality, J. Climate, 23, 6133–6142, https://doi.org/10.1175/2010JCLI3700.1, 2010.

Avdievitch, N. N., Ehlers, T. A., and Glotzbach, C.: Slow Long-Term Exhumation of the West Central Andean Plate Boundary, Chile, Tectonics, 37, 2243–2267, https://doi.org/10.1029/2017TC004944, 2018.

Bellard, C., Bertelsmeier, C., Leadley, P., Thuiller, W., and Courchamp, F.: Impacts of climate change on the future of biodiversity, Ecol. Lett., 15, 365–377, https://doi.org/10.1111/j.1461-0248.2011.01736.x, 2012.

Bonnet, S. and Crave, A.: Landscape response to climate change: Insights from experimental modeling and implications for tectonic versus climatic uplift of topography, Geology, 31, 123–126, https://doi.org/10.1130/0091-7613(2003)031<0123:Lrtcci>2.0.Co;2, 2003.

Braun, J., Voisin, C., Gourlan, A. T., and Chauvel, C.: Erosional response of an actively uplifting mountain belt to cyclic rainfall variations, Earth Surf. Dynam., 3, 1–14, https://doi.org/10.5194/esurf-3-1-2015, 2015.

Breckle, S.-W.: Walter's Vegetation of the Earth, XX, 4th Edn., Springer-Verlag, Berlin, Heidelberg, 527 pp., 2002.

Collins, D. B. G., Bras, R. L., and Tucker, G. E.: Modeling the effects of vegetation-erosion coupling on landscape evolution, J. Geophys. Res., 109, F03004, https://doi.org/10.1029/2003jf000028, 2004.

Davy, P. and Lague, D.: Fluvial erosion/transport equation of landscape evolution models revisited, J. Geophys. Res., 114, F03007, https://doi.org/10.1029/2008jf001146, 2009.

Dixon, J. L., Heimsath, A. M., and Amundson, R.: The critical role of climate and saprolite weathering in landscape evolution, Earth Surf. Proc. Land., 34, 1507–1521, https://doi.org/10.1002/esp.1836, 2009.

Dosseto, A., Hesse, P. P., Maher, K., Fryirs, K., and Turner, S.: Climatic and vegetation control on sediment dynamics during the last glacial cycle, Geology, 38, 395–398, https://doi.org/10.1130/g30708.1, 2010.

Dunne, T., Malmon, D. V., and Mudd, S. M.: A rain splash transport equation assimilating field and laboratory measurements, J. Geophys. Res., 115, F01001, https://doi.org/10.1029/2009jf001302, 2010.

Fernandes, N. F. and Dietrich, W. E.: Hillslope evolution by diffusive processes: The timescale for equilibrium adjustments, Water Resour. Res., 33, 1307–1318, https://doi.org/10.1029/97wr00534, 1997.

Gerten, D., Luo, Y., Le Maire, G., Parton, W. J., Keough, C., Weng, E., Beier, C., Ciais, P., Cramer, W., Dukes, J. S., Hanson, P. J., Knapp, A. A. K., Linder, S., Nepstad, D., Rustad, L., and Sowerby, A.: Modelled effects of precipitation on ecosystem carbon and water dynamics in different climatic zones, Global Change Biol., 14, 2365–2379, https://doi.org/10.1111/j.1365-2486.2008.01651.x, 2008.

Gilbert, G. K.: Report on the geology of the Henry Mountains, US Government Printing Office, Washington, DC, https://doi.org/10.3133/70039916, 1877.

Hancock, G. S. and Anderson, R. S.: Numerical modeling of fluvial strath-terrace formation in response to oscillating climate, GSA Bull., 114, 1131–1142, https://doi.org/10.1130/0016-7606(2002)114<1131:NMOFST>2.0.CO;2, 2002.

Heimsath, A. M., Dietrich, W. E., Nishiizumi, K., and Finkel, R. C.: The soil production function and landscape equilibrium, Nature, 388, 358–361, https://doi.org/10.1038/41056, 1997.

Herman, F., Rhodes, E. J., Braun, J., and Heiniger, L.: Uniform erosion rates and relief amplitude during glacial cycles in the Southern Alps of New Zealand, as revealed from OSL-thermochronology, Earth Planet. Sc. Lett., 297, 183–189, https://doi.org/10.1016/j.epsl.2010.06.019, 2010.

Hobley, D. E. J., Adams, J. M., Nudurupati, S. S., Hutton, E. W. H., Gasparini, N. M., Istanbulluoglu, E., and Tucker, G. E.: Creative computing with Landlab: an open-source toolkit for building, coupling, and exploring two-dimensional numerical models of Earth-surface dynamics, Earth Surf. Dynam., 5, 21–46, https://doi.org/10.5194/esurf-5-21-2017, 2017.

Howard, A. D.: A detachment-limited model of drainage basin evolution, Water Resour. Res., 30, 2261–2285, https://doi.org/10.1029/94WR00757, 1994.

Huntley, B., Allen, J. R., Collingham, Y. C., Hickler, T., Lister, A. M., Singarayer, J., Stuart, A. J., Sykes, M. T., and Valdes, P. J.: Millennial climatic fluctuations are key to the structure of last glacial ecosystems, PLoS One, 8, e61963, https://doi.org/10.1371/journal.pone.0061963, 2013.

Huxman, T. E., Smith, M. D., Fay, P. A., Knapp, A. K., Shaw, M. R., Loik, M. E., Smith, S. D., Tissue, D. T., Zak, J. C., Weltzin, J. F., Pockman, W. T., Sala, O. E., Haddad, B. M., Harte, J., Koch, G. W., Schwinning, S., Small, E. E., and Williams, D. G.: Convergence across biomes to a common rain-use efficiency, Nature, 429, 651–654, https://doi.org/10.1038/nature02561, 2004.

Hyun, S., Ahagon, N., and Yoon, H.-I.: Milankovitch cycles and paleoceanographic evolution within sediments from ODP Sites 980 and 983 of the North Atlantic Ocean, Geosci. J., 9, 235–242, https://doi.org/10.1007/BF02910583, 2005.

Istanbulluoglu, E. and Bras, R. L.: Vegetation-modulated landscape evolution: Effects of vegetation on landscape processes, drainage density, and topography, J. Geophys. Res., 110, F02012, https://doi.org/10.1029/2004jf000249, 2005.

Istanbulluoglu, E. and Bras, R. L.: On the dynamics of soil moisture, vegetation, and erosion: Implications of climate variability and change, Water Resour. Res., 42, W06418, https://doi.org/10.1029/2005wr004113, 2006.

Jeffery, M. L., Yanites, B. J., Poulsen, C. J., and Ehlers, T. A.: Vegetation-precipitation controls on Central Andean topography, J. Geophys. Res.-Earth, 119, 1354–1375, https://doi.org/10.1002/2013jf002919, 2014.

Johnstone, S. A. and Hilley, G. E.: Lithologic control on the form of soil-mantled hillslopes, Geology, 43, 83–86, https://doi.org/10.1130/g36052.1, 2014.

Kelly, A. E. and Goulden, M. L.: Rapid shifts in plant distribution with recent climate change, P. Natl. Acad. Sci. USA, 105, 11823, https://doi.org/10.1073/pnas.0802891105, 2008.

Kirby, E. and Whipple, K. X.: Expression of active tectonics in erosional landscapes, J. Struct. Geol., 44, 54–75, https://doi.org/10.1016/j.jsg.2012.07.009, 2012.

Knapp, A. K., Ciais, P., and Smith, M. D.: Reconciling inconsistencies in precipitation–productivity relationships: implications for climate change, New Phytol., 214, 41–47, https://doi.org/10.1111/nph.14381, 2017.

Kojima, S., Soto, I., Quiroz, M., Valencia, P., and Fernandez, I.: Geological and Geochemical Characteristics of the Intrusion-Related Vein-Type Gold Deposits in the El Morado District, Coastal Cordillera, Northern Chile, Resour. Geol., 67, 197–206, https://doi.org/10.1111/rge.12129, 2017.

Lague, D., Crave, A., and Davy, P.: Laboratory experiments simulating the geomorphic response to tectonic uplift, J. Geophys. Res.-Solid, 108, ETG 3-1–ETG 3-20, https://doi.org/10.1029/2002jb001785, 2003.

Martin, Y.: Modelling hillslope evolution: linear and nonlinear transport relations, Geomorphology, 34, 1–21, https://doi.org/10.1016/S0169-555X(99)00127-0, 2000.

McPhillips, D., Bierman, P. R., Crocker, T., and Rood, D. H.: Landscape response to Pleistocene-Holocene precipitation change in the Western Cordillera, Peru: ^{10}Be concentrations in modern sediments and terrace fills, J. Geophys. Res.-Earth, 118, 2488–2499, https://doi.org/10.1002/2013jf002837, 2013.

Melnick, D.: Rise of the central Andean coast by earthquakes straddling the Moho, Nat. Geosci., 9, 401–407, https://doi.org/10.1038/ngeo2683, 2016.

Miller, S. R., Sak, P. B., Kirby, E., and Bierman, P. R.: Neogene rejuvenation of central Appalachian topography: Evidence for differential rock uplift from stream profiles and erosion rates, Earth Planet. Sc. Lett., 369–370, 1–12, https://doi.org/10.1016/j.epsl.2013.04.007, 2013.

Mishra, A. K., Placzek, C., and Jones, R.: Coupled influence of precipitation and vegetation on millennial-scale erosion rates derived from ^{10}Be, PLoS One, 14, e0211325, https://doi.org/10.1371/journal.pone.0211325, 2019.

Mowll, W., Blumenthal, D. M., Cherwin, K., Smith, A., Symstad, A. J., Vermeire, L. T., Collins, S. L., Smith, M. D., and Knapp, A. K.: Climatic controls of aboveground net primary production in semi-arid grasslands along a latitudinal gradient portend low sensitivity to warming, Oecologia, 177, 959–969, https://doi.org/10.1007/s00442-015-3232-7, 2015.

Oeser, R. A., Stroncik, N., Moskwa, L.-M., Bernhard, N., Schaller, M., Canessa, R., van den Brink, L., Köster, M., Brucker, E., Stock, S., Fuentes, J. P., Godoy, R., Matus, F. J., Oses Pedraza, R., Osses McIntyre, P., Paulino, L., Seguel, O., Bader, M. Y., Boy, J., Dippold, M. A., Ehlers, T. A., Kühn, P., Kuzyakov, Y., Leinweber, P., Scholten, T., Spielvogel, S., Spohn, M., Übernickel, K., Tielbörger, K., Wagner, D., and von Blanckenburg, F.: Chemistry and microbiology of the Critical Zone along a steep climate and vegetation gradient in the Chilean Coastal Cordillera, Catena, 170, 183–203, https://doi.org/10.1016/j.catena.2018.06.002, 2018.

Owen, J. J., Amundson, R., Dietrich, W. E., Nishiizumi, K., Sutter, B., and Chong, G.: The sensitivity of hillslope bedrock erosion to precipitation, Earth Surf. Proc. Land., 36, 117–135, https://doi.org/10.1002/esp.2083, 2011.

Pelletier, J. D.: Fluvial and slope-wash erosion of soil-mantled landscapes: detachment- or transport-limited?, Earth Surf. Proc. Land., 37, 37–51, https://doi.org/10.1002/esp.2187, 2012.

Perron, J. T.: Climate and the Pace of Erosional Landscape Evolution, Annu. Rev. Earth Planet. Sci., 45, 561–591, https://doi.org/10.1146/annurev-earth-060614-105405, 2017.

Rossel, K., Aguilar, G., Salazar, E., Martinod, J., Carretier, S., Pinto, L., and Cabré, A.: Chronology of Chilean Frontal Cordillera building from geochronological, stratigraphic and geomorphological data insights from Miocene intramontane-basin deposits, Basin Res., 30, 289–310, https://doi.org/10.1111/bre.12221, 2018.

Routschek, A., Schmidt, J., and Kreienkamp, F.: Impact of climate change on soil erosion – A high-resolution projection on catchment scale until 2100 in Saxony/Germany, Catena, 121, 99–109, https://doi.org/10.1016/j.catena.2014.04.019, 2014.

Sala, O. E., Parton, W. J., Joyce, L. A., and Lauenroth, W. K.: Primary Production of the Central Grassland Region of the United States, Ecology, 69, 40–45, https://doi.org/10.2307/1943158, 1988.

Schaller, M. and Ehlers, T. A.: Limits to quantifying climate driven changes in denudation rates with cosmogenic radionuclides, Earth Planet. Sc. Lett., 248, 153–167, https://doi.org/10.1016/j.epsl.2006.05.027, 2006.

Schaller, M., Blanckenburg, F. von, Hovius, N., Veldkamp, A., van den Berg, M. W., and Kubik, P. W.: Paleoerosion Rates from Cosmogenic ^{10}Be in a 1.3 Ma Terrace Sequence: Response of the River Meuse to Changes in Climate and Rock Uplift, J. Geol., 112, 127–144, https://doi.org/10.1086/381654, 2004.

Schaller, M., Ehlers, T. A., Lang, K. A. H., Schmid, M., and Fuentes-Espoz, J. P.: Addressing the contribution of climate and vegetation cover on hillslope denudation, Chilean Coastal Cordillera (26°–38° S), Earth Planet. Sc. Lett., 489, 111–122, https://doi.org/10.1016/j.epsl.2018.02.026, 2018.

Schaller, M., Dal Bo, I., Ehlers, T. A., Klotzsche, A., Drews, R., Fuentes Espoz, J. P., and van der Kruk, J.: Comparison of regolith physical and chemical characteristics with geophysical data along a climate and ecological gradient, Chilean Coastal Cordillera (26 to 38° S), Soil, 6, 629–647, https://doi.org/10.5194/soil-6-629-2020, 2020.

Schmid, M., Ehlers, T. A., Werner, C., Hickler, T., and Fuentes-Espoz, J.-P.: Effect of changing vegetation and precipitation on denudation – Part 2: Predicted landscape response to transient climate and vegetation cover over millennial to million-year timescales, Earth Syst. Dynam., 6, 859–881, https://doi.org/10.5194/esurf-6-859-2018, 2018.

Seybold, H., Rothman, D. H., and Kirchner, J. W.: Climate's watermark in the geometry of stream networks, Geophys. Res. Lett., 44, 2272–2280, https://doi.org/10.1002/2016gl072089, 2017.

Shobe, C. M., Tucker, G. E., and Barnhart, K. R.: The SPACE 1.0 model: a Landlab component for 2-D calculation of sediment transport, bedrock erosion, and landscape evolution, Geosci. Model Dev., 10, 4577–4604, https://doi.org/10.5194/gmd-10-4577-2017, 2017.

Slater, L. J. and Singer, M. B.: Imprint of climate and climate change in alluvial riverbeds: Continental United States, 1950–2011, Geology, 41, 595–598, https://doi.org/10.1130/g34070.1, 2013.

Smith, B., Wårlind, D., Arneth, A., Hickler, T., Leadley, P., Siltberg, J., and Zaehle, S.: Implications of incorporating N cycling and N limitations on primary production in an individual-based dynamic vegetation model, Biogeosciences, 11, 2027–2054, https://doi.org/10.5194/bg-11-2027-2014, 2014.

Smith, M. D., Wilcox, K. R., Power, S. A., Tissue, D. T., and Knapp, A. K.: Assessing community and ecosystem sensitivity to climate change – toward a more comparative approach, J. Veg. Sci., 28, 235–237, https://doi.org/10.1111/jvs.12524, 2017.

Starke, J., Ehlers, T. A., and Schaller, M.: Latitudinal effect of vegetation on erosion rates identified along western South America, Science, 367, 1358, https://doi.org/10.1126/science.aaz0840, 2020.

Tucker, G. E.: Drainage basin sensitivity to tectonic and climatic forcing: implications of a stochastic model for the role of entrainment and erosion thresholds, Earth Surf. Proc. Land., 29, 185–205, https://doi.org/10.1002/esp.1020, 2004.

Tucker, G. E., Lancaster, S. T., Gasparini, N. M., and Bras, R. L.: Modeling floodplain dynamics and stratigraphy: implications for geoarchaeology, Final Technical Report (Part II-C), Contract Number DACA88-95-C-0017, USACERL – US Army Corps of Engineers Construction Engineering Research Laboratory, 16 pp., 1999.

Tucker, G. E., Lancaster, S. T., Gasparini, N. M., Bras, R. L., and Rybarczyk, S. M.: An object-oriented framework for distributed hydrologic and geomorphic modeling using triangulated irregular networks, Comput. Geosci., 27, 959–973, https://doi.org/10.1016/S0098-3004(00)00134-5, 2001.

Turowski, J. M., Lague, D., Crave, A., and Hovius, N.: Experimental channel response to tectonic uplift, J. Geophys. Res.-Earth, 111, F03008, https://doi.org/10.1029/2005jf000306, 2006.

van Dongen, R., Scherler, D., Wittmann, H., and von Blanckenburg, F.: Cosmogenic ^{10}Be in river sediment: where grain size matters and why, Earth Surf. Dynam., 7, 393–410, https://doi.org/10.5194/esurf-7-393-2019, 2019.

Werner, C., Schmid, M., Ehlers, T. A., Fuentes-Espoz, J. P., Steinkamp, J., Forrest, M., Liakka, J., Maldonado, A., and Hickler, T.: Effect of changing vegetation and precipitation on denudation – Part 1: Predicted vegetation composition and cover over the last 21 thousand years along the Coastal Cordillera of Chile, Earth Surf. Dynam., 6, 829–858, https://doi.org/10.5194/esurf-6-829-2018, 2018.

Whipple, K. X.: The influence of climate on the tectonic evolution of mountain belts, Nat. Geosci., 2, 730–730, https://doi.org/10.1038/ngeo638, 2009.

Whipple, K. X. and Tucker, G. E.: Dynamics of the stream-power river incision model: Implications for height limits of mountain ranges, landscape response timescales, and research needs, J. Geophys. Res.-Solid, 104, 17661–17674, https://doi.org/10.1029/1999jb900120, 1999.

Willgoose, G., Bras, R. L., and Rodriguez-Iturbe, I.: A coupled channel network growth and hillslope evolution model: 1. Theory, Water Resour. Res., 27, 1671–1684, https://doi.org/10.1029/91WR00935, 1991.

Xia, J., Chen, J., Piao, S., Ciais, P., Luo, Y., and Wan, S.: Terrestrial carbon cycle affected by non-uniform climate warming, Nat. Geosci., 7, 173–180, https://doi.org/10.1038/ngeo2093, 2014.

Yang, Y., Fang, J., ma, W., and Wang, W.: Relationship between variability in aboveground net primary production and precipitation in global grasslands. Geophys. Res. Lett., 35, L23710, https://doi.org/10.1029/2008GL035408, 2008.

Yanites, B. J. and Ehlers, T. A.: Global climate and tectonic controls on the denudation of glaciated mountains, Earth Planet. Sc. Lett., 325–326, 63–75, https://doi.org/10.1016/j.epsl.2012.01.030, 2012.

Yetemen, O., Istanbulluoglu, E., and Duvall, A. R.: Solar radiation as a global driver of hillslope asymmetry: Insights from an ecogeomorphic landscape evolution model, Water Resour. Res., 51, 9843–9861, https://doi.org/10.1002/2015WR017103, 2015.

Yetemen, O., Saco, P. M., and Istanbulluoglu, E.: Ecohydrology Controls the Geomorphic Response to Climate Change, Geophys. Res. Lett., 46, 8852–8861, https://doi.org/10.1029/2019GL083874, 2019.

Zhang, Y., Xiao, X., Guanter, L., Zhou, S., Ciais, P., Joiner, J., Sitch, S., Wu, X., Nabel, J., Dong, J., Kato, E., Jain, A. K., Wiltshire, A., and Stocker, B. D.: Precipitation and carbon-water coupling jointly control the interannual variability of global land gross primary production, Scient. Rep., 6, 39748, https://doi.org/10.1038/srep39748, 2016.

3.2 Effects of seasonal variations in vegetation and precipitation on catchment-scale erosion rates in Chilean Coastal Cordillera

3.2.1 Declarations of contribution of all co-authors in the manuscript

This section of the dissertation comprises the manuscript in late stage of preparation for a potential publication. The title of the manuscript is designed as *"Effects of seasonal variations in vegetation and precipitation on catchment-scale erosion rates along a climate and ecological gradient (Chile): Insights from numerical modelling"*.

The manuscript was prepared and contributed by two authors, namely Hemanti Sharma (HS), and Todd A. Ehlers (TAE). Hemanti Sharma and Todd Ehlers jointly developed the research idea. The model input data was procured and processed by Hemanti Sharma followed by model modifications and simulation runs. The manuscript was written by Hemanti Sharma with the help of Todd Ehlers.

The detailed contributions of each author for the above publication are presented in Table 2.

Table 2. Contribution of authors (in percentage) in the manuscript with the title *"Effects of seasonal variations in vegetation and precipitation on catchment-scale erosion rates along a climate and ecological gradient (Chile): Insights from numerical modelling"*.

Author	Author position	Scientific ideas [%]	Data generation [%]	Analysis & interpretation [%]	Paper writing [%]
HS	1	70	90	60	70
TAE	2	30	10	40	30

3.2.2 Manuscript Draft: Effects of seasonal variations in vegetation and precipitation on catchment-scale erosion rates along a climate and ecological gradient (Chile): Insights from numerical modelling

Effects of seasonal variations in vegetation and precipitation on catchment-scale erosion rates along a climate and ecological gradient (Chile): Insights from numerical modelling.

Hemanti Sharma[1], Todd A. Ehlers[1]

[1]Department of Geosciences, University of Tübingen, 72076, Tübingen, Germany

Abstract

Precipitation in wet seasons influences catchment erosion and significantly contributes to annual erosion rates. However, wet seasons are also associated with increased vegetation cover, which helps resist erosion. This study investigates the effect of present-day seasonal variations in rainfall and spatially variable vegetation cover on erosion rates for four catchments along with the extreme climate and ecological gradient (from arid to temperate) in the Chilean Coastal Cordillera (~26 °S – ~38 °S). We do this using the Landlab-SPACE landscape evolution model modified to account for vegetation-dependent hillslope-fluvial processes and hillslope hydrology. Model inputs include SRTM DEM (90m) for initial catchment conditions; MODIS NDVI for vegetation seasonality; weather station observations of precipitation (between 2000 – 2019); and evapotranspiration obtained from GLDAS NOAH. Simulations were conducted with a step-wise increase in complexity to quantify the sensitivity of catchment scale erosion rates to seasonal variations in precipitation and vegetation cover. The simulations were conducted for 1,000 years (20 years of vegetation and precipitation observations repeated 50 times). After detrending the results for long-term transient changes, the last 20 years were analyzed. Results indicate that when vegetation cover is varied but precipitation is held constant, the amplitude of change in erosion rates ranges between 6.5% (humid-temperate) to 36% (Mediterranean setting). In contrast, in simulations with variable precipitation change and constant vegetation cover, the amplitude of change in erosion rates is higher and ranges between 13% (arid) to 91% (Mediterranean setting). Finally, simulations with coupled precipitation and vegetation cover variations demonstrate variations in catchment erosion of 13% (arid) to 97% (Mediterranean setting). Taken together, we find that precipitation variations more strongly influence seasonal variations in erosion rates. However, the effects of seasonal variations in vegetation on erosion are also significant (between 5-36%). Finally, seasonal variations in vegetation are most pronounced in semi-arid to Mediterranean settings and least prevalent in arid and humid-temperature settings.

Keywords: Landlab, SPACE, Chilean Coastal Cordillera, vegetation cover, seasonality in precipitation

1 Introduction

Catchment scale erosion rates vary spatially and temporally (Wang et al., 2021) and depend on topography (slope), vegetation cover, type (Zhang et al., 2011, 2014; Starke et al., 2020), and precipitation rates (Cerdà, 1998). Over annual timescales, temporal variations in catchment erosion occur in response to seasonal precipitation and vegetation cover variations. For example, previous work has found that a significant fraction of annual erosion occurs during wet seasons with high runoff rates (e.g., Hancock and Lowry, 2021; Leyland et al., 2016; Gao et al., 2021; Wulf et al., 2010). However, this increase in precipitation during wet seasons also promotes vegetation growth, which in turn retards the erosion rates (e.g., Langbein and Schumm, 1958; Zheng, 2006; Schmid et al., 2018). Seasonality in both precipitation and vegetation cover plays a crucial role in intra-annual changes in erosion rates (Istanbulluoglu and Bras, 2006; Yetemen et al., 2015). The intensity, frequency, and seasonality of precipitation and vegetation cover change depend on the climate and ecological conditions of the area of interest (Herrmann and Mohr, 2011). One means of investigating the effects of seasonality in precipitation and (or) vegetation cover on erosion rates is through landscape evolution modeling (LEM), which can be parameterized for variations in vegetation-dependent hillslope and fluvial processes over seasonal time scales.

Previous modeling and observational studies have investigated the effects of seasonality in precipitation and vegetation on catchment erosion. For example, Bookhagen et al. (2005), Wulf et al. (2010), and Deal et al. (2017) investigated the effects of stochastic variations in precipitation on erosion and sediment transport in the Himalayas. They found that high variability in rainstorm days (>80% of MAP) during the wet season (summer monsoon) caused high variability in suspended sediment load. Work by Chakrapani (2005) documents the control of mean local relief and seasonality in precipitation on sediment load in rivers. Similar seasonality in sediment loads was reported in a field study in Iran, using sediment traps and erosion pins. These authors concluded that wet seasons have maximum erosion rates (>70% of annual), which decreases in the dry season (<10% of annual) (Mosaffaie et al., 2015). Field observations in the heavily vegetated Columbian Andes concluded that soil erosion and nutrient losses are significantly influenced by precipitation seasonality (Suescún et al., 2017). In contrast, work by Steegen et al. (2000) in a loamy agricultural catchment in central Belgium found that suspended sediment concentrations in the streams were lower during summer (wet) than winters (dry) due to the development in vegetation cover in the wet season. Other workers have found a dependence of seasonal erosion on ecosystem type. For example, Istanbulluoglu et al. (2006) found a reduction in soil loss potential to storm frequency in humid ecosystems compared to arid and semi-arid regions. Work by Wei et al. (2015) documented that differences in vegetation cover may contribute to long-term erosion and sedimentation. However, seasonal variations in runoff and sediment yield are mainly contributed by intra-annual rainfall variations. Previous work in a Mediterranean environment, e.g., Gabarrón-Galeote

et al. (2013) described rainfall intensity as the main factor in determining hydrological erosive response, regardless of the rainfall depth of an event.

When looking at seasonal vegetation changes in more detail, several different studies suggest these changes are important for catchment erosion. For example, Garatuza-Payán et al. (2005) emphasized that seasonal patterns in erosion are strongly influenced by plant phenology demonstrated by the changes in vegetation cover (as measured by NDVI). A similar study on the Loess Plateau, China, by Zheng (2006) documented decreasing soil erosion as vegetation cover increases during the wet season. Work conducted in a forested setting (Zhang et al., 2014) documents the importance of tree cover as an effective filter for decreasing the effects of rainfall intensity on soil structure, runoff, and sediment yield. Numerical modeling studies have also found a significant impact of vegetation on erosion. For example, Zhang et al. (2019) found that when precipitation is kept constant, the effect of vegetation cover change on sediment yields is significant (20-30% of total flux). Also, during the early to the mid-wet season, the richness and evenness of plant cover play an essential role in reducing erosion rates during low rainfall events (Hou et al., 2020). However, in the case of high-intensity rainfall events at the start of a wet season, when vegetation cover is low, the duration and intensity of rainfall were found to significantly affect erosion rates (Hancock and Lowry, 2015). Other work conducted in a Mediterranean environment points to the coincidence of peak rainfall erosivity in low vegetation cover settings, leading to an increased risk of soil erosion (Ferreira and Panagopoulos, 2014). Despite potentially conflicting results in the previous studies, what is clear is that seasonality in precipitation and vegetation covers are associated with variations in catchment erosion. However, which factor (precipitation or vegetation) plays the dominant role is unclear.

This study complements the previous work by applying a Landscape Evolution Model (LEM) to investigate seasonal transients in catchment erosion due to variations in precipitation and vegetation. We do this for four locations in the extreme climate and ecological gradient (i.e., arid, semi-arid, Mediterranean, and humid temperate) of the Chilean Coastal Cordillera. Our efforts are focused on testing two hypotheses: (1) if precipitation is the first-order driver of seasonal erosion rates, then the influence of seasonal changes in vegetation cover would be of low significance, and (2) catchment erosion in arid and semi-arid regions is more sensitive to seasonality in precipitation and vegetation than the Mediterranean and humid temperate regions. To test the above hypotheses, we conduct a sensitivity analysis of fluvial and hillslope erosion over four Chilean study areas to investigate the individual effects of seasonal changes in vegetation cover and precipitation compared to simulations with coupled variations in precipitation and vegetation cover. We do this using a two-dimensional LEM (the Landlab-SPACE software), which explicitly handles bedrock and sediment entrainment and deposition. We build upon the approach of Sharma et al. (2021) with the additional consideration of soil-water infiltration. The input parameters include SRTM DEMs (90 m) of four regions in different climate/ecological

settings (Fig. 1) as initial topographies; MODIS NDVI (between 2000 – 2019) as a proxy of vegetation cover; and weather station observations of precipitation (between 2000 – 2019).

2 Study Areas

This section summarizes the geologic, climate, and vegetation settings of the four selected catchments (Fig. 1) investigated in the Chilean Coastal Cordillera. These catchments are located in the Pan de Azúcar National Park (arid, ~26°S), Santa Gracia nature preserve (semi-arid, ~30°S), and the La Campana (mediterranean, ~33°S) and Nahuelbuta (temperate-humid, ~38°S) national parks. Together, these study areas span ~1,300 km of the Coastal Cordillera. These study areas are chosen for their steep climate and ecological gradient from North (arid environment with small shrubs) to South (humid temperate environment with evergreen mixed forests) (Schaller et al., 2020). The study areas are part of the German-Chilean priority research program EarthShape (www.earthshape.net) and ongoing research efforts within these catchments.

The bedrock of the four study areas is composed of granitoid rocks, including granites, granodiorites, and tonalites in Pan de Azúcar, La Campana, and Nahuelbuta, respectively, and gabbro and diorites in Santa Gracia (Oeser et al., 2018). The soil types in each catchment based on grain size distribution are defined as a sandy loam in three northern catchments (with high bulk density: 1300 – 1500 kg m^{-3}) and sandy clay loam in Nahuelbuta (with lower bulk density: 800 kg m^{-3}) (Bernhard et al., 2018). The western margin of Chile along the latitudes of the different study areas is characterized by a similar tectonic setting whereby an oceanic plate (currently the Nazca plate) has been subducting under the South American plate since the Palaeozoic. Despite this common tectonic setting along, slight differences in modern rock uplift rates are documented in the regions surrounding the three northern catchments (i.e., < 0.1 mm yr^{-1} for ~ 26 °S to ~33 °S) (Melnick, 2016) and the southern catchment (i.e., 0.04 to > 0.2 mm yr^{-1} for ~38 °S over the last 4±1.2 Ma) (Glodny et al., 2008; Melnick et al., 2009). Over geologic (millennial) timescales, measured denudation rates in the region range between ~0.005 to ~0.6 mm yr^{-1} (Schaller et al., 2018). To facilitate a comparison between the study areas and focus on erosion variations from seasonal changes in precipitation and vegetation, we assume a uniform rock uplift rate of 0.05 mm yr^{-1} for this study. This rate is broadly consistent with the range of previously reported values.

The climate gradient in the study areas ranges from an arid climate in Pan de Azúcar (north) with mean annual precipitation (MAP) of ~11 mm yr^{-1} to semi-arid in Santa Gracia (MAP: ~ 88 mm yr^{-1}), the Mediterranean in La Campana (MAP: ~350 mm yr^{-1}), and a temperate-humid climate in Nahuelbuta (south) with a MAP of 1400 mm yr^{-1} (Ziese et al., 2020). The observed mean annual temperatures (MAT) also vary with latitude ranging from ~20°C in the north to ~5°C in the south (Übernickel et al.,

2020). The previous gradients in MAP and MAT and latitudinal variations in solar radiation result in a southward increase in vegetation density (Bernhard et al., 2018). The vegetation gradient evident from mean MODIS Normalized Difference Vegetation Index (NDVI) values range from ~0.1 in Pan de Azúcar (north) to ~0.8 in Nahuelbuta (south) (Didan, Kamel, 2015). In this study, NDVI values are used as a proxy of vegetation cover density, similar to the approach of Schmid et al. (2018).

This gradient in climate and vegetation cover from north to south in the Chilean Coastal Cordillera provides an opportunity to study the effects of seasonal variations in vegetation cover and precipitation on catchment-scale erosion rates in different environments.

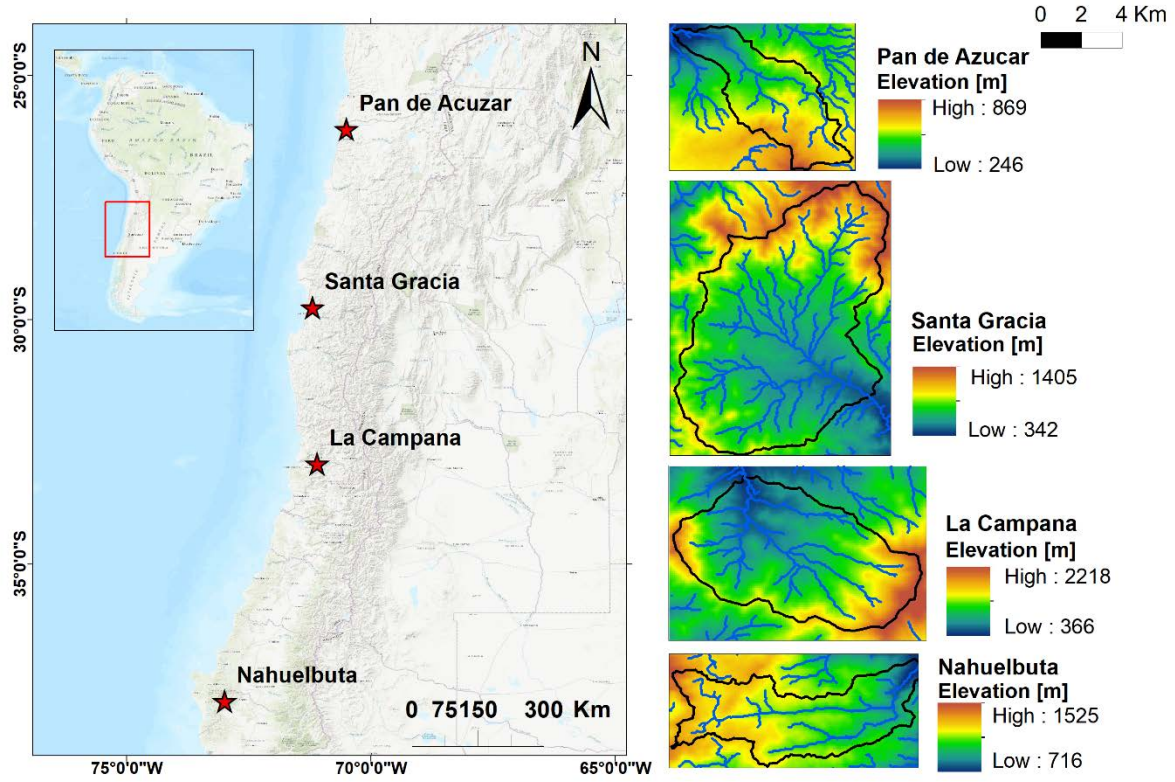

Figure 1. Study areas in Coastal Chilean Cordillera ranging from (north to south) an arid environment in the North (Pan de Azúcar), semi-arid grasslands and shrubs (Santa Gracia), Mediterranean shrubs and forests (La Campana), and temperate-humid forests in the South (Nahuelbuta). (Earth Resources Observation And Science (EROS) Center, 2017)

3 Methods

This section comprises a description of model inputs (section 3.1), estimation of runoff rates (section 3.2), model setup (section 3.3), and initial and boundary conditions (section 3.4). This is followed by an overview of simulations conducted (section 3.5) and a brief description of detrending the model results for long-term transients (section 3.6).

3.1. Data used for model inputs

In contrast to previous modeling studies (Schmid et al., 2018; Sharma et al., 2021) conducted in the same region, we used current topography in the study areas as the initial condition for simulations instead of a synthetic topography produced during a model spin-up phase in LandLab. Initial topography for the four selected catchments was obtained by cropping the SRTM digital elevation model (DEM) in rectangular shapes encapsulating the catchment area (Fig. 1). The DEM has a spatial resolution of 90 m; this indicates the cell size used in the model (dx and dy) (Earth Resources Observation And Science (EROS) Center, 2017). Maximum relief of ~1852 m is observed in La Campana (~33 °S), followed by ~1063 m in Santa Gracia (~30 °S), ~809 m in Nahuelbuta (~38 °S) and ~623 m Pan de Azúcar (~26 °S). Catchment sizes considered vary between ~64 km^2 in Pan de Azúcar, ~142.5 km^2 in Santa Gracia, ~106.8 km^2 in La Campana and ~68.7 km^2 in Nahuelbuta. We note that present-day topography as the initial condition in simulations can introduce an initial transient in erosion rates due to model erosional parameters (e.g., erodibility, hillslope diffusivity) differing from actual parameters within the catchment.

Precipitation data applied over each study area (Fig. 3b) was acquired from the Global Precipitation Climatology Centre (GPCC) for the period 01/03/2000 to 31/12/2019 (DD/MM/YEAR). The data has a spatial resolution of 1° (~111 km) and a 1-day temporal resolution and comprises daily land-surface precipitation from rain gauges built on Global Telecommunication System-based and historical data (Ziese et al., 2020). The previous data was augmented with daily precipitation weather station data from 01/02/2020 to 28/02/2020 obtained from Übernickel et al. (2020). We do this to include all the seasons between 2000 to 2019, i.e., from the Autumn of 2000 to the Summer of 2019. The periods (months of a year) of specific seasons in the Chilean Coastal Cordillera are illustrated in Table 1. Seasonal precipitation rates were calculated by summing up daily precipitation rates at three-month intervals. The seasonality and intensity of precipitation in the wet season (winter) increase from arid (Pan de Azúcar) to humid temperate (Nahuelbuta) region.

Table 1. Months of a year corresponding to specific seasons in the Chilean Coastal Cordillera

Seasons	Months
Summer[d*]	December - February
Autumn[w*]	March - May
Winter[w*]	June - August
Spring[d*]	September - November

*d: dry season, w: wet season

NDVI derived from remote sensing imagery has been proven effective for estimating seasonal changes in vegetation cover density (Garatuza-Payán et al., 2005). Normalized difference vegetation

index (NDVI) obtained from MODIS (Didan, Kamel, 2015) is used as a proxy for changes in vegetation cover in the catchments. The NDVI data were acquired for 20 years (01/03/2000 – 28/02/2020), with a spatial resolution of 250 m and temporal resolution of 16 days. For optimization during the model simulations, the vegetation cover dataset was resampled to match the spatial resolution (90 m) of SRTM DEM and temporal resolution of 3 months. To summarize, season variations in precipitation rate and vegetation cover were applied to the simulations between 01/03/2000 and 28/02/2020.

Additional aspects of the catchment hydrologic cycle were determined using the following approaches for the same periods. First, evapotranspiration (ET) data was obtained from the Global Land Data Assimilation System (GLDAS) Noah version 2.1, with a monthly temporal resolution and spatial resolution of 0.25° (~28 km) (Beaudoing, H. et al., 2020; Rodell et al., 2004). The data was obtained from March-2000 to February-2020. Due to the coarse resolution of the dataset, ET is assumed to be uniform over the entire catchment area.

Soil characteristics such as the grain size distribution (sand, silt, and clay fraction) and bulk density were adapted from Bernhard et al. (2018) to estimate soil water infiltration capacity in each study area. Based on these soil properties, the soils have been classified as a sandy loam (in Pan de Azúcar, Santa Gracia, and La Campana) and sandy clay loam (Nahuelbuta). Average bulk density values of 1300 kg m^{-3}, 1500 kg m^{-3}, 1300 kg m^{-3}, and 800 kg m^{-3} were used for Pan de Azúcar, Santa Gracia, La Campana, and Nahuelbuta, respectively (Bernhard et al., (2018).

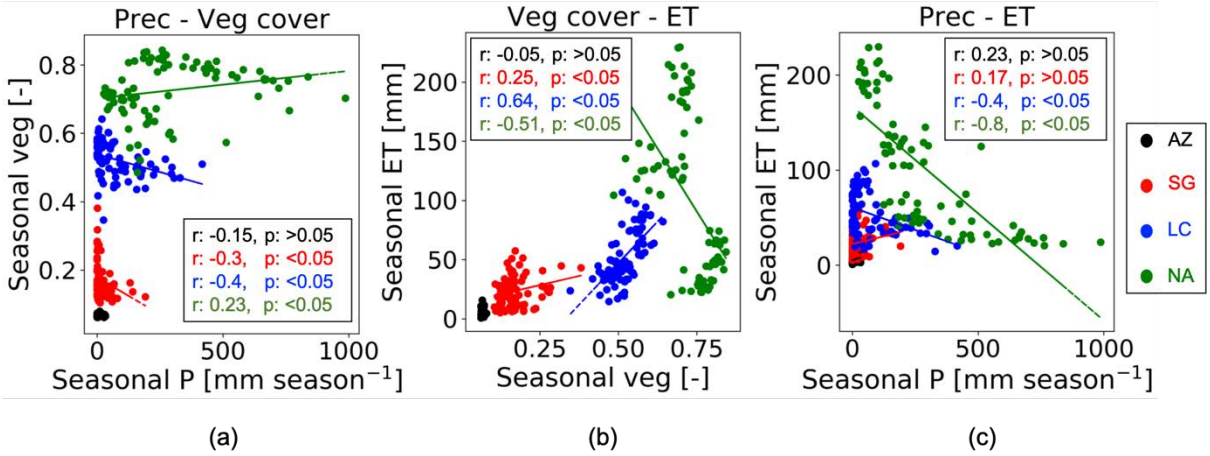

Figure 2. Parameter correlation for model input data (i.e., seasonal precipitation, vegetation cover and evapotranspiration) including: (a) seasonal precipitation [mm season^{-1}] and fraction of vegetation cover [-], (b) fractional seasonal vegetation cover [-] and evapotranspiration [mm], and (c) seasonal precipitation [mm season^{-1}] and evapotranspiration [mm]. The plots represent dataset corresponding to Autumn of 2000 to Summer of 2019.

Figure 2 shows correlations between the model input data, such as variable climatic variables (i.e., precipitation and evapotranspiration) and vegetation cover for each study area investigated. The relationships, and regression lines, show for each area in different climate-ecological zones the general

seasonal relationships over the 20 years (i.e., Autumn of 2000 – Summer of 2019) of data. For example, the correlation between seasonal precipitation and vegetation cover (Fig. 2a) illustrates a moderate negative correlation (r > -0.4) in semi-arid (SG) and Mediterranean (LC) regions. In contrast, vegetation in the humid temperate region (NA) is positively correlated (r: 0.23). ET and vegetation cover are positively correlated (Fig. 2b) in the semi-arid (SG) and Mediterranean regions (LC). However, the correlations are negative in the humid-temperate region (NA). The correlation between seasonal precipitation and ET (Fig. 2c) is slightly positive (r: ~0.2) in the semi-arid region (SG) and moderately negative (r: -0.4) in the Mediterranean (LC) study area. However, we observe a strong negative correlation (r: -0.8) between precipitation and ET in humid-temperate and Mediterranean regions (LC and NA, Fig. 2c). This negative correlation is owed to the steep negative gradient in temperature (e.g., ~2.5 °C in NA) and solar radiation (Übernickel et al., 2020) during winters (wet season) in southern latitudes (LC and NA).

3.2. Estimation of runoff rates

The precipitation rates [m season^{-1}] are subjected to soil-water infiltration [m season^{-1}] and evapotranspiration [m season^{-1}] to estimate the runoff rates (R). The runoff rates at every time step (t) are calculated using actual soil-water infiltration (I_a) and evapotranspiration (ET) as follows,

$$R(t) = P(t) - I_a(t) - ET(t), \quad (1)$$

where *P* is the precipitation amount in one season. This relation is followed in the model grid cells with non-zero sediment thickness.

The soil-water infiltration rate was estimated by applying the Green-Ampt equation (Green and Ampt, 1911; Julien et al., 1995),

$$f(t) = K_e \left(1 + \frac{\psi \cdot \Delta\theta}{F}\right), \quad (2)$$

where f(t) is the infiltration rate [m s^{-1}] at time t, K_e is the effective hydraulic conductivity [m s^{-1}], F is cumulative infiltration [m], Ψ is suction at the wetting front [m], and Δθ is the difference between saturated and initial volumetric moisture content [m^3 m^{-3}]. Effective hydraulic conductivity is highly complex and anisotropic; hence, it was considered uniform with 1×10^{-6} m s^{-1} for each catchment.

Following the approach of Istanbulluoglu and Bras. (2006) for loamy soils, the soil-water infiltration was modified to account for variable vegetation cover in each grid cell, as follows:

$$I_c(t) = f(t)(1 - V(t)) + 4f(t)(V(t)), \quad (3)$$

$$I_a(t) = Min[P(t), I_c(t)], \quad (4)$$

where I_c is the infiltration capacity and V is the vegetation cover (between 0 and 1) in a model grid cell at time-step *t*.

3.3. Model setup

We applied a python-based landscape evolution model, Landlab (Hobley et al., 2017), combined with the SPACE 1.0 module of Shobe at al. (2017). The SPACE module allows coupled detachment-transport limited fluvial processes with simultaneous bedrock erosion and sediment entrainment. The Landlab-SPACE programs were modified for vegetation-dependent hillslope processes (Johnstone and Hilley, 2014) and vegetation-dependent overland flow and fluvial erosion using the approach described in Schmid et al. (2018) and Sharma et al. (2021). In addition, the geomorphic processes considered involve weathering and regolith production (Barnhart et al., 2019) and infiltration of surface water into the soil (Rengers et al., 2016) based on the Green-Ampt method (Green and Ampt, 1911), and runoff modeling.

The model parameters (Table. A1) are calibrated to the distinct climate and ecological settings in the Chilean Coastal Cordillera observations of Schaller et al. (2018). The model state parameters (i.e., erosion, diffusion, lithological, tectonic, etc.) in the simulations are adapted from Sharma et al. (2021). The model was simulated at a seasonal scale (time step of three months) from the Autumn of 2000 (01/03/2000) to the Summer of 2019 (28/02/2020). Simulations were conducted for a total time of 1000 years with a time-step of 1 season (3 months) with 20 years (2000 – 2019) of observations in vegetation and precipitation, with repetitions of 50 times, to tap long-term transient trends in the model results. The combined effect of temporally variable (at seasonal scale) precipitation and vegetation cover (also spatially variable) on catchment-scale erosion rates is simulated in the model.

3.4. Boundary and initial conditions

The boundaries are closed (no flow) on all sides, with a single stream outlet at the point of minimum elevation at boundary nodes (Fig. 3). Initial sediment cover thickness is considered uniform across the model domain, based on the observations by Schaller et al. (2018), which is 0.2 m in arid (AZ), 0.45 m in semi-arid (SG), 0.6 m in the Mediterranean (LC), and 0.7 m in humid temperate (NA) catchments. The initial rock uplift rate is kept constant throughout the entire model run as 0.05 mm yr^{-1}, adapted from a similar study (Sharma et al., 2021).

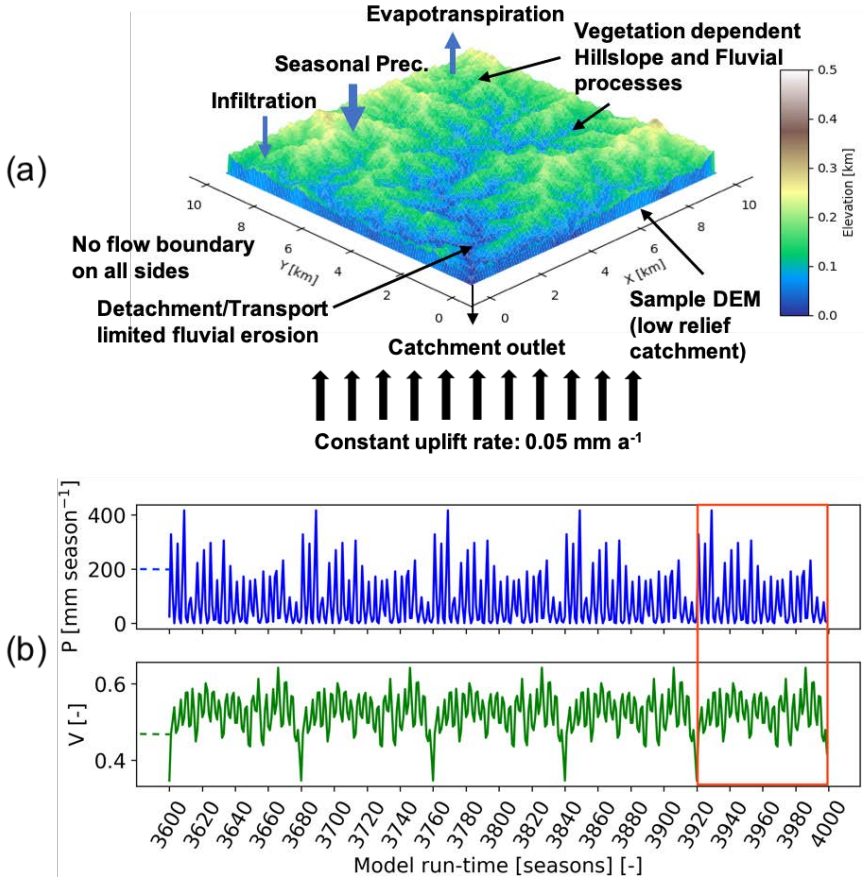

Figure 3. A simplified model geometry with seasonal precipitation and vegetation forcings used in this study. (a) Model setup representing sample DEM (low relief catchment) with no flow boundaries on all sides and a single catchment outlet. The model involves vegetation-dependent seasonal hillslope and fluvial processes and rainfall-infiltration-runoff modeling. (b) Seasonal precipitation and vegetation cover dataset (Mediterranean setting) for the last five iterations of model simulations. The results of highlighted iterations (after detrending for long-term transients) are analyzed in consecutive sections.

3.5. Overview of simulations conducted

The simulations were designed to identify the sensitivity of erosion rates to seasonal variations in either precipitation rates or vegetation cover and the more realistic scenario of coupled seasonal variations in both vegetation cover and precipitation. We evaluated this sensitivity with a step-wise increase in model complexity. Three sets of simulations were designed for the four selected study areas, which are as follows,

1. Scenario 1: Influence of constant precipitation with seasonal variations in vegetation cover catchment-scale erosion rates.
2. Scenario 2: Influence of seasonal variation in precipitation and constant vegetation cover on catchment-scale erosion rates.

3. Scenario 3: Influence of coupled seasonal variations in both precipitation and vegetation cover on catchment-scale erosion rates.

The results for scenarios 1 – 3 are illustrated in sections 4.1, 4.2, and 4.3, respectively.

3.6. Detrending of results for long term transients

Model simulations were conducted for 1,000 years using 20 years [March-2000 – Feb-2020] of observations in vegetation cover and precipitation repeated 50 times. Simulations presented here were conducted on the present-day topography to allow for the application of observed time series of precipitation and vegetation change in different ecosystems and study areas. This choice of setting comes with the compromise that the tectonic (e.g., rock uplift rates) and erosional parameters (e.g., diffusivity, erodibility, etc.) used in the model are likely not the same as those that led to the present-day catchment topography. As a result, a long-term transient in erosion rates is expected as the model tries to reach an equilibrium with assumed erosional parameters. In order to correct for any long-term transients in erosion influencing our interpretations, we conducted a linear detrending of the results to remove any long-term variations. Hence, the model results' last 20 years (detrended) were analyzed and discussed in sections 4 and 5.

4 Results

In the following sections, we focus our analysis on the mean catchment erosion rates at seasonal scales (3 months) in the Southern Hemisphere (see Table. 1). The rock uplift rate was kept constant at 0.05 mm yr^{-1} following Sharma et al. (2021). For simple representation, the results of the last five years of the last cycle of transient simulations starting from Autumn-2015 to Summer-2019 are displayed in Fig. 4, 6, and 8 (after detrending, see section 3.6). The results for the entire time series (Autumn-2000 – Summer-2019) are available in the supplement (Fig. 1 – 3). The precipitation and erosion rates are shown with the units [mm $season^{-1}$].

4.1. Scenario 1: Influence of constant precipitation and seasonal variations in vegetation cover on erosion rates

In scenario 1, vegetation cover (MODIS NDVI from March 2000 to February 2020) fluctuates seasonally (Fig. 4b), and precipitation rates are kept constant at the seasonal mean (i.e., MAP divided by the number of seasons in a year) during the entire time-series (Fig. 4a) (Ziese et al., 2020). The range of seasonal vegetation cover variation (and mean seasonal precipitation rates) are observed as 0.06 – 0.08 [-] (3.92 mm $season^{-1}$), 0.1 – 0.4 [-] (20.16 mm $season^{-1}$), 0.35 – 0.65 [-] (79 mm $season^{-1}$), and 0.5

– 0.85 [-] (292 mm season^{-1}) for Pan de Azúcar, Santa Gracia, La Campana and Nahuelbuta, respectively.

The predicted mean catchment seasonal erosion rates range between $0 - 6 \times 10^{-4}$ mm season^{-1}, $0 - 9.4 \times 10^{-4}$ mm season^{-1}, $0 - 2.3 \times 10^{-3}$ mm season^{-1}, and $1.2 \times 10^{-3} - 4 \times 10^{-3}$ mm season^{-1} in Pan de Azúcar, Santa Gracia, La Campana, and Nahuelbuta, respectively (Fig. 4c). The mean catchment seasonal erosion rates have an inverse linear relationship with seasonal vegetation cover for arid, semi-arid, and Mediterranean settings (Fig. 5). However, this relationship is positive in the humid-temperate setting, i.e., erosion increases with an increase in vegetation cover with a relatively lower gradient (3×10^{-3}).

The maximum gradient between vegetation cover and erosion rates is observed in the Mediterranean region (La Campana, gradient: -6×10^{-3}). The slopes in the vegetation cover – erosion rate relationship (Fig. 5) represent the sensitivity of each catchment to changes in seasonal vegetation cover, which indicates that the Mediterranean region (La Campana) is ~4.5 times more sensitive than the semi-arid region (Santa Gracia). Due to very low precipitation in the arid region (Pan de Azúcar), no significant range in erosion rates is observed (e.g. Pearson r: 0.17; p: >0.05). The results (Fig. 4 and 5) suggest high sensitivity of erosion in the Mediterranean setting to changes in seasonal vegetation cover (i.e., erosion rates decrease with an increase in vegetation cover). The erosion rates are lower (e.g., <0.005 mm season-1) due to low mean precipitation rates subjected to infiltration and evapotranspiration.

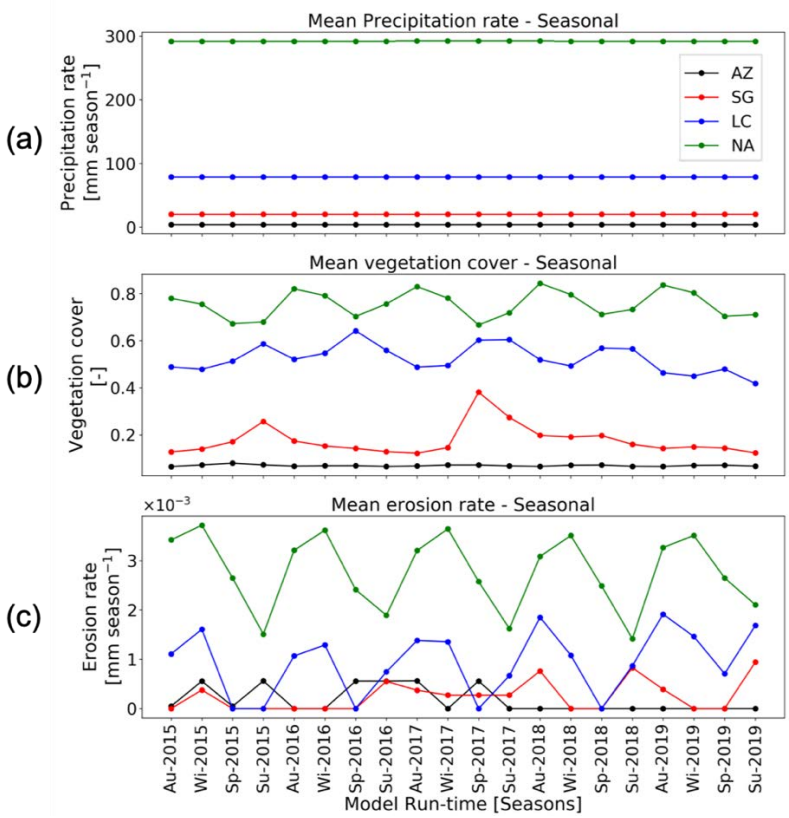

Figure 4. Results of simulations with constant seasonal precipitation and variable vegetation over last 5 years (Autumn-2015 – Summer-2019) of last cycle of transient-state model run representing: (a) mean catchment seasonal precipitation rates [mm season^{-1}], (b) mean catchment seasonal vegetation cover [-], and (c) mean catchment seasonal erosion rates [mm season^{-1}].

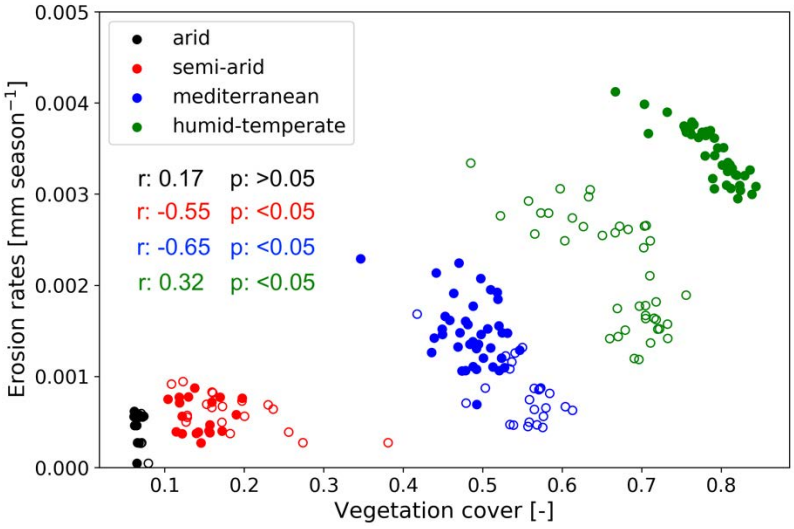

Figure 5. Correlation of vegetation cover [-] and erosion rates [mm season^{-1}] obtained from simulations with constant seasonal precipitation and variable vegetation over the last cycle of the transient state model run (Autumn-2000 – Summer-2019). * *Hollow circles: dry season; filled circles: wet season.*

4.2. Scenario 2: Influence of seasonal variations in precipitation and constant vegetation cover on erosion rates

In scenario 2, seasonal vegetation cover (MODIS NDVI from Mar-2000 – Feb-2020) is kept constant (Fig. 6b) and precipitation rates are fluctuating seasonally (Mar-2000 – Feb-2020) (Fig. 6a). The range of seasonal precipitation rate variations (and mean seasonal vegetation cover) are observed in the range of 0 – 32.42 mm season^{-1} (0.07 [-]), 0 – 191.66 mm season^{-1} (0.17 [-]), 0.03 – 417 mm season^{-1} (0.52 [-]), and 26 – 987 mm season^{-1} (0.73 [-]) for Pan de Azúcar, Santa Gracia, La Campana and Nahuelbuta, respectively.

The simulated mean catchment seasonal erosion rates are observed in the range of $0 - 2 \times 10^{-3}$ mm season^{-1}, $0 - 8.3 \times 10^{-3}$ mm season^{-1}, $0 - 1.37 \times 10^{-2}$ mm season^{-1}, and $0 - 1.3 \times 10^{-2}$ mm season^{-1} in Pan de Azúcar, Santa Gracia, La Campana, and Nahuelbuta, respectively (Fig. 6c). The mean catchment seasonal erosion rates are observed in a linear relationship with seasonal precipitation rates (Fig. 7), with a maximum gradient in the arid region (AZ, gradient: ~1.3×10^{-4}).

The gradients in precipitation – erosion rate relationship (Fig. 7) represent the sensitivity of each catchment to changes in seasonal precipitation rates, which indicates that the arid region (AZ) is ~2.7, ~3.2, and ~8 times more sensitive than semi-arid (SG), Mediterranean (LC) and humid-temperate region (NA), respectively. The results (Fig. 6 and 7) suggest high sensitivity of erosion in the arid and semi-arid settings to changes in seasonal precipitation rates (i.e., erosion increases at relatively higher rates with an increase in precipitation). The erosion rates are higher than in scenario 1 (e.g., 0 – 0.014 mm season^{-1}) due to higher precipitation rates in scenario 2.

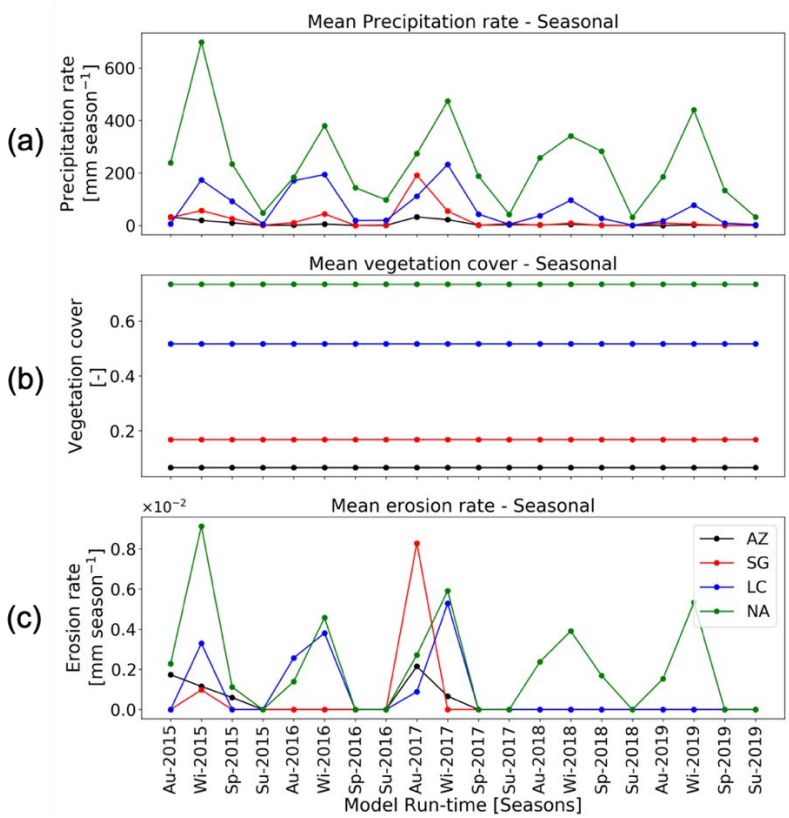

Figure 6. Results of simulations with variable seasonal precipitation and constant vegetation over last 5 years (Autumn-2015 – Summer-2019) of last cycle of transient-state model run representing: (a) mean catchment seasonal precipitation rates [mm season^{-1}], (b) mean catchment seasonal vegetation cover [-], and (c) mean catchment seasonal erosion rates [mm season^{-1}].

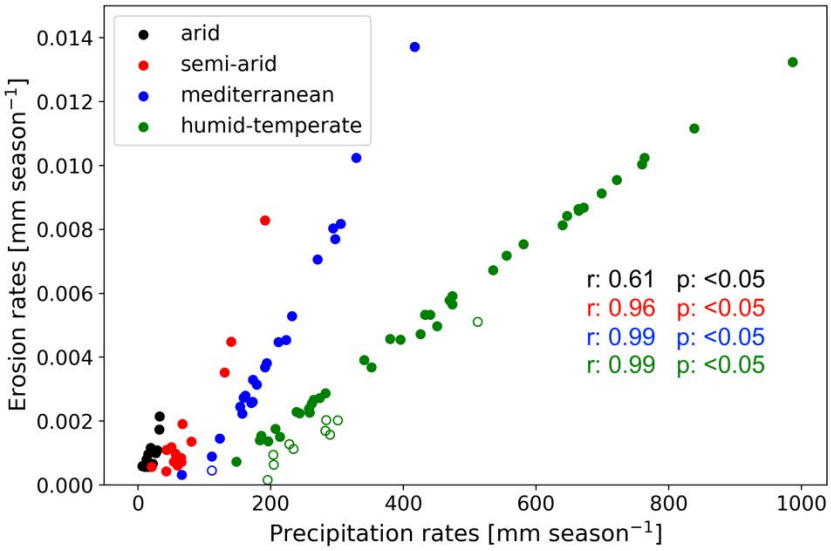

Figure 7. Correlation of precipitation rates [mm season^{-1}] and erosion rates [mm season^{-1}] obtained from simulations with variable seasonal precipitation and constant vegetation over the last cycle of the transient state model run (Autumn-2000 – Summer-2019). * *Hollow circles: dry season; filled circles: wet season.*

4.3. Scenario 3: Influence of coupled seasonal variations in both precipitation and vegetation cover on erosion rates

In this scenario, coupled variations in seasonal vegetation cover (MODIS NDVI from Mar-2000 – Feb-2020) (Fig. 8b) and precipitation rates are presented for the years 2000 - 2019 (Fig. 8a). The range of seasonal precipitation rates (and seasonal vegetation cover) variations are 0 – 32.42 mm season^{-1} (0.06 – 0.08 [-]), 0 – 191.66 mm season^{-1} (0.1 – 0.38 [-]), 0.03 – 417 mm season^{-1} (0.35 – 0.65 [-]), and 26 – 987 mm season^{-1} (0.5 – 0.85 [-]) for Pan de Azúcar, Santa Gracia, La Campana and Nahuelbuta, respectively.

The mean catchment seasonal erosion rates are observed in the range of $0 - 2 \times 10^{-3}$ mm season^{-1}, $0 - 1 \times 10^{-2}$ mm season^{-1}, $0 - 1.4 \times 10^{-2}$ mm season^{-1}, and $0 - 1.4 \times 10^{-2}$ mm season^{-1} in Pan de Azúcar, Santa Gracia, La Campana, and Nahuelbuta, respectively (Fig. 8c). Similar to scenario 2, mean catchment seasonal erosion rates are observed in a linear relationship with seasonal precipitation rates (Fig. 9), with a maximum gradient in an arid region (AZ, gradient: ~1.3×10^{-4}). The slopes in the precipitation – erosion rate relationship (Fig. 9) represent the sensitivity of each catchment to coupled variations in seasonal precipitation rates and vegetation cover. The results (Fig. 8 and 9) indicate that the arid region (AZ) is ~2.3, ~3, and ~8 times more sensitive than the semi-arid (SG), Mediterranean (LC), and humid-temperate region (NA), respectively. The similarity in results obtained from scenarios 2 and 3 suggest the first-order control of seasonal precipitation changes on erosion rates (e.g., Pearson $r > 0.6$ for arid setting, Fig. 9a), with relatively less significance of changing vegetation cover (Pearson $r < -0.19$ for semi-arid setting, Fig. 9b). However, the mean vegetation cover per model cell in a catchment plays a significant role.

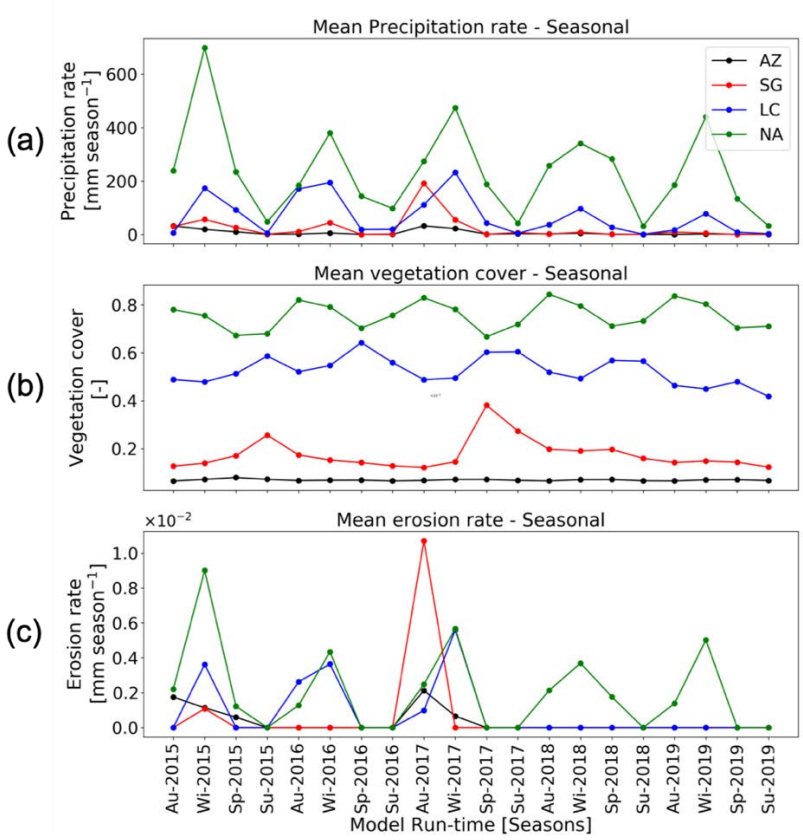

Figure 8. Results of simulations with coupled variations in seasonal precipitation and vegetation over the last five years (Autumn-2015 – Summer-2019) of the last cycle of transient-state model run representing: (a) mean catchment seasonal precipitation rates [mm season^{-1}], (b) mean catchment seasonal vegetation cover [-], and (c) mean catchment seasonal erosion rates [mm season^{-1}].

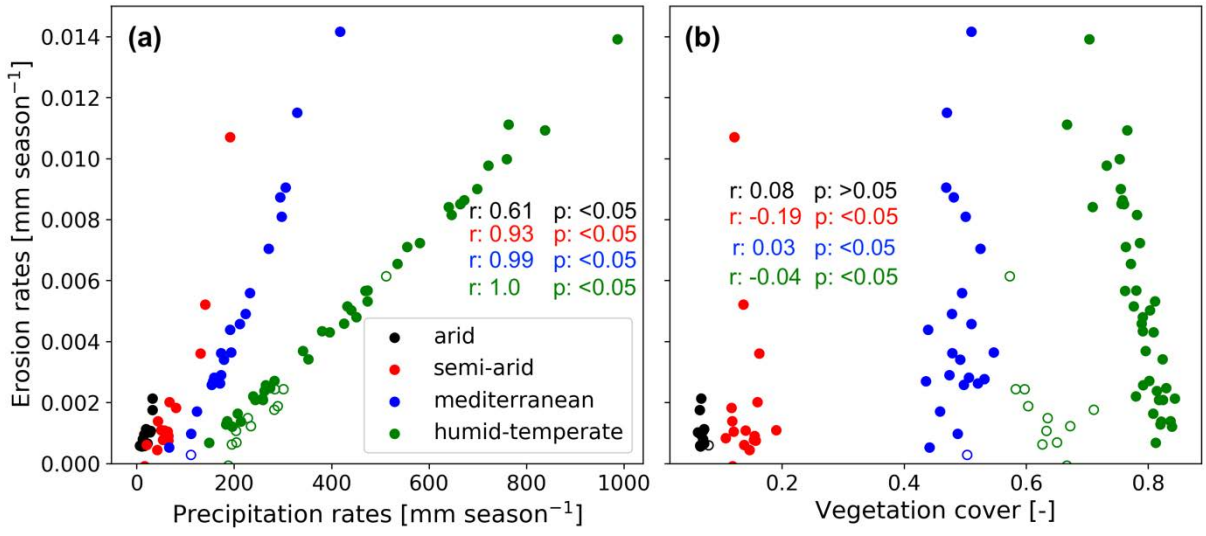

Figure 9. Correlation between (a) precipitation rates [mm season^{-1}] and (b) vegetation cover and erosion rates [mm season^{-1}] obtained from simulations with coupled variations in seasonal precipitation and vegetation over the last cycle of the transient simulation (Autumn-2000 – Summer-2019). * Hollow circles: dry season; filled circles: wet season.

5 Discussion

This section synthesizes the amplitude of change in erosion rates for scenarios 1 - 3 (section 5.1), followed by discussing the effect of variability in vegetation and precipitation rates on seasonal erosion rates (section 5.2). Next, the synthesis of catchment-scale erosion rate variability is presented over wet and dry seasons (section 5.3). Lastly, the results are compared with previously published studies (section 5.4), followed by the model limitations description (section 5.5).

5.1. Synthesis of the amplitude of change in erosion rates for model scenarios 1-3

Here we discuss the change amplitude of mean catchment erosion rates [in percentage] at a seasonal scale (Fig. 10) in the study areas. The amplitude of change in erosion rates to their respective mean values is estimated using the coefficient of variation in percent (standard deviation divided by the mean of a dataset). The coefficient of variation is defined as a statistical tool to compare multiple variables free from scale effects, i.e., it is a dimensionless quantity (Brown, 1998). This comparison represents the sensitivity of each catchment to changing seasonal weather for all three model scenarios (section 4.1 – 4.3).

In scenario 1, with seasonal variations in vegetation cover and constant seasonal precipitation (Fig. 10a), the amplitude of change in erosion rates ranges between 6.5% in the humid-temperate setting and 23% and 36% in semi-arid and Mediterranean settings, respectively. The above results support the findings of Zhang et al. (2019), which observed 20-30% of the total change in sediment yield with constant precipitation and variable vegetation cover. The above study used the soil and water assessment tool (SWAT) based on NDVI and climate parameters. Also, a 5.5% change in amplitude in erosion rates is observed in the arid setting. However, due to an insignificant correlation between vegetation cover and erosion rates (i.e., Pearson r: 0.17 and $p>0.05$, Fig. 5) and negligible vegetation cover ($V < 0.1$), it is unclear if these changes in erosion rates are due to changes in vegetation cover.

In scenario 2, with constant vegetation cover and variable precipitation rates (Fig. 10b), the amplitude of change in erosion rates ranges from 13% in the arid setting (AZ) to 52%, 65%, and 91% in humid-temperate (NA), semi-arid (SG) and Mediterranean (LC) settings, respectively. A similar trend is observed in scenario 3 with coupled variations in vegetation cover and precipitation rates (Fig. 10c), with amplitude of change in erosion rates between 13% in the arid setting to 50%, 86%, and 97% in humid-temperate, semi-arid and Mediterranean settings, respectively. The amplitude of erosion rate changes is amplified in scenario 3, especially in the semi-arid setting (e.g., ~21% increase in change amplitude from scenario 2 to scenario 3). This could be owed to the 35% change in amplitude of vegetation change in the semi-arid setting (Fig. 8). Overall, these observations indicate high sensitivity of erosion in semi-arid and Mediterranean environments over arid and humid-temperate settings.

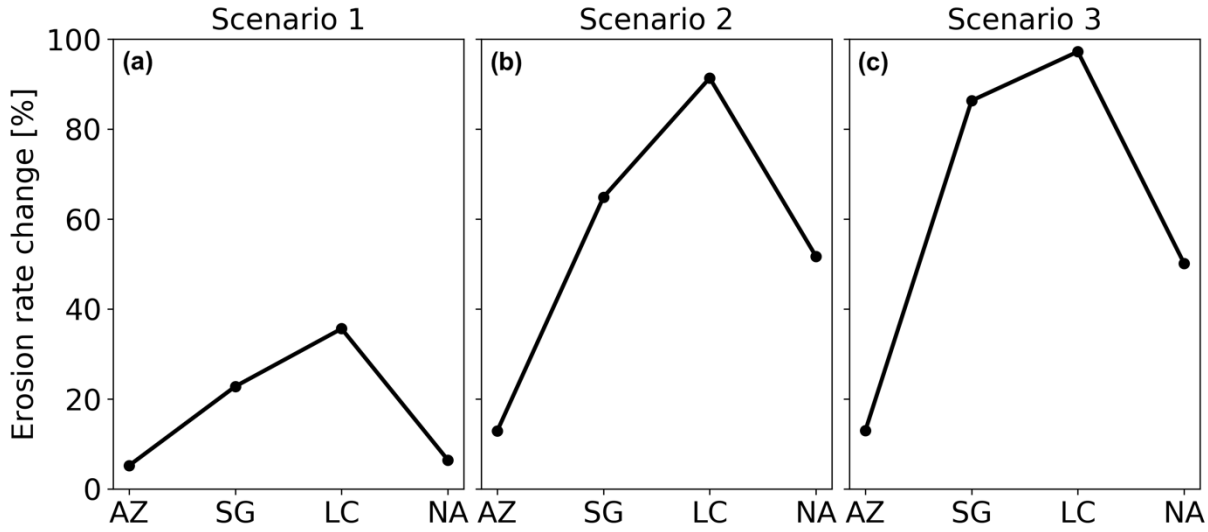

Figure 10. The amplitude of change in seasonal erosion rates (relative to their respective means) in (a) scenario 1: with variable vegetation cover and constant precipitation rates, (b) scenario 2: with constant vegetation cover and variable precipitation rates, and (c) scenario 3: with coupled variations in vegetation cover and precipitation rates.

The pattern of erosion rate changes in scenarios 1-3 implies the first-order control of precipitation variation (over vegetation cover variation) on erosion rates at a seasonal scale. For example, a plot-scale study by Gabarrón-Galeote et al. (2013) in the Mediterranean environment in Belgium concluded that rainfall intensity was the main factor in determining seasonal soil hydrological and erosive response. Another field study by Suescún et al. (2017) in the Columbian Andes highlighted the significant influence of precipitation seasonality (over vegetation cover seasonality) on runoff and erosion rates. An observational catchment-scale study in the semi-arid Chinese Loess Plateau by Wei et al. (2015) indicated that intra-annual precipitation variation significantly contributes to monthly runoff and sediment yield variations.

5.2. Synthesis of catchment erosion rates over wet and dry seasons

In this section, we discuss the ratio of MAP (Fig. 11a) and mean annual erosion (MAE) (Fig. 11b) during different seasons (i.e., autumn – summer) in a year, averaged over the entire time series (2000 – 2019). This analysis is performed for the simulation results of scenario 3 for different climate and ecological settings (i.e., arid to humid-temperate). We do this specifically with scenario 3 results to capture the trends in erosion rates with coupled variations in model input (i.e., precipitation and vegetation cover).

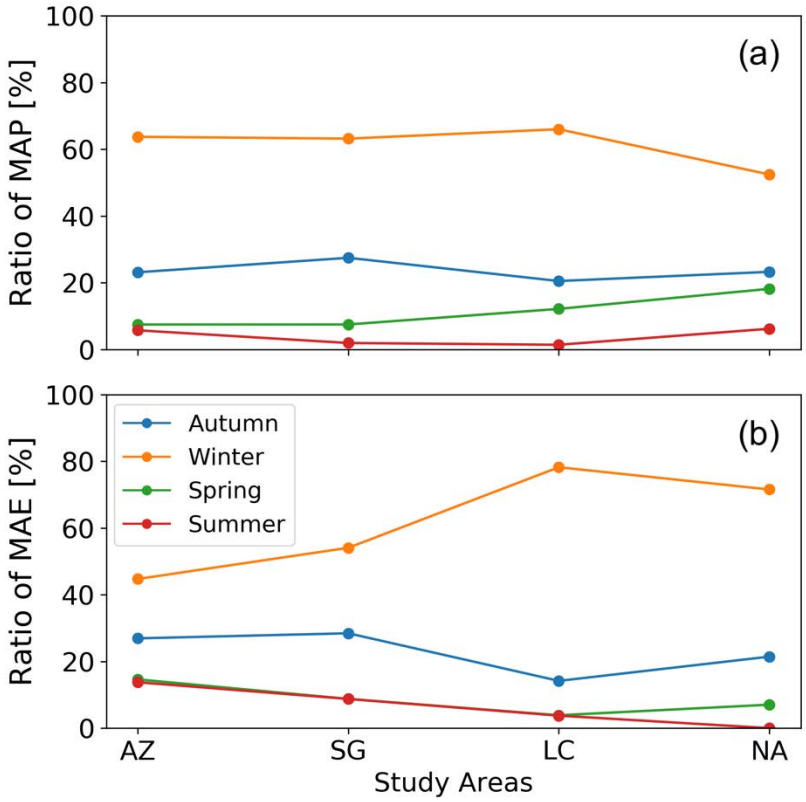

Figure 11. The ratio of model variables to annual means during all the seasons in a year for simulation results from scenario 3 (coupled seasonal variations in precipitation and vegetation cover). Each point represents a unique climate and ecological setting i.e., arid (Pan de Azúcar, AZ), semi-arid (Santa Gracia, SG), Mediterranean (La Campana, LC), and humid-temperate settings (Nahuelbuta, NA). The plots correspond to (a) ratio of MAP per season [%] and (b) ratio of MAE per season [%].

The distribution of the ratio of MAP during different seasons (Fig. 11a) depicts winter (June-August) and summer (December-February) as the wettest and driest seasons of the year, respectively. For example, all study areas receive >50% and <6% of MAP during winters and summers. The same is reflected in Fig. 11b with 45%, 55%, 78%, and 71% of MAE in arid, semi-arid, Mediterranean, and humid-temperate settings, respectively, during winters. On the contrary, during summers, the share of MAE decreases from 14% in the arid setting to 1% in the humid-temperate setting. The Autumn (March-May) receives milder precipitation amounts ranging from 20–30% of MAP in the study areas. Arid and semi-arid settings experience a relatively higher share of MAE (e.g., ~30%) than the Mediterranean and humid temperate settings (e.g., ~15-20%). The Spring season experiences relatively higher erosion rates despite a lower MAP share in arid and semi-arid settings. For example, arid and semi-arid settings experience 10-14% of MAE for ~7% of MAP. At the same time, the Mediterranean and humid-temperate settings experience 5-7% of MAE for ~12-18% of MAP during Spring. Overall, we found out that arid and semi-arid settings experience <15% and ~50% of MAE during wet (winter) and dry (summer) seasons. The above relationship is amplified for the Mediterranean and humid-temperate

settings with <5% and >70% of MAE during wet and dry seasons. The latter is in line with an observational study by Mosaffaie et al. (2015) in a Mediterranean catchment in Iran. The above study used field observations from 2012-2013 to conclude that maximum erosion rates (>70%) are observed during the wet season, which decreases in dry the season (<10%).

5.3. Comparison to previous studies

In this section, we correlate the broad findings of this study to the previously published field and observational studies. For example, in an observational study in an agrarian drainage basin in the Belgian Loam Belt, Steegen et al. (2000) evaluated sediment transport over various time scales (including seasonal). The above research observed lower sediment fluxes during the seasons with high vegetation cover. An observational study by Zheng (2006) quantifying the effect of vegetation changes on soil erosion in Loess Plateau, China, concluded that soil erosion was significantly reduced (up to ~50%) after vegetation restoration. Another observational study in semi-arid grasslands in Loess Plateau, China, by Hou et al. (2020) highlighted a considerable reduction in erosion rates due to the development of richness and evenness of plant community in the early to the mid wet season. Results of scenario 1 (seasonal variations in vegetation cover with constant precipitation rates) support the findings of the above studies with a negative correlation (Pearson r: ~ –0.6 and $p < 0.05$) between vegetation cover and erosion rates for semi-arid and Mediterranean settings. For example, erosion rates decrease with an increase in vegetation cover in Santa Gracia (semi-arid) and La Campana (Mediterranean) (see Fig. 5). However, a positive correlation (Pearson r: ~0.3 and $p<0.05$) is observed in humid-temperate setting from dry season to wet season (see Fig. 5).

A catchment-scale observational study in Baspa Valley, NW Himalayas (Wulf et al., 2010) analyzed seasonal precipitation gradients and their impact on fluvial erosion using weather station observations (1998 – 2007). The study observed a direct relationship between precipitation and sediment yield variability, demonstrating the summer monsoon's first-order control on erosion processes. An observational study by Wei et al. (2015) in Loess Plateau, China, evaluated erosion and sediment transport under various vegetation types and precipitation variations. The above study highlighted that significant changes in vegetation cover might contribute to long-term soil dynamics. However, seasonal variations in runoff and sediment yield are mainly contributed by rainfall seasonality. The similarity in the patterns of erosion rates in scenario 2 (variable precipitation and constant vegetation cover) and scenario 3 (coupled variations in precipitation and vegetation) confirms the above findings. For example, the amplitude of change in erosion rates (Fig. 10) in scenarios 2 and 3 differ by 0%, 6%, and –2% in arid, Mediterranean, and humid-temperate settings. However, this difference is enhanced in the semi-arid region (i.e., ~23%) due to a relatively high degree of variation (~25%) in vegetation cover change.

An observational study in Columbian Andes by Suescún et al. (2017) assessed the impact of seasonality on vegetation cover and precipitation and found higher erosion rates in regions with steeper slopes. Another study by Chakrapani (2005) emphasized the direct impact of local relief and channel slope on sediment yield in natural rivers. The broad findings of the above studies agree with our results of scenarios 1-3, as we find higher erosion rates in the Mediterranean and humid-temperate regions with steeper topography (mean slope ~20 deg), which encounter high seasonality (and intensity) in precipitation.

5.4. Model Limitations

The model setup used in this study was designed to quantify the sensitivity of erosion rates in different climate and ecological settings with variations in precipitation rates and vegetation cover at seasonal scales. We represent the degree of variations in erosion rates in terms of change amplitude (with respect to the mean) for different model scenarios (see sections 4.1 – 4.3). This study was intended to introduce temporal downscaling (from millennial to seasonal time scales) to the approach of previous similar modeling studies (e.g., Schmid et al., 2018; Sharma et al., 2021).

Our modeling approach uses several simplistic assumptions that warrant discussion and potential investigation in future studies. For example, our model successfully captures major surface processes, including vegetation-dependent erosion and infiltration, sediment transport, and surface runoff. However, groundwater flow is not considered in the current study, and how it can impact the model by groundwater entering into the streams. The reason is that groundwater flow modeling includes a high amount of heterogeneity and anisotropy and requires much finer grid sizes (<1m) and smaller time steps (in seconds to hours). Thus, due to the large grid-cell size (90 m) and timescales (monthly), the inclusion of robust groundwater flow modeling is out of scope for this study. Also, this study assumed uniform lithological and hydrological parameters (e.g., vertical hydraulic conductivity, initial soil moisture, evapotranspiration, erodibility, etc.) over the entire catchment. As said earlier, these properties are subjected to a high level of uncertainty and heterogeneity, the best fitting parameters, based on previously published literature (e.g., Schaller et al., 2018; Bernhard et al., 2018; Schmid et al., 2018; Sharma et al., 2021) are used for the model simulations. However, the heterogeneity in vegetation cover and related soil-water infiltration per grid cell is used in this study. For the heterogeneity in vegetation cover, we use MODIS-derived NDVI as a proxy of vegetation cover. According to Garatuza-Payán et al. (2005), NDVI is assumed as an effective tool for estimating seasonal changes in vegetation cover density. However, the spatial resolution (250 m) of the NDVI dataset is relatively lower than that of the SRTM DEM (90 m) used in the study. The difference in spatial resolution of vegetation cover and topography might introduce ambiguity in the model results.

Another limitation arises with best-fitting generalized model parameters (e.g., rock uplift rate, erodibility, diffusivity, etc.) on the SRTM DEM (as initial topography) rather than a steady-state topography. We did this to capture the effects of seasonality in precipitation and vegetation cover in modern times (2000 - 2019). However, the current topography might not have evolved with the same tectonic and lithological parameters, and the long-term transients were evident in the model results. To handle this limitation, we simulated the model for 50 iterations and detrended the model results to remove those transient effects (see section 3.6). This limitation can be handled in future studies by parameterizing the model to the current topography using stochastic (e.g., Bayesian) techniques (e.g., Stephenson et al., 2006; Avdeev et al., 2011). As this study aimed to capture the control of seasonal precipitation and (or) vegetation changes on the relative variability of erosion rates, the above limitation may not pose a problem in the model results.

6 Summary and Conclusions

In this study, we applied a numerical modeling approach (using Landlab-SPACE) to quantify the impact of seasonal variations in precipitation and vegetation on catchment averaged erosion rates. We performed this in regions with varied climate and ecological settings: arid, semi-arid, Mediterranean, and humid-temperate. Three sets of simulations were designed to model erosion rates for (a) scenario 1: constant precipitation and variable vegetation cover, (b) scenario 2: variable precipitation and constant vegetation cover, and (c) coupled variations in precipitation and vegetation cover. The main conclusions of this study are as follows:

1. Scenario 1, with variable vegetation cover and constant precipitation (Fig. 4), resulted in slight variations in seasonal erosion rates (<0.02 mm yr^{-1}) in comparison to the other scenarios. The amplitude of change in seasonal erosion rates (relative to the mean) is the smallest in humid-temperate setting and the maximum in the Mediterranean setting (Fig. 10a). For example, it ranges from 6.5% in humid-temperate setting (Nahuelbuta) to 23% and 36% in semi-arid (Santa Gracia) and Mediterranean settings (La Campana), respectively.
2. Scenario 2, with constant vegetation cover and variable precipitation (Fig. 6), results in relatively higher seasonal erosion rates (<0.06 mm yr^{-1}) in comparison to scenario 1. The amplitude of change in seasonal erosion rates (relative to the mean) is smallest in the arid setting and the largest in the Mediterranean setting (Fig. 10b). For example, it ranges from 13% in the arid setting (Pan de Azúcar) to 52%, 65%, and 91% in humid-temperate (Nahuelbuta), semi-arid (Santa Gracia), and Mediterranean settings (La Campana), respectively.
3. Scenario 3, with coupled variations in vegetation cover and precipitation (Fig. 8), results in similar seasonal erosion rates (<0.06 mm yr^{-1}) to scenario 2. Similarly, the amplitude of change in seasonal erosion rates (relative to the mean) is the smallest in the arid setting and the largest

in the Mediterranean setting (Fig. 10c). For example, it ranges from 13% in the arid setting (Pan de Azúcar) to 50%, 86%, and 97% in humid-temperate (Nahuelbuta), semi-arid (Santa Gracia), and Mediterranean settings (La Campana), respectively. A significant increase (from scenario 2) in variation in erosion rates (~21%) is owed to the ~25% variation in vegetation cover in semi-arid settings.

4. All study areas experience maximum and minimum erosion during wet and dry seasons, respectively (Fig. 11b). However, the difference (in maximum and minimum) is amplified from arid (~30%) to the Mediterranean and humid-temperate settings (~70-75%). This is owed to the range of amplitude of precipitation rates (Fig. 7) from arid (e.g., ~9 mm) to humid-temperate settings (e.g., ~543 mm) in wet and dry seasons.

Broadly, we conclude that precipitation changes are the primary driver of erosion changes over seasonal timescales, and changes in vegetation cover effects on erosion are secondary. For example, the amplitude of change in erosion rates in scenarios 2 and 3 is similar (Fig. 10b-c; with a difference < 6%) for arid, Mediterranean, and humid-temperate settings. However, this difference is amplified in the semi-arid setting (~65-86%) due to the influence of significant vegetation cover change. Also, this amplitude of change is determined by the ecological setting of the area of interest. For example, the sensitivity of erosion rates to changing precipitation (Fig. 10b-c) increases from arid (~13%) to Mediterranean settings (~91-97%) and again decreases in humid-temperate setting (~50-52%) due to abundance of vegetation cover.

Appendix

Table A1. Input parameters with corresponding units for the landscape evolution model

Model Parameters	Values
Grid spacing (dx)	90 m
Model runtime (totalT)	1000 years (2000 – 2019 repeated over 50 times)
time-step (dt)	1 season (3 months)
Rock uplift rate (U)[1]	1.25×10^{-5} [m season^{-1}] (or 0.05 [mm a^{-1}])
Initial sediment thickness (H_initial)[2]	20 (AZ), 0.45 (SG), 0.6 (LC), 0.7 (NA) [cm]
Bedrock erodibility (Kr)[1]	2×10^{-9} [m^{-1}]
Sediment erodibility (Ks)[1]	2×10^{-8} [m^{-1}]
Reach scale bedrock roughness (H*)[1]	1 [m]
Porosity (φ)[1]	0.2 [-]
Fraction of fine sediments (Ff)[1]	0.2 [-]
Effective terminal settling velocity (Vs)[1]	2.5 [m season^{-1}]
m, n[1]	0.6, 1 [-]
Bedrock erosion threshold stream power (ω_cr)[1]	1.25×10^{-5} [m season^{-1}]
Sed. entr. threshold stream power (ω_cs)[1]	1.25×10^{-6} [m season^{-1}]
Bare soil diffusivity (K_b)[1]	2.5×10^{-4} [m^2 season^{-1}]
Exponential decay coefficient (α)[1]	0.3 [-]
Critical channel formation area (A_{crit})[3]	1×10^{6} [m^2]
Reference vegetation cover (V_r)[3]	1 (100%)
Manning's number for bare soil (n_s)[3]	0.01 [-]
Manning's number for ref. vegetation (n_v)[3]	0.6 [-]
Sacling factor for vegetation influence (w)[3]	1 [-]
Soil bulk density (B)[4]	1300 (AZ), 1500 (SG), 1300 (LC), 800 (NA) [kg m^{-3}]
Soil type[4]	sandy loam (AZ, SG, LC); sandy clay loam (NA)
Initial soil moisture (s)[4]	0.058 (AZ), 0.02 (SG), 0.053 (LC), 0.15 (NA) [m^3 m^{-3}]

[1] Sharma et al. (2021), [2] Schaller et al. (2018), [3] Schmid et al. (2018), [4] Bernhard et al. (2018).

Acknowledgments:

Hemanti Sharma and Todd A. Ehlers acknowledge support from the Open Access Publishing Fund of the University of Tübingen. We also acknowledge support from the Research Training Group 1829 Integrated Hydrosystem Modelling, funded by the German Research Foundation (DFG). In addition, Todd A. Ehlers acknowledges support from the German priority research program "EarthShape: Earth Surface Shaping by Biota" (SPP-1803; EH329/14-2). We thank xxx and yyy for their constructive reviews.

References

Avdeev, B., Niemi, N. A., and Clark, M. K.: Doing more with less: Bayesian estimation of erosion models with detrital thermochronometric data, Earth Planet. Sci. Lett., 305, 385–395, https://doi.org/10.1016/j.epsl.2011.03.020, 2011.

Barnhart, K. R., Glade, R. C., Shobe, C. M., and Tucker, G. E.: Terrainbento 1.0: a Python package for multi-model analysis in long-term drainage basin evolution, Geosci. Model Dev., 12, 1267–1297, https://doi.org/10.5194/gmd-12-1267-2019, 2019.

Beaudoing, H., Rodell, M., and NASA/GSFC/HSL: GLDAS Noah Land Surface Model L4 monthly 0.25 x 0.25 degree, Version 2.1, https://doi.org/10.5067/SXAVCZFAQLNO, 2020.

Bernhard, N., Moskwa, L.-M., Schmidt, K., Oeser, R. A., Aburto, F., Bader, M. Y., Baumann, K., von Blanckenburg, F., Boy, J., van den Brink, L., Brucker, E., Büdel, B., Canessa, R., Dippold, M. A., Ehlers, T. A., Fuentes, J. P., Godoy, R., Jung, P., Karsten, U., Köster, M., Kuzyakov, Y., Leinweber, P., Neidhardt, H., Matus, F., Mueller, C. W., Oelmann, Y., Oses, R., Osses, P., Paulino, L., Samolov, E., Schaller, M., Schmid, M., Spielvogel, S., Spohn, M., Stock, S., Stroncik, N., Tielbörger, K., Übernickel, K., Scholten, T., Seguel, O., Wagner, D., and Kühn, P.: Pedogenic and microbial interrelations to regional climate and local topography: New insights from a climate gradient (arid to humid) along the Coastal Cordillera of Chile, CATENA, 170, 335–355, https://doi.org/10.1016/j.catena.2018.06.018, 2018.

Bookhagen, B., Thiede, R. C., and Strecker, M. R.: Abnormal monsoon years and their control on erosion and sediment flux in the high, arid northwest Himalaya, Earth Planet. Sci. Lett., 231, 131–146, https://doi.org/10.1016/j.epsl.2004.11.014, 2005.

Brown, C. E.: Coefficient of Variation, in: Applied Multivariate Statistics in Geohydrology and Related Sciences, Springer, Berlin, Heidelberg, 1998.

Cerdà, A.: The influence of aspect and vegetation on seasonal changes in erosion under rainfall simulation on a clay soil in Spain, Can. J. Soil Sci., 78, 321–330, https://doi.org/10.4141/S97-060, 1998.

Chakrapani, G. J.: Factors controlling variations in river sediment loads, Curr. Sci., 88, 569–575, 2005.

Deal, E., Favre, A. C., and Braun, J.: Rainfall variability in the Himalayan orogen and its relevance to erosion processes: RAINFALL VARIABILITY IN THE HIMALAYAS, Water Resour. Res., 53, 4004–4021, https://doi.org/10.1002/2016WR020030, 2017.

Didan, Kamel: MOD13Q1 MODIS/Terra Vegetation Indices 16-Day L3 Global 250m SIN Grid V006, https://doi.org/10.5067/MODIS/MOD13Q1.006, 2015.

Earth Resources Observation And Science (EROS) Center: Shuttle Radar Topography Mission (SRTM) Void Filled, https://doi.org/10.5066/F7F76B1X, 2017.

Ferreira, V. and Panagopoulos, T.: Seasonality of Soil Erosion Under Mediterranean Conditions at the Alqueva Dam Watershed, Environ. Manage., 54, 67–83, https://doi.org/10.1007/s00267-014-0281-3, 2014.

Gabarrón-Galeote, M. A., Martínez-Murillo, J. F., Quesada, M. A., and Ruiz-Sinoga, J. D.: Seasonal changes in the soil hydrological and erosive response depending on aspect, vegetation type and soil water repellency in different Mediterranean microenvironments, Solid Earth, 4, 497–509, https://doi.org/10.5194/se-4-497-2013, 2013.

Gao, P., Li, Z., and Yang, H.: Variable discharges control composite bank erosion in Zoige meandering rivers, CATENA, 204, 105384, https://doi.org/10.1016/j.catena.2021.105384, 2021.

Garatuza-Payán, J., Sánchez-Andrés, R., Sánchez-Carrillo, S., and Navarro, J. M.: Using remote sensing to investigate erosion rate variability in a semiarid watershed, due to changes in vegetation cover, IAHS Publ, 292, 144–151, 2005.

Glodny, J., Gräfe, K., Echtler, H., and Rosenau, M.: Mesozoic to Quaternary continental margin dynamics in South-Central Chile (36–42°S): the apatite and zircon fission track perspective, Int. J. Earth Sci., 97, 1271–1291, https://doi.org/10.1007/s00531-007-0203-1, 2008.

Green, W. H. and Ampt, G. A.: Studies on Soil Phyics., J. Agric. Sci., 4, 1–24, https://doi.org/10.1017/S0021859600001441, 1911.

Hancock, G. and Lowry, J.: Hillslope erosion measurement—a simple approach to a complex process, Hydrol. Process., 29, 4809–4816, 2015.

Hancock, G. and Lowry, J.: Quantifying the influence of rainfall, vegetation and animals on soil erosion and hillslope connectivity in the monsoonal tropics of northern Australia, Earth Surf. Process. Landf., 46, 2110–2123, https://doi.org/10.1002/esp.5147, 2021.

Herrmann, S. M. and Mohr, K. I.: A Continental-Scale Classification of Rainfall Seasonality Regimes in Africa Based on Gridded Precipitation and Land Surface Temperature Products, J. Appl. Meteorol. Climatol., 50, 2504–2513, https://doi.org/10.1175/JAMC-D-11-024.1, 2011.

Hobley, D. E. J., Adams, J. M., Nudurupati, S. S., Hutton, E. W. H., Gasparini, N. M., Istanbulluoglu, E., and Tucker, G. E.: Creative computing with Landlab: an open-source toolkit for building, coupling, and exploring two-dimensional numerical models of Earth-surface dynamics, Earth Surf. Dyn., 5, 21–46, https://doi.org/10.5194/esurf-5-21-2017, 2017.

Hou, J., Zhu, H., Fu, B., Lu, Y., and Zhou, J.: Functional traits explain seasonal variation effects of plant communities on soil erosion in semiarid grasslands in the Loess Plateau of China, Catena, v. 194, 104743-, https://doi.org/10.1016/j.catena.2020.104743, 2020.

Istanbulluoglu, E. and Bras, R. L.: On the dynamics of soil moisture, vegetation, and erosion: Implications of climate variability and change, Water Resour. Res., 42, 2006.

Johnstone, S. A. and Hilley, G. E.: Lithologic control on the form of soil-mantled hillslopes, Geology, 43, 83–86, https://doi.org/10.1130/G36052.1, 2014.

Julien, P. Y., Saghafian, B., and Ogden, F. L.: RASTER-BASED HYDROLOGIC MODELING OF SPATIALLY-VARIED SURFACE RUNOFF1, JAWRA J. Am. Water Resour. Assoc., 31, 523–536, https://doi.org/10.1111/j.1752-1688.1995.tb04039.x, 1995.

Langbein, W. B. and Schumm, S. A.: Yield of sediment in relation to mean annual precipitation, Eos Trans. Am. Geophys. Union, 39, 1076–1084, https://doi.org/10.1029/TR039i006p01076, 1958.

Leyland, J., Hackney, C. R., Darby, S. E., Parsons, D. R., Best, J. L., Nicholas, A. P., Aalto, R., and Lague, D.: Extreme flood-driven fluvial bank erosion and sediment loads: direct process measurements using integrated Mobile Laser Scanning (MLS) and hydro-acoustic techniques: Direct measurement of flood-driven erosion using MLS and MBES, Earth Surf. Process. Landf., 42, 334–346, https://doi.org/10.1002/esp.4078, 2016.

Melnick, D.: Rise of the central Andean coast by earthquakes straddling the Moho, Nat. Geosci., 9, 401–407, https://doi.org/10.1038/ngeo2683, 2016.

Melnick, D., Bookhagen, B., Strecker, M. R., and Echtler, H. P.: Segmentation of megathrust rupture zones from fore-arc deformation patterns over hundreds to millions of years, Arauco peninsula, Chile: EARTHQUAKE SEGMENTATION AT ARAUCO, J. Geophys. Res. Solid Earth, 114, https://doi.org/10.1029/2008JB005788, 2009.

Mosaffaie, J., Ekhtesasi, M. R., Dastorani, M. T., Azimzadeh, H. R., and Zare Chahuki, M. A.: Temporal and spatial variations of the water erosion rate, Arab. J. Geosci., 8, 5971–5979, https://doi.org/10.1007/s12517-014-1628-z, 2015.

Oeser, R. A., Stroncik, N., Moskwa, L.-M., Bernhard, N., Schaller, M., Canessa, R., Brink, L. van den, Köster, M., Brucker, E., Stock, S., Fuentes, J. P., Godoy, R., Matus, F. J., Pedraza, R. O., McIntyre, P. O., Paulino, L., Seguel, O., Bader, M. Y., Boy, J., Dippold, M. A., Ehlers, T. A., Kühn, P., Kuzyakov, Y., Leinweber, P., Scholten, T., Spielvogel, S., Spohn, M., Übernickel, K., Tielbörger, K., Wagner, D., and Blanckenburg, F. von: Chemistry and microbiology of the Critical Zone along a steep climate and vegetation gradient in the Chilean Coastal Cordillera, CATENA, 170, 183–203, https://doi.org/10.1016/j.catena.2018.06.002, 2018.

Rengers, F. K., McGuire, L., Kean, J. W., Staley, D. M., and Hobley, D. E. J.: Model simulations of flood and debris flow timing in steep catchments after wildfire, Water Resour. Res., 52, 6041–6061, https://doi.org/10.1002/2015WR018176, 2016.

Rodell, M., Houser, P. R., Jambor, U., Gottschalck, J., Mitchell, K., Meng, C.-J., Arsenault, K., Cosgrove, B., Radakovich, J., Bosilovich, M., Entin, J. K., Walker, J. P., Lohmann, D., and Toll, D.: The Global Land Data Assimilation System, Bull. Am. Meteorol. Soc., 85, 381–394, https://doi.org/10.1175/BAMS-85-3-381, 2004.

Schaller, M., Ehlers, T. A., Lang, K. A. H., Schmid, M., and Fuentes-Espoz, J. P.: Addressing the contribution of climate and vegetation cover on hillslope denudation, Chilean Coastal Cordillera (26°–38°S), Earth Planet. Sci. Lett., 489, 111–122, https://doi.org/10.1016/j.epsl.2018.02.026, 2018.

Schaller, M., Dal Bo, I., Ehlers, T. A., Klotzsche, A., Drews, R., Fuentes Espoz, J. P., and van der Kruk, J.: Comparison of regolith physical and chemical characteristics with geophysical data along a climate and ecological gradient, Chilean Coastal Cordillera (26 to 38\degree\,S), SOIL, 6, 629–647, https://doi.org/10.5194/soil-6-629-2020, 2020.

Schmid, M., Ehlers, T. A., Werner, C., Hickler, T., and Fuentes-Espoz, J.-P.: Effect of changing vegetation and precipitation on denudation – Part 2: Predicted landscape response to transient climate and vegetation cover over millennial to million-year timescales, Earth Surf. Dyn., 6, 859–881, https://doi.org/10.5194/esurf-6-859-2018, 2018.

Sharma, H., Ehlers, T. A., Glotzbach, C., Schmid, M., and Tielbörger, K.: Effect of rock uplift and Milankovitch timescale variations in precipitation and vegetation cover on catchment erosion rates, Earth Surf. Dyn., 9, 1045–1072, https://doi.org/10.5194/esurf-9-1045-2021, 2021.

Shobe, C. M., Tucker, G. E., and Barnhart, K. R.: The SPACE 1.0 model: A Landlab component for 2-D calculation of sediment transport, bedrock erosion, and landscape evolution, Geosci. Model Dev. Discuss., 1–38, https://doi.org/10.5194/gmd-2017-175, 2017.

Starke, J., Ehlers, T. A., and Schaller, M.: Latitudinal effect of vegetation on erosion rates identified along western South America, Science, 367, 1358–1361, https://doi.org/10.1126/science.aaz0840, 2020.

Steegen, A., Govers, G., Nachtergaele, J., Takken, I., Beuselinck, L., and Poesen, J.: Sediment export by water from an agricultural catchment in the Loam Belt of central Belgium, Geomorphology, 33, 25–36, https://doi.org/10.1016/S0169-555X(99)00108-7, 2000.

Stephenson, J., Gallagher, K., and Holmes, C.: A Bayesian approach to calibrating apatite fission track annealing models for laboratory and geological timescales, Geochim. Cosmochim. Acta, 70, 5183–5200, https://doi.org/10.1016/j.gca.2006.07.027, 2006.

Suescún, D., Villegas, J. C., León, J. D., Flórez, C. P., García-Leoz, V., and Correa-Londoño, G. A.: Vegetation cover and rainfall seasonality impact nutrient loss via runoff and erosion in the Colombian Andes, Reg. Environ. Change, 17, 827–839, https://doi.org/10.1007/s10113-016-1071-7, 2017.

Übernickel, K., Ehlers, T. A., Ershadi, M. R., Paulino, L., Fuentes Espoz, J.-P., Maldonado, A., Oses-Pedraza, R., and von Blanckenburg, F.: Time series of meteorological station data in the EarthShape study areas of in the Coastal Cordillera, Chile, https://doi.org/10.5880/FIDGEO.2020.043, 2020.

Wang, L., Zheng, F., Liu, G., Zhang, X. J., Wilson, G. V., Shi, H., and Liu, X.: Seasonal changes of soil erosion and its spatial distribution on a long gentle hillslope in the Chinese Mollisol region, Int. Soil Water Conserv. Res., 9, 394–404, https://doi.org/10.1016/j.iswcr.2021.02.001, 2021.

Wei, W., Chen, L., Zhang, H., and Chen, J.: Effect of rainfall variation and landscape change on runoff and sediment yield from a loess hilly catchment in China, Environ. Earth Sci., 73, 1005–1016, https://doi.org/10.1007/s12665-014-3451-y, 2015.

Wulf, H., Bookhagen, B., and Scherler, D.: Seasonal precipitation gradients and their impact on fluvial sediment flux in the Northwest Himalaya, Geomorphology, 118, 13–21, https://doi.org/10.1016/j.geomorph.2009.12.003, 2010.

Yetemen, O., Istanbulluoglu, E., Flores-Cervantes, J. H., Vivoni, E. R., and Bras, R. L.: Ecohydrologic role of solar radiation on landscape evolution, Water Resour. Res., 51, 1127–1157, https://doi.org/10.1002/2014wr016169, 2015.

Zhang, S., Li, Z., Hou, X., and Yi, Y.: Impacts on watershed-scale runoff and sediment yield resulting from synergetic changes in climate and vegetation, Catena, 179, 129–138, https://doi.org/10.1016/j.catena.2019.04.007, 2019.

Zhang, W., An, S., Xu, Z., Cui, J., and Xu, Q.: The impact of vegetation and soil on runoff regulation in headwater streams on the east Qinghai–Tibet Plateau, China, Catena, 87, 182–189, https://doi.org/10.1016/j.catena.2011.05.020, 2011.

Zhang, X., Yu, G. Q., Li, Z. B., and Li, P.: Experimental Study on Slope Runoff, Erosion and Sediment under Different Vegetation Types, Water Resour. Manag., 28, 2415–2433, https://doi.org/10.1007/s11269-014-0603-5, 2014.

Zheng, F. L.: Effect of Vegetation Changes on Soil Erosion on the Loess Plateau1 1Project supported by the Chinese Academy of Sciences (No. KZCX3-SW-422) and the National Natural Science Foundation of China (Nos. 9032001 and 40335050)., Pedosphere, 16, 420–427, https://doi.org/10.1016/S1002-0160(06)60071-4, 2006.

Ziese, M., Rauthe-Schöch, A., Becker, A., Finger, P., Rustemeier, E., and Schneider, U.: GPCC Full Data Daily Version 2020 at 1.0°: Daily Land-Surface Precipitation from Rain-Gauges built on GTS-based and Historic Data: Gridded Daily Totals (2020), https://doi.org/10.5676/DWD_GPCC/FD_D_V2020_100, 2020.

3.3 Effects of extreme precipitation events on catchment erosion along a climate and ecological gradient in Chilean Coastal Cordillera

3.3.1 Declarations of contribution of all co-authors in the manuscript

This section of the dissertation comprises the manuscript in late stage of preparation for a potential publication. The title of the manuscript is designed as *"Effects of extreme precipitation events on catchment erosion along a climate and ecological gradient in the Chilean Coastal Cordillera"*.

The manuscript was prepared and contributed by three authors, namely Hemanti Sharma (HS), Todd A. Ehlers (TAE), and Christoph Glotzbach (CG). Hemanti Sharma and Todd Ehlers jointly developed the idea with further refinements suggested by Christoph Glotzbach. The model input data for Landlab and SWAT was procured and processed by Hemanti Sharma followed by model setup and simulation runs. The visualization, interpretation of results and manuscript preparation was done by Hemanti Sharma with the help of Todd Ehlers. The detailed contributions of each author for the above publication are presented in Table 3.

Table 3. Contribution of authors (in percentage) in the manuscript with the title *"Effects of extreme precipitation events on catchment erosion along a climate and ecological gradient in the Chilean Coastal Cordillera"*.

Author	Author position	Scientific ideas [%]	Data generation [%]	Analysis & interpretation [%]	Paper writing [%]
HS	1	70	90	70	80
TAE	2	20	10	30	20
CG	3	10	0	0	0

3.3.2 Manuscript Draft: Effects of extreme precipitation events on catchment erosion along a climate and ecological gradient in the Chilean Coastal Cordillera

Effects of extreme precipitation events on catchment erosion along a climate and ecological gradient in the Chilean Coastal Cordillera.

Hemanti Sharma[1], Todd A. Ehlers[1], Christoph Glotzbach[1]

[1]Department of Geosciences, University of Tübingen, 72076, Tübingen, Germany

Abstract

Extreme precipitation events can play an essential role in shaping landscapes. The effect of these events on catchment erosion is expected to depend upon the intensity and duration of the event and the density and type of vegetation present (amongst other factors). This study complements previous efforts and applies the Landlab landscape evolution model (LEM) to investigate the vegetation-dependent erosional response from a daily time series of precipitation events along the steep climate and ecological gradient in the Chilean Coastal Cordillera. Results are presented for four study areas ranging from (arid) barren land in the north (~26 °S) to (humid-temperate) dense forest in the south (~39 °S). Simulations were conducted for 1,900 years using precipitation observations from 1982 to 2019 (repeated 50 times). The LEM (area-normalized) surface water discharge rates at the catchment outlet were cross-checked to predictions from the Soil and Water Analysis Tool (SWAT) hydrological model. The results suggest that during extreme precipitation events, erosion rate changes in (arid) barren land are ~14%, ~86%, and ~93% more sensitive to precipitation changes relative to (semi-arid) grassland, (Mediterranean) shrubland, and (humid-temperate) dense forest, respectively. This sensitivity is attributed to (1) a higher prevalence of low frequency, high magnitude precipitation events in the northern (arid) setting during El Niño periods; and (2) the absence of erosionally resilient plant function types (PFT) in northern catchments (i.e., arid and semi-arid settings). In addition, a strong positive correlation (Pearson $r > 0.8$, >95% significance level) of (area-normalized) runoff rates was observed between the Landlab LEM and the SWAT hydrological model. This underscores the utility of the Landlab LEM (as modified here to account for variable PFTs) for simulating shorter timescale catchment processes.

Keywords: Landscape evolution model, hydrological model, plant functional types, Landlab, SWAT.

1 Introduction

The frequency, magnitude, and duration of precipitation are significant drivers of erosion and sedimentation processes in river catchments at shorter timescales (e.g., Bezak et al., 2021; Medeiros and de Araújo, 2013; Meusburger et al., 2012; Farhan and Alnawaiseh, 2018). The impact of these processes on runoff and catchment erosion also depends on the spatial distribution of land use and land cover (LULC) types (Nunes et al., 2011; Serpa et al., 2015; Sharma et al., 2011). The LULC also includes vegetation density and distribution of plant functional types (PFT) such as trees, shrubs, and grasses. Vegetation types are important because they impact flow resistance and infiltration (Stolte, 2003). In some settings, a significant fraction of mean annual precipitation (MAP) occurs during specific heavy precipitation events that last hours to days, strongly affecting the catchment erosion. This is owed to the scale-dependent connectivity of runoff and sediment (Lesschen et al., 2009). The spatial extent of changes in erosion and sedimentation patterns that occurred during these flood events can be investigated using the landscape evolution modeling technique (Zellou and Rahali, 2017). However, the landscape evolution models (LEM) are conventionally designed to quantify topographic evolution and associated catchment erosion over longer (e.g., millions of years) timescales (e.g., Coulthard, 2001; Tucker and Hancock, 2010; Willgoose, 2005). This timescale gap between short, and long-term surface processes poses challenges when trying to understand the impact of extreme events on landform development (Tucker and Hancock, 2010). For example, understanding the variability of erosion and sedimentation rates across timescales is essential for knowing which processes lead to a bias in estimating sediment fluxes leaving the catchment outlet (Kirchner et al., 2001; Vanacker et al., 2007). For example, the combined effects of vegetation cover (and type) and variable precipitation distribution make it difficult (amongst other factors) to quantify transients in catchment erosion. This study investigates how vegetation density and type and stochastic variations in precipitation influence catchment erosion.

Previous observational and modeling studies have emphasized the importance of short-term temporal heterogeneity in precipitation (e.g., daily) on catchment erosion. For example, in a review, Brunsden and Thornes (1979) demonstrated the episodic behavior of landscape change due to extreme precipitation events. An observational study by Hooke and Mant (2000) in SE Spain reported a strong relationship between catchment erosion response and flood magnitude in a semi-arid setting, using a digital elevation model and field surveys. In another observational study in a semi-arid catchment in Southern Bolivia, Coppus and Imeson (2002) concluded that extreme events significantly contribute to annual erosion and sediment transport. Also, in their analysis, Gonzàlez-Hidalgo et al. (2009) and Gonzalez-Hidalgo et al. (2010) documented the asymmetric contribution of low frequency and high magnitude precipitation events to annual catchment erosion in arid and semi-arid settings. In an observational study using mobile laser scanning and acoustic techniques, Leyland et al. (2016) reported

a two-fold and four-fold increase in bank erosion and suspended sediment volumes, respectively, during flooding in the Mekong river. Also, recent developments in modeling approaches include temporal downscaling of non-steady-state LEMs to account for daily erosion events. These LEMS are either parameterized or integrated with the simplistic short-term event- and physically-based models. For example, Baartman et al. (2013) calibrated LAPSUS LEM to the simulation results of an event-based soil erosion model (OpenLISEM) to incorporate the effect of short-term precipitation variability in long-term landscape development. The above study documented that very high magnitude (or frequency) extreme events (beyond natural climate variability) leave a signal in the landscape. For the simulation of catchment erosion during flood events, Coulthard et al. (2013) coupled the CASER landscape evolution model (Coulthard et al., 2002) and a hydrodynamic model LISFLOOD-FP (Bates and De Roo, 2000; Bates et al., 2010) to create CEASER-LF. The above model is computationally efficient with a solid physical basis and has been extensively applied in short timescale landscape evolution modeling studies to simulate flood events (e.g., Walsh et al., 2020; Zellou and Rahali, 2017).

The changes in land use and land cover, including vegetation cover and type, have been documented to affect short-term catchment erosion and runoff significantly. For example, a modeling study by Boix-Fayos et al. (2008) reported a reduction of 54% in sediment yield, linked with a three-fold increase in forest cover (between 1956 and 1997) in a catchment in SE Spain. An observational study in a sub-humid Mediterranean catchment in Portugal by Nunes et al. (2011) demonstrated a significant reduction in soil erosion and an increase in infiltration capacity with an increase in shrub and tree cover. A study by Sharma et al. (2011) using the universal soil loss equation (USLE) and geographic information system (GIS) reported an increase in mean soil erosion potential of the watershed resulting from the conversion of forest patches to cropland. A plot-scale study by Meng et al. (2021), using revised-USLE, demonstrated that earth bank terraces experienced more erosion, while slopes with hedgerows (shrubs) had lower erosion rates during moderate or heavy rainfall events. A modeling study by Serpa et al. (2015) evaluated the impact of climate and land-use changes on sediment transport in humid and arid settings for projected emission and land cover change scenarios (i.e., 2071-2100). The above study highlighted the importance of climate-induced LULC change on catchment erosion to isolated changes in climate. The previous studies underscored the significance of changes in climate and vegetation cover (and type) on the variations in catchment erosion. However, it is not clear which factor (i.e., vegetation type or precipitation variability) plays a more vital role in influencing catchment erosion at daily timescales.

This study investigates the influence of vegetation cover, PFT-dependent coupled hillslope and fluvial processes, soil-water infiltration, and evapotranspiration on catchment-scale erosion rates at a daily timescale using a complex landscape evolution model. Emphasis is placed on the sensitivity of erosion to different land cover types and precipitation variations, including extreme events. We do this

by testing two hypotheses, i.e., (a) if LULC poses first-order control on catchment erosion, then regions with less resilient vegetation cover (barren or grasses) would experience more erosion during extreme events, despite the prevalence of high magnitude precipitation in regions with more resilient vegetation cover (e.g., shrubs and trees), (b) if Landlab LEM (modified to account for PFTs) provide a reliable output at shorter timescales, then its results should be comparable with that of a physically-based model. To test the first hypothesis, we apply the Landlab-SPACE LEM at daily time steps for ~4 decades. The LEM couples PFT-dependent detachment-transport limited fluvial processes (Shobe et al., 2017), vegetation-dependent hillslope diffusion (Johnstone and Hilley, 2014), and soil-water infiltration (Rengers et al., 2016; Green and Ampt, 1911) to compute catchment erosion. The simulations are subjected to daily precipitation input obtained from weather stations (1982 – 2019) (Ziese et al., 2020) and actual evapotranspiration obtained from Global Land Evaporation Amsterdam Model version-3 (GLEAM v3) (Martens et al., 2017). We do this for four study areas along the climate and ecological gradient of Chilean Coastal Cordillera, with landcover types ranging from barren land in the north to dense forest in the south. To test the second hypothesis, the surface water discharge rates are normalized by domain area, obtained from LEM (Landlab-SAPCE) (Hobley et al., 2017), and hydrological model (Soil and Water Assessment Tool) (Winchell et al., 2013) are compared and correlated for validation of LEM results.

2 Study Area

This section includes the description of land cover types and topographic characteristics in the four selected catchments, along with an abrupt climate and ecological gradient in the Chilean Coastal Cordillera (~26 °S – ~38 °S) (Schaller et al., 2020). These catchments are located in the Pan de Azúcar National Park (arid, ~26°S), Santa Gracia nature preserve (semi-arid, ~30°S), and the La Campana (mediterranean, ~33°S) and Nahuelbuta (temperate-humid, ~38°S) national parks (Fig. 1). The study areas are part of the German-Chilean priority research program EarthShape (www.earthshape.net) and ongoing research efforts within these catchments.

Mean annual precipitation (1982 – 2019) in these regions ranges from 20.5 mm yr^{-1} in the north to 1350 mm yr^{-1} in the south (Ziese et al., 2020). The northern catchments (i.e., Pan de Azúcar and Santa Gracia) experience distinct climate patterns from El Niño Southern Oscillations (ENSO). The El Niño (warm phase of ENSO) events pose anomalies in climate, leading to severe flooding events in the northern latitudes of South America (Valdés-Pineda et al., 2016). However, the ENSO effects dampen in southern latitudes; hence southern study areas, i.e., La Campana and Nahuelbuta, are not affected by El Niño.

The selected catchments in Pan de Azúcar (~26 °S), Santa Gracia (~29.75 °S), La Campana (~33 °S), and Nahuelbuta (~38 °S) are hereafter referred to as barren land, grassland, shrubland, and dense

forest, respectively, based on the PFT distribution as per LULC dataset (Zanaga et al., 2021). The topographic characteristics (i.e., area, elevation, slope, etc.) extracted from DEM (Earth Resources Observation And Science (EROS) Center, 2017) and PFT distribution (% coverage of barren, grasses, bushes, and trees) of the selected catchments are illustrated in Table 1.

Table 1. Topographic characteristics (SRTM DEM) and plant functional types distribution (ESA LULC) of selected catchments in Chilean Coastal Cordillera (Z: topographic elevation, S: topographic slope).

Study Areas	Topographic Characteristics						PFT Distribution			
	Area [km^2]	Mean Z [m]	Max. Z [m]	Min. Z [m]	Relief [m]	Mean S [°]	Barren [%]	Grass [%]	Shrubs [%]	Trees [%]
AZ	12.53	431	666	245	421	9.8	99.94	0.04	0.02	-
SG	20.7	675	991	497	494	13	66	29	5	-
LC	9.37	653	977	388	589	16	1.4	1.5	91.7	5.4
NA	6.74	1117	1236	903	333	11.2	-	0.9	-	99.1

**AZ: Pan de Azucar, SG: Santa Gracia, LC: La Campana, and NA: Nahuelbuta.*

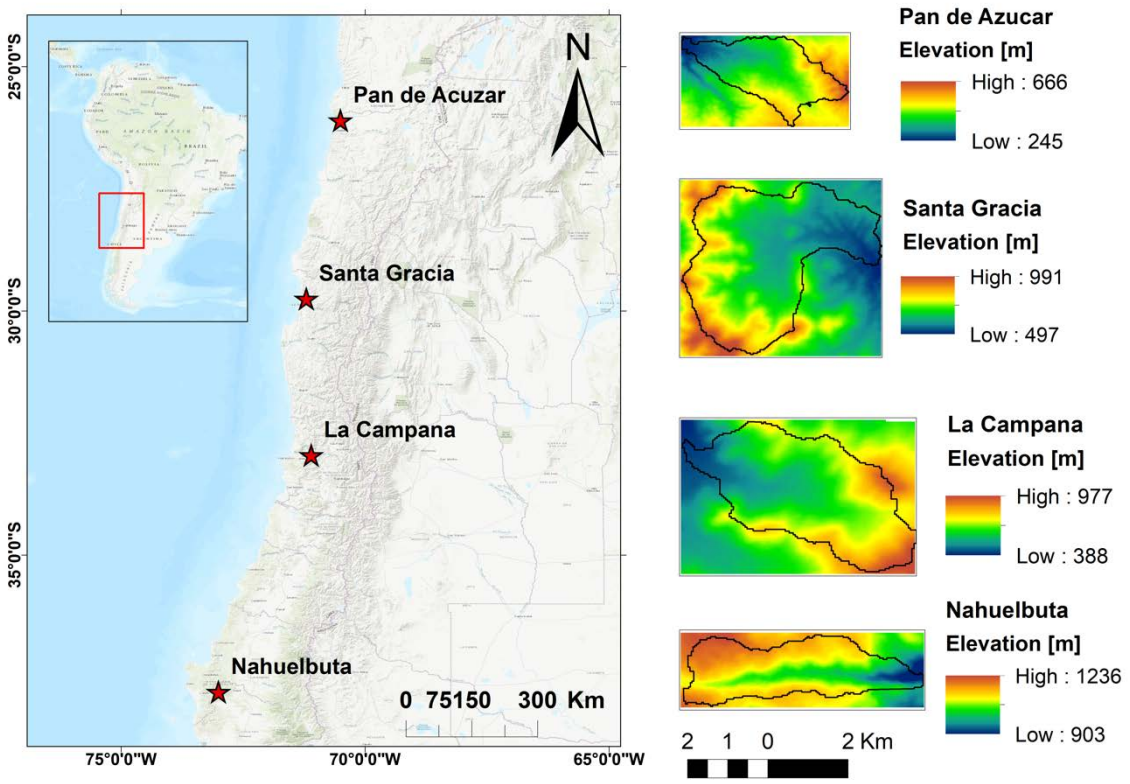

Figure 1. Study areas in Chilean Coastal Cordillera with catchments in arid – barren land in the North (Pan de Azúcar), semi-arid – grassland (Santa Gracia), Mediterranean – shrubland (La Campana), and humid temperate – dense forest (Nahuelbuta) in the South (Earth Resources Observation And Science (EROS) Center, 2017).

3 Methods

This section includes the description of datasets and models used in this study. We applied a coupled landscape evolution modeling technique at daily time steps to quantify the role of temporal variability of precipitation (frequency and magnitude) in selected catchments with different landcover types (ranging from barren land to dense forest). We also use a hydrological model, ArcSWAT, an ArcGIS extension of the Soil and Water Assessment Tool (SWAT), to generate surface runoff in the study areas to validate LEM results.

3.1. Data used for model setup and simulations

The datasets used for setting up Landlab simulations include present-day digital elevation models (DEMs) for initial topography, daily precipitation and evapotranspiration data (1982 - 2019), and land use land cover (LULC) maps. We also use a soil classification map (HWSD) in conjunction with the above datasets for SWAT simulations.

We use Space Radar Topography Mission (SRTM) DEM version 3.0, at a 1-Arc-second (30 m) spatial resolution (Earth Resources Observation And Science (EROS) Center, 2017), clipped in rectangular shapes encapsulating the catchment areas (Fig. 1), as initial topography in both Landlab and SWAT simulations. The catchment (model domain) sizes range from ~6.74 km^2 in Nahuelbuta (humid-temperate) to ~20.7 km^2 (~500 m) in Santa Gracia (semi-arid) (see Table. 1). As we use finer grids (30 m * 30 m) in the model domain to capture high-intensity events during shorter time steps (daily), smaller sub-catchments are analyzed in this study to compensate for the computational expense of LEM simulations.

The daily precipitation data [mm day^{-1}] (01/01/1982 – 31/12/2019) was obtained from the Global Precipitation Climatology Centre (GPCC) (Ziese et al., 2020). The data has a spatial resolution of 1 degree (i.e., ~111 km). The precipitation frequency and intensity data used show an increase in precipitation from the north (Pan de Azúcar) to the south (Nahuelbuta) (Fig. 2). However, a significant number of days with high-intensity events occur in the northern arid region (Pan de Azúcar) and decrease to the southern humid temperate region (Nahuelbuta). This trend can be attributed to a more prominent influence of ENSO in the northern study areas (i.e., Pan de Azúcar and Santa Gracia). The evapotranspiration [mm day^{-1}] dataset (1982 – 2019) is obtained from the Global Land Evapotranspiration Model version 3 (GLEAM v3) (see Fig. A1), which applies the Priestly and Taylor equation to estimate potential evapotranspiration using observations of surface net radiations and near-surface temperature (Martens et al., 2017). The GLEAM estimates the evapotranspiration using multiplicative stress based on vegetation depth and soil moisture.

The soil database used for the SWAT model was obtained from the Harmonised World Soil Database (in SWAT format) (Abbaspour and Vaghefi, 2019). The dataset is prepared by the Food and Agricultural Organization of the United Nations (FAO) and the International Institute of Applied Systems Analysis (IIASA). It combines available regional and national soil information with the data contained in the FAO-UNESCO soil map and HWSD v_121 and soil hydrological parameters. The dataset has a spatial resolution of 30 arc seconds (1 km) and represents a maximum of 1 m soil depth (i.e., 30 cm topsoil layer and 70 cm sub-soil layer). It contains the information on soil texture (e.g., percentage of sand, silt, and clay), chemistry (e.g., organic carbon, electrical conductivity, and pH), and hydrological parameters (e.g., bulk density, soil water capacity, hydraulic conductivity, etc.) estimated using pedotransfer functions by Abbaspour et al. (2019).

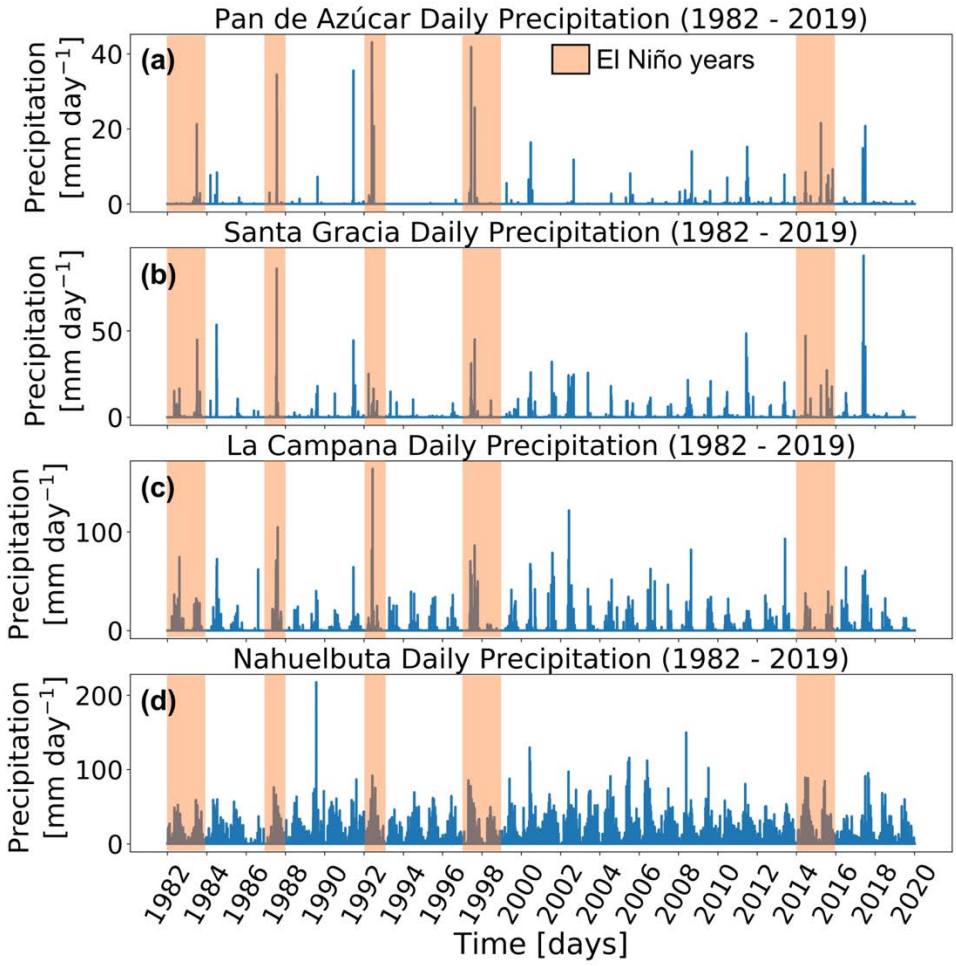

Figure 2. Observed precipitation rates [mm day^{-1}] for 1982 – 2019 obtained from GPCC Full Data Daily Product version (Ziese et al., 2020) in (a) arid – barren land (Pan de Azúcar), (b) semi-arid – grassland (Santa Gracia), (c) Mediterranean – shrubland (La Campana), and (d) humid temperate – dense forest (Nahuelbuta).

The LULC dataset is obtained from the European Space Agency (ESA) WorldCover 10 m 2020 product based on Sentinel-1 and 2 data and has a spatial resolution of 10 m (Zanaga et al., 2021). The

data is divided into 11 land cover classes aligned with the UN-FAO Land Cover Classification System. Our study areas are broadly divided into four landcover classifications, i.e., trees, shrubs, grass, and barren land (Fig. 3). The landcover classifications define Manning's number in each model cell based on the plant functional types (PFT). Manning's numbers for each PFT (Table. A1) are based on the approach of Kalyanapu et al. (2010). The catchments are broadly classified as barren (Pan de Azúcar), mixed grassland (Santa Gracia), shrubland (La Campana), and dense forest (Nahuelbuta). The LULC data is resampled to a spatial resolution of 30 m to match the DEM resolution (model cell size). However, the model is set up for ~4 decades of precipitation variability; we assume the same LULC classification for an entire model run, ignoring the dynamic vegetation growth in that period.

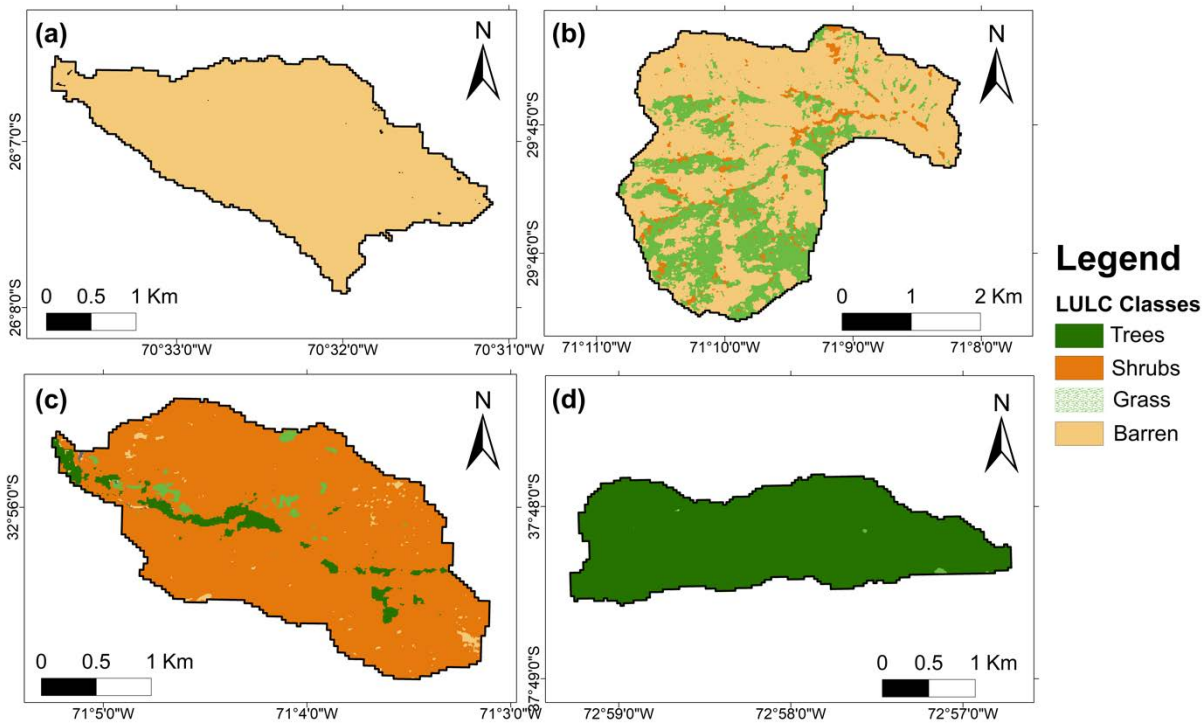

Figure 3. ESA Landcover dataset (2020) – PFT product (10 m spatial resolution), Landcover classes broadly classified into tree cover, shrubland, grassland, built-up area, and barren land (Zanaga et al., 2021) in (a) arid – barren land (Pan de Azúcar), (b) semi-arid – grassland (Santa Gracia), (c) Mediterranean – shrubland (La Campana), and (d) humid temperate – dense forest (Nahuelbuta).

3.2. Model Setup

This section describes the model setups and input parameters for the landscape evolution model (Landlab-SAPCE) and hydrological model (ArcSWAT).

3.2.1. Landscape evolution model – Landlab-SPACE setup

The model domain consists of rectangular grids with catchment sizes varying from ~7 km^2 to ~21 km^2 (based on the modern-day DEM) and experiences a constant uplift rate of 1.37×10^{-7} mm day^{-1} (or 0.05 mm yr^{-1}). We use the two-dimensional, python-based landscape evolution model, LandLab (Hobley et al., 2017), which allows coupling of detachment-transport limited fluvial processes (Shobe et al., 2017), hillslope diffusion (Johnstone and Hilley, 2014), flow accumulation (Braun and Willett, 2013), evapotranspiration (Martens et al., 2017), and soil-water infiltration (Green and Ampt, 1911) modules (Fig. 4a). The simulations are designed to capture the erosion response of temporally constant land cover distribution (Zanaga et al., 2021) to variable precipitation input (1982 – 2019) (Ziese et al., 2020) at daily time steps. The precipitation is subjected to evapotranspiration and soil-water infiltration, depending on the infiltration capacity of the sediment layer and surface water available in each model cell at each model time-step. The model parameters are calibrated to the distinct climate and ecological settings in the Chilean Coastal Cordillera observations of Schaller et al. (2018), which have predominantly granitoid lithology (Kojima et al., 2017; Rossel et al., 2018; Oeser et al., 2018). The model state parameters (i.e., erosion, diffusion, lithological, tectonic, etc.) in the simulations are adapted from Sharma et al. (2021). The model parameters with respective units and references are illustrated in Table A1. The combined effects of daily precipitation variations and vegetation cover and type on catchment-scale erosion rates are simulated in the model. The (area-normalized) surface water discharge rates at the catchment outlet obtained from Landlab are cross-checked with the predictions of the SWAT hydrological model for validation of the results.

The land cover classification defines Manning's roughness coefficients based on plant functional types (PFT) (see table A1). These Manning's numbers are hence used to estimate the modified bedrock and sediment erodibilities, using the approach of Sharma et al. (2021). Also, we use the mean vegetation cover fraction in the entire model domain to estimate the vegetation-dependent diffusion coefficient (for hillslope processes), using the approach of Istanbulluoglu and Bras (2005) and Schmid et al. (2018).

Simulations were conducted for 1,900 years (38 years of precipitation and ET input repeated over 50 times). We did this to tap long-term transients in the model results arising due to the choice of model parameters (e.g., erosivity, uplift rates), which are likely not the same resulting in the present-day topography. We conducted a linear detrending of the results for the correction of any long-term

transients in erosion rates. Hence, the model results' last 38 years (detrended) were analyzed and discussed in sections 4 and 5.

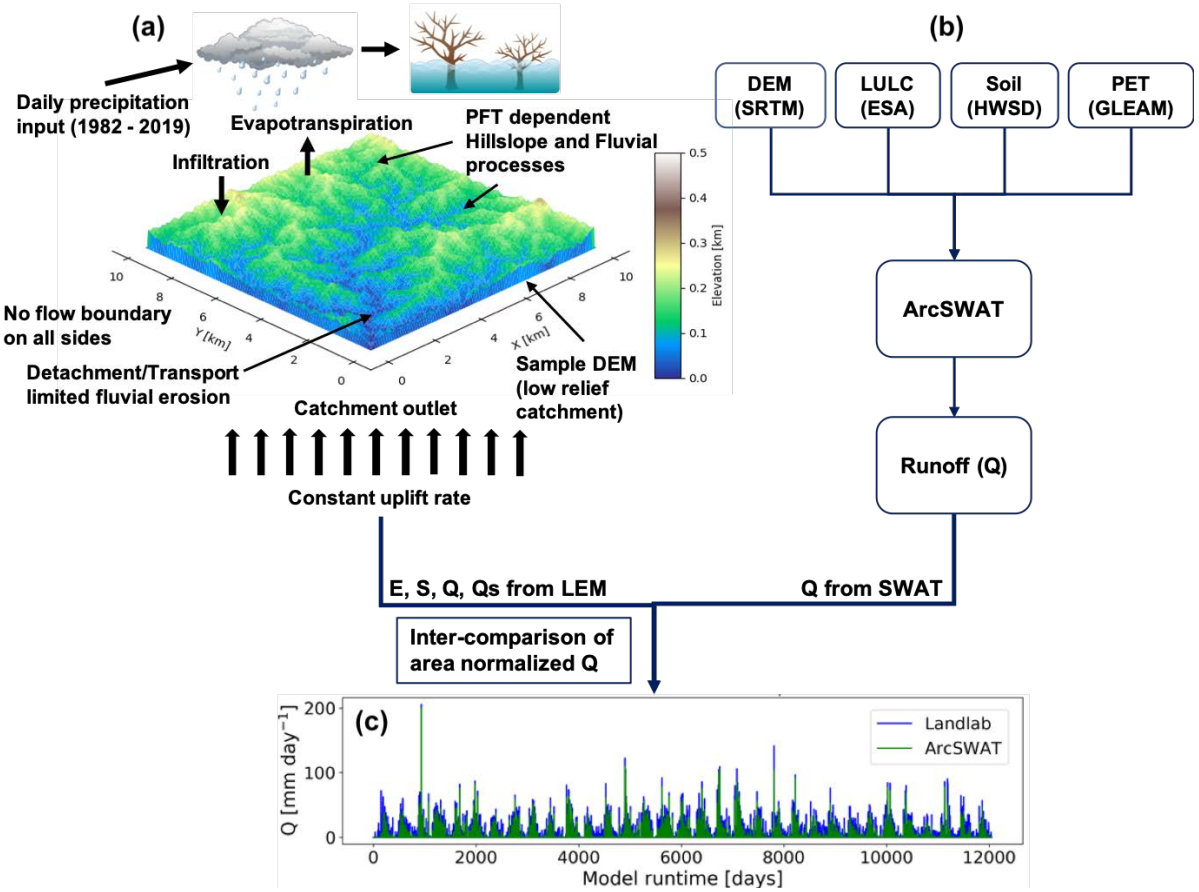

Figure 4. Model setup for (a) Landscape evolution model (Landlab) with no flow boundaries on all sides and a single catchment outlet. Daily precipitation and annual Landcover datasets (PFT distribution) are used as input parameters. The model experiences constant rock uplift rates, infiltration, evapotranspiration, and PFT-dependent hillslope and fluvial processes. (b) Hydrological model (ArcSWAT), with digital elevation model (DEM), land use land cover (LULC) obtained from European Space Agency (ESA) (Zanaga et al., 2021), soil dataset obtained from Harmonised World soil Database (HWSD) (Abbaspour and Vaghefi, 2019), and potential evapotranspiration (PET) obtained from Global Land Evapotranspiration Model (GLEAM v3) (Martens et al., 2017) as input parameters to calculate surface water discharge rates. (c) Sample plot showing inter-comparison of surface water discharge rates (normalized by catchment area) obtained from LEM and Hydrological model for correlation of model outputs.

3.2.2. Hydrological model – ArcSWAT setup

ArcSWAT is the ArcView extension of the Soil and Water Assessment Tool (SWAT). SWAT is a physically-based, semi-distributed hydrological model based on the water balance concept. Catchment processes, including runoff, evapotranspiration, sediment, nutrient transport, and crop growth, are simulated based on topographical, meteorological, soil, and land cover data (Winchell et al., 2013). The model is developed to predict the impact of land management practices on water, sediment, and agricultural sediment yields in large and complex watersheds with varying soil and land cover over long periods (Arnold et al., 1998). It is a computationally efficient model enabling the study of long-term impacts. However, it is a continuous-time model and is not designed to simulate detailed, single event flood routing.

A watershed is discretized into several sub-basins to enhance accuracy and provide a better physical description of the water balance. Input information for each sub-basin is grouped into different categories, i.e., climate, hydrologic response units (HRUs), groundwater, and main channel (reach) draining the sub-basin. Each HRU contains a unique combination of land cover, soil type, and topographic slope. Surface runoff is predicted for each HRU and routed to obtain total runoff for the watershed.

We use current topography (same as LEM) in the SWAT model to define the flow routing and stream network. We further define the catchment outlet (same as LEM, see section 3.2.1) to delineate the catchment geometry. The model input includes meteorological data, land cover and soil classification, and potential evapotranspiration (Fig. 4b). The meteorological data includes weather station precipitation observations at daily time steps (Ziese et al., 2020). The land covers were classified into four categories, i.e., trees, shrubs, grasses, and barren land (Zanaga et al., 2021). Soil classification data (compatible with SWAT) was obtained from Harmonized World Soil Database (HWSD_v121) (Abbaspour and Vaghefi, 2019). The potential evapotranspiration (PET), estimated using the Priestly and Taylor method (Priestley and Taylor, 1972) obtained from GLEAM v3 (Martens et al., 2017), is used as the input parameter to estimate actual ET. This is as per the ET obtained from the same dataset (see section 3.2.1) used in the Landlab LEM. The model spins up for the first five years of the simulation run. Hence, the results for 33 years (1987 – 2019) are used for analysis. SWAT provides a variety of outputs; however, we only analyze surface water discharge rates to validate LEM results.

3.2.3. Correlation of Landlab and SWAT output

The resultant (area normalized) surface water discharge rates ($Q_{LANDLAB}$) at catchment outlet obtained from Landlab-LEM simulations are compared and correlated with the (area normalized) surface runoff (Q_{SWAT}) obtained from SWAT simulations to validate the model results (Fig. 4c) in

section 5.3. We normalized the runoff rates by catchment area, as Landlab is simulated over the entire rectangular domain encompassing the catchment shape. However, SWAT is simulated specifically over delineated catchment (ignoring areas outside the catchment). Therefore, it is required to remove the area effects to correlate the model outputs efficiently.

3.3. Boundary and initial conditions

The LEM and hydrological model domains consist of the topography with no-flow boundaries on each side and a single catchment outlet. In LEM, initial sediment cover thickness and soil moisture content are considered uniform across the model domain. These are based on the observations of Schaller et al. (2018) and weather station data (Übernickel et al., 2020), respectively, which are 20 cm (0.06 m^3 m^{-3}) in barren land (AZ), 45 cm (0.02 m^3 m^{-3}) in grassland (SG), 60 cm (0.05 m^3 m^{-3}) in shrubland (LC), and 70 cm (0.15 m^3 m^{-3}) in dense-forest (NA). The initial rock uplift rate is kept constant throughout the entire model run as 0.05 mm yr^{-1}, adapted from a similar study (Sharma et al., 2021).

4 Results

This section includes a delineation of days with probable flood events from 1982 to 2019, with particular emphasis on El Niño events in the regions of northern catchments, i.e., Pan de Azúcar (~26 °S) and Santa Gracia (~29 °S). It is followed by representing erosion rates obtained from PFT-dependent Landlab LEM. Lastly, we present together the surface water discharge rates obtained from LEM (Landlab) and hydrological model (SWAT) for inter-comparison of results from both models.

4.1. Delineation of days with probable flood events

This section defines the precipitation threshold to delineate the days when probable flood event(s) would have occurred. Various methods are available to trace flood events (e.g., Santos and Fragoso, 2016; Norbiato et al., 2008). However, for simplification, the flood threshold is defined as half of the maximum precipitation amount in the entire precipitation record (i.e., 1982 – 2019) for all four catchments. The flooded day thresholds are estimated as 21.5 mm d^{-1}, 46.8 mm d^{-1}, 82 mm d^{-1}, and 108.8 mm d^{-1} for Pan de Azúcar, Santa Gracia, La Campana, and Nahuelbuta, respectively. We observe a maximum number of probable days with flood events in Pan de Azúcar (9 days), followed by La Campana and Nahuelbuta (7 days) and Santa Gracia (6 days) (Fig. 5).

The number of days with probable flood events during El Niño years for northern regions (Pan de Azúcar and Santa Gracia) are shown in Table 2. We observed that all of the flood events (delineated above) in northern catchments occurred during ENSO periods in South America (Cai et al., 2020) in the northernmost region (Pan de Azúcar). Also, five out of six flood events in Santa Gracia occurred during

ENSO periods, except a recent event (Autumn – 2017) with precipitation of ~94 mm day^{-1}, which is 22 mm higher than the MAP (i.e., 72 mm) in this region.

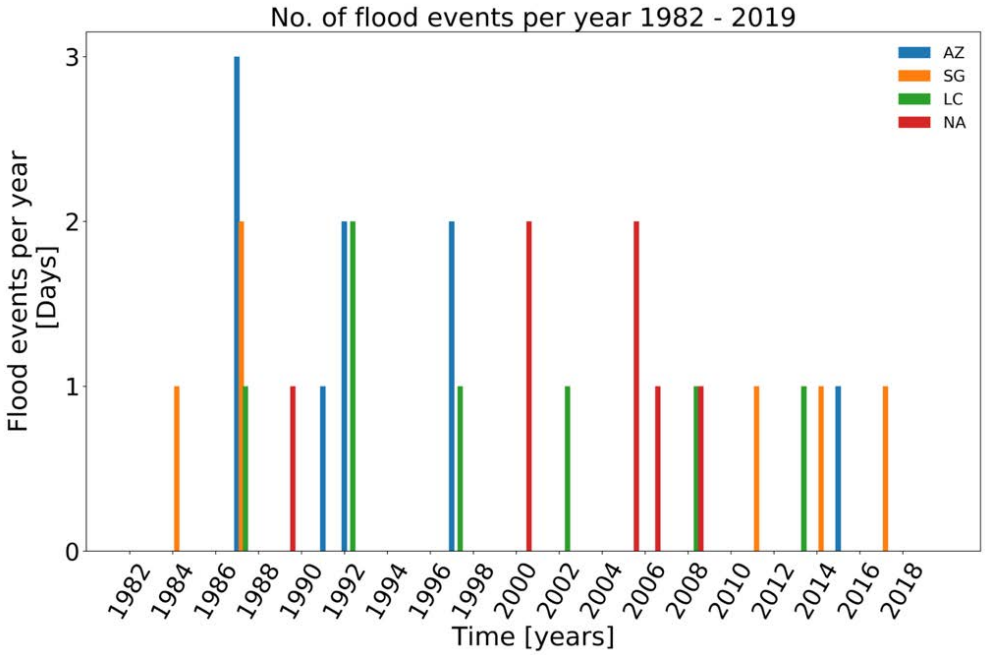

Figure 5. The number of extreme events per year between 1982 – 2019, based on the thresholds of half magnitude of maximum precipitation event in (a) arid - barren land (AZ), (b) semi-arid - grassland (SG), (c) Mediterranean - shrubland (LC), and (d) humid temperate - dense forest (NA).

Table 2. Number of days with probable events in Pan de Azúcar and Santa Gracia during El Niño years (1982 – 2019).

El Niño years	Pan de Azúcar (26 °S)	Santa Gracia (29 °S)
1982	-	-
1983	1 (Winter)	1 (Winter)
1987	3 (Winter)	2 (Winter)
1992	2 (Autumn)	-
1997	2 (Autumn)	1 (Winter)
1998	-	-
2014	-	1 (Winter)
2015	1 (Autmn)	-

* Flood events in La Campana and Nahuelbuta do not have corresponding effects due to ENSO effects

4.2. Effect of variable precipitation rates on erosion rates using Landlab LEM

Variations in daily precipitation rates (1982 – 2019) are explored here (Fig. 2), with constant land cover distribution simulated to observe the pattern in erosion rates. The range of precipitation rates (and PFT distribution) is 0 – 43 mm day^{-1} (mostly barren), 0 – 94 mm day^{-1} (grassland), 0 – 164 mm day^{-1} (mixed shrubland), and 0 - 217 mm day^{-1} (dense forest) in Pan de Azúcar, Santa Gracia, La Campana, and Nahuelbuta, respectively.

The mean catchment daily erosion rates are observed in the range of $0 - 6.25 \times 10^{-3}$ mm day^{-1}, $0 - 1.75 \times 10^{-2}$ mm day^{-1}, $0 - 5.17 \times 10^{-3}$ mm day^{-1}, and $0 - 3.1 \times 10^{-3}$ mm day^{-1} in Pan de Azúcar, Santa Gracia, La Campana, and Nahuelbuta, respectively. Mean catchment daily erosion rates are observed linearly with precipitation rates (Fig. 6a), with a higher gradient in the semi-arid region (SG, gradient: ~2.1×10^{-4}). The slopes in the precipitation – erosion rate relationship represent the sensitivity of each catchment to variable daily precipitation rates. It indicates that the semi-arid region (SG) is 19%, 84%, and 93% more sensitive than arid (AZ), Mediterranean (LC), and humid-temperate area (NA), respectively. However, during the days with possible flood events, slopes in the erosion – precipitation relationship (Fig. 6b) indicate that catchment erosion in the arid catchment is 14%, 86%, and 93% more sensitive than semi-arid, Mediterranean, and humid temperate catchments, respectively.

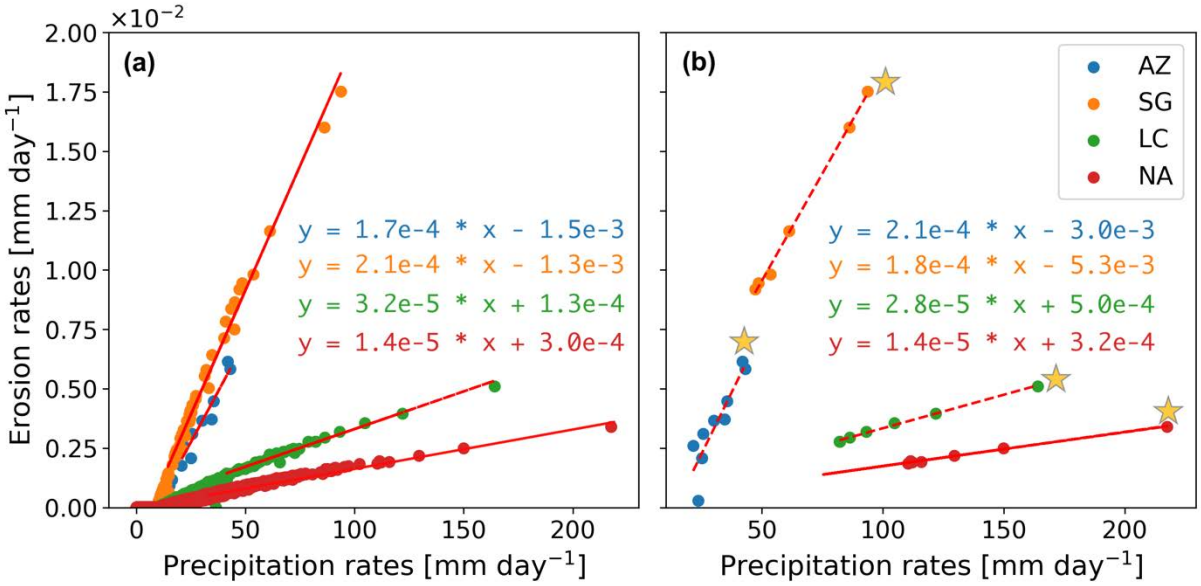

Figure 6. Relation of precipitation rates [mm day^{-1}] and erosion rates [mm day^{-1}] in study areas, obtained from simulations with variable daily precipitation and constant plant functional type distribution for (a) the last cycle of the transient state model run (1982 – 2019) and (b) delineated extreme events between 1982 and 2019.

4.3. Discharge rates from LEM (Landlab) and hydrological model (SWAT)

This section presents the surface water discharge rates normalized by catchment area [mm day^{-1}] obtained from the SWAT and the last iteration of Landlab simulations with variable daily precipitation (Fig. 7). We do this to compare the efficacy of our LEM results with that of a hydrological model over a short time scale (33 years). The results from both models are compared for the precipitation input of 1987 – 2019, as SWAT uses the first five years of a simulation run for model spin-up.

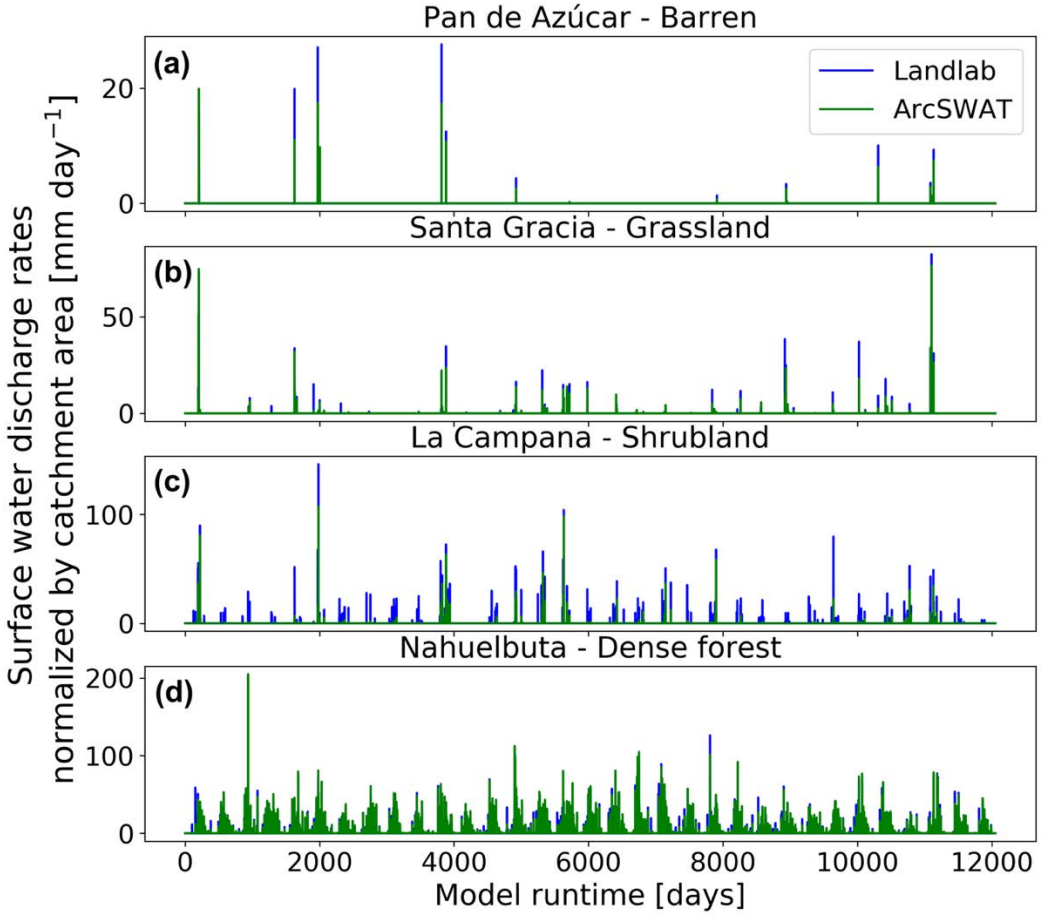

Figure 7. Surface water discharge rates normalized by catchment area, Q_n [mm day^{-1}] obtained from SWAT and Landlab model simulations, plotted against model runtime with ground-based precipitation input (1987 – 2019) for the catchments in (a) arid – barren land (Pan de Azúcar), (b) semi-arid – grassland (Santa Gracia), (c) Mediterranean – shrubland (La Campana), and (d) humid temperate – dense forest (Nahuelbuta).

We observe relatively lower surface water discharge rates in SWAT simulation results than that of Landlab. The Landlab derived surface water discharges are observed in the range of $0 - 29.4$ mm day^{-1}, $0 - 82.3$ mm day^{-1}, $0 - 148.8$ mm day^{-1}, and $0 - 197.2$ mm day^{-1} in Pan de Azúcar (Fig. 7a), Santa Gracia (Fig. 7b), La Campana (Fig. 7c) and Nahuelbuta (Fig. 7d), respectively. At the same time, SWAT-derived discharge rates deviate negatively from Landlab results for the northern three

catchments (Fig. 7a, b, and c) but fit well in the southern catchment (Fig. 7d). For example, the maximum SWAT derived (area-normalized) discharge rates are 32%, 6.5%, and 28% lower than Landlab output in Pan de Azúcar, Santa Gracia, and La Campana, respectively. However, in Nahuelbuta, we observe ~4% higher surface discharge rates in SWAT results.

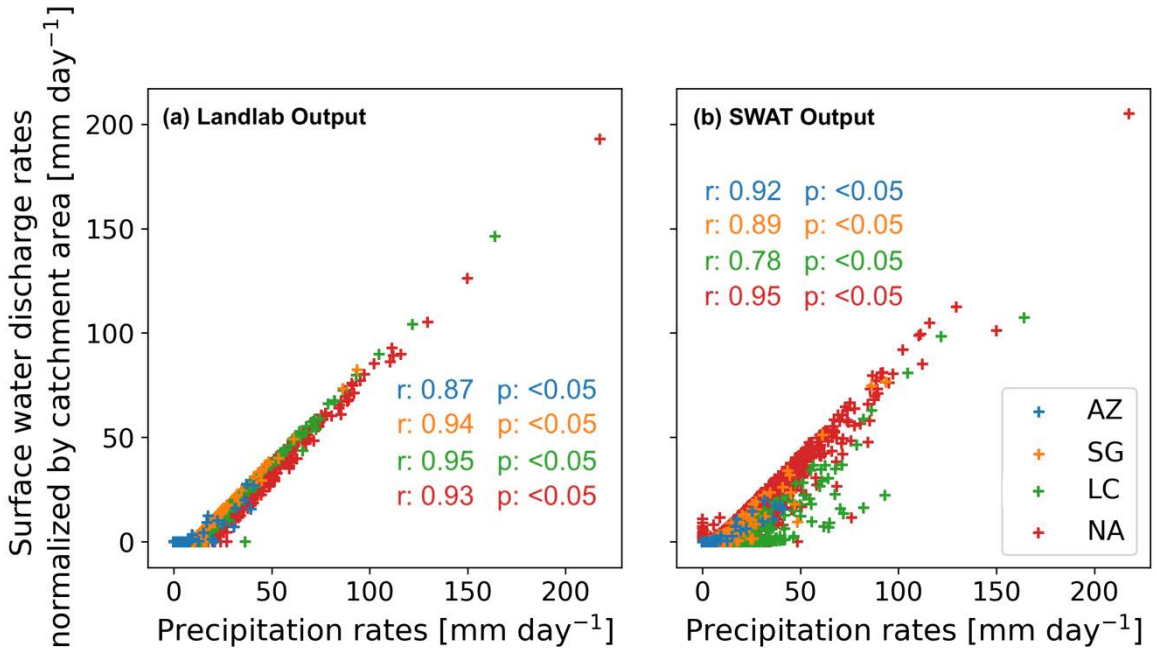

Figure 8. Catchment outlet (daily) surface water discharge rates [mm day^{-1}] in study areas, normalized by catchment area for (a) Landlab-SPACE simulations and (b) ArcSWAT simulations during 1982 – 2019.

The area-normalized surface water discharge rates [mm day^{-1}] obtained from Landlab and SWAT model simulations are plotted against the precipitation rates in Figures 8a and 8b. A linear response is observed in the results from both models; however, in SWAT results, the discharge rates are rather more scattered. Also, we find significantly lower surface water discharge rates in La Campana in SWAT simulation results. This is owing to higher simulated soil water infiltration and evapotranspiration in this catchment due to differences in the implementation of geomorphic and weather-related processes in both models.

5 Discussion

This section discusses the amplitude of change in erosion rates (due to daily precipitation variations) in the different land cover and climate settings (section 5.1). This is followed by analyzing the effect of extreme precipitation events on spatial changes in erosion rates (section 5.2). Next, we compare the runoff estimates from the Landlab-SPACE landscape evolution model and the SWAT hydrological model (section 5.3). Lastly, we present the model limitations and outlook for future studies (section 5.4).

5.1. The amplitude of change in erosion rates in distinct land cover and climate settings

In this section, we discuss the amplitude of change in catchment erosion (in percentage) with respect to the daily means in the study areas with different land cover (PFT distribution) and climate settings, ranging from arid, barren land (Pan de Azúcar) to humid temperate dense-forest (Nahuelbuta) (Fig. 9). The amplitude of change in erosion rates to their respective mean values is represented as the coefficient of variation (Brown, 1998) in percentage (standard deviation divided by the mean of a dataset).

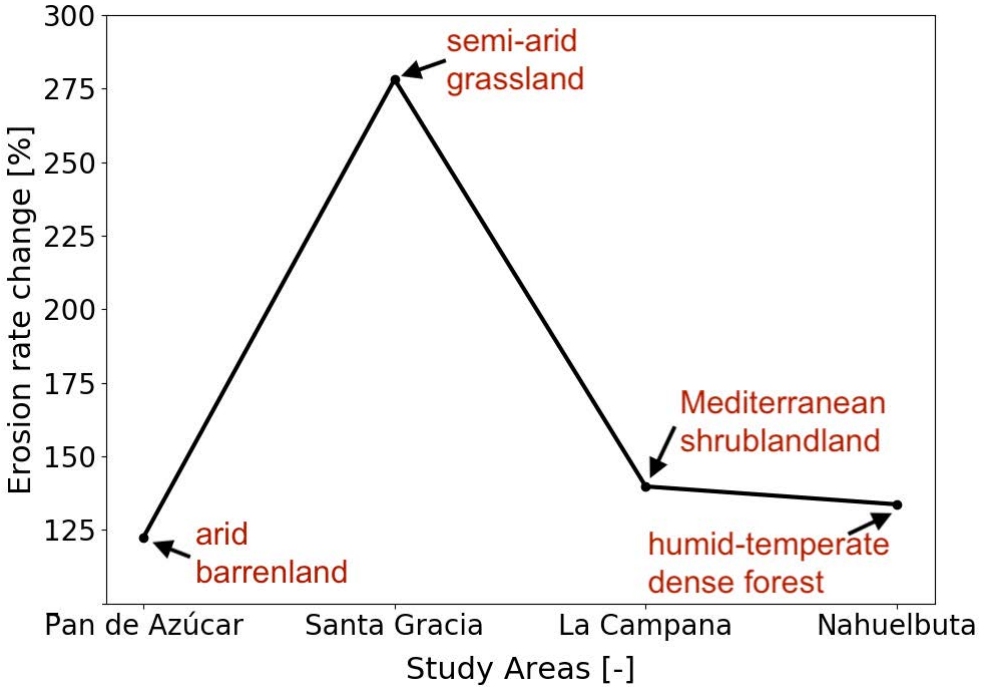

Figure 9. The amplitude of change in daily erosion rates (relative to their respective means) with variable precipitation rates (from 1982 to 2019) for the catchments in arid – barren land (Pan de Azúcar), semi-arid – grassland (Santa Gracia), Mediterranean – shrubland (La Campana), and humid temperate – dense forest (Nahuelbuta).

The minimum amplitude of change in erosion rates (with respect to mean) is observed in the catchment in an arid setting with mostly barren land (i.e., 122% in Pan de Azúcar). It increases significantly in the semi-arid setting (i.e., 278% in Santa Gracia) with a combination of barren land and ~29% grass cover. This abrupt increase in the amplitude of change in erosion rates is owed to a significant increase in precipitation magnitude (e.g., 43 to 94 mm day^{-1}) and marginal difference in vegetation cover (i.e., <10% to 20%) from the arid to the semi-arid setting. Also, the disproportional contribution of low frequency – high magnitude precipitation events leads to high variance in erosion rates, especially in arid and semi-arid regions (e.g., Brunsden and Thornes, 1979; Gonzalez-Hidalgo et al., 2009, 2010; Hooke and Mant, 2000). The catchments in the Mediterranean and humid temperate settings with extensive shrubs and tree cover (i.e., >90% vegetation cover) experience a moderate

change in erosion (i.e., 135 – 140%). The above changes in extensively vegetated catchments are still quite significant (e.g., >100%), owing to occasional flood events in these regions (see section 5.2). The above variability in erosion rates for different landcover types agrees with Garatuza-Payán et al. (2005), which used remote sensing techniques to investigate erosion rates in a semi-arid watershed. The above study found that >98% of the variance in erosion rates could be explained by vegetation type and height.

5.2. Analysis of the effect of maximum precipitation event on spatial changes in erosion rates

This section discusses the spatial distribution of erosion rate change (with respect to mean annual erosion rates per grid cell) during an extreme event (the day with maximum daily precipitation from 1982 to 2019) in the study areas. The catchment annual mean erosion rates (between 1982 and 2019) are in the range of $2.6 \times 10^{-7} - 0.04$ mm yr^{-1}, $1.4 \times 10^{-6} - 0.73$ mm yr^{-1}, $8 \times 10^{-7} - 1.2$ mm yr^{-1}, and $2 \times 10^{-7} - 1.9$ mm yr^{-1} in Pan de Azúcar, Santa Gracia, La Campana, and Nahuelbuta, respectively.

The maximum erosion rate change (i.e., ~0.6 mm day^{-1}) is visible in the semi-arid setting (Santa Gracia, Fig. 10b), with hillslope erosion ranging from 0.01 – 0.06 mm day^{-1}, with a catchment scale mean of ~0.02 mm day^{-1} for 94 mm day^{-1} precipitation rate. No significant hillslope processes are visible in the arid setting (Pan de Azúcar, Fig. 10a) due to lower relief in Pan de Azúcar with a maximum erosion change of ~0.5 mm day^{-1} and a moderate catchment mean of ~0.005 mm day^{-1}. In the Mediterranean setting (La Campana, Fig. 10c) and humid temperate setting (Nahuelbuta, Fig. 10d), the erosion rate changes are relatively much lower (<0.02 mm day^{-1}), and the catchment means are estimated as ~0.004 mm day^{-1} due to the flow resistance provided by extensive vegetation cover. Also, hillslope erosion is negligible in La Campana and Nahuelbuta, owing to vegetation-stabilized slopes in these catchments. In addition, sedimentation of up to ~1.5 mm day^{-1} is observed in the higher-order stream in Nahuelbuta, despite a heavy precipitation amount of 217 mm day^{-1}.

Significant erosion rate changes are attributed to fluvial processes in the study areas. For example, maximum erosion change (~0.5 – 0.6 mm day^{-1}) is observed in higher-order streams in Pan de Azúcar and Santa Gracia (see Fig. 10a and 10b). This occurs when shear stress exceeds the critical stream power to initiate erosion during the extreme precipitation events (Snyder et al., 2003). Overall, we observe a decreasing effect of precipitation on catchment erosion from arid and semi-arid settings (comprising barren land and grasses) to the Mediterranean and humid temperate settings (with shrubs and extensive tree cover). For example, the precipitation magnitude during extreme events increases from 94 – 217 mm day^{-1} from semi-arid to humid temperate settings, with decreasing (catchment mean) erosion rates from 0.02 – 0.004 mm day^{-1}. The above observations align with the broader findings of Baartman et al. (2013), which compared an event-based erosion model to a LEM and suggested that land cover change may significantly impact erosion dynamics over climate variability.

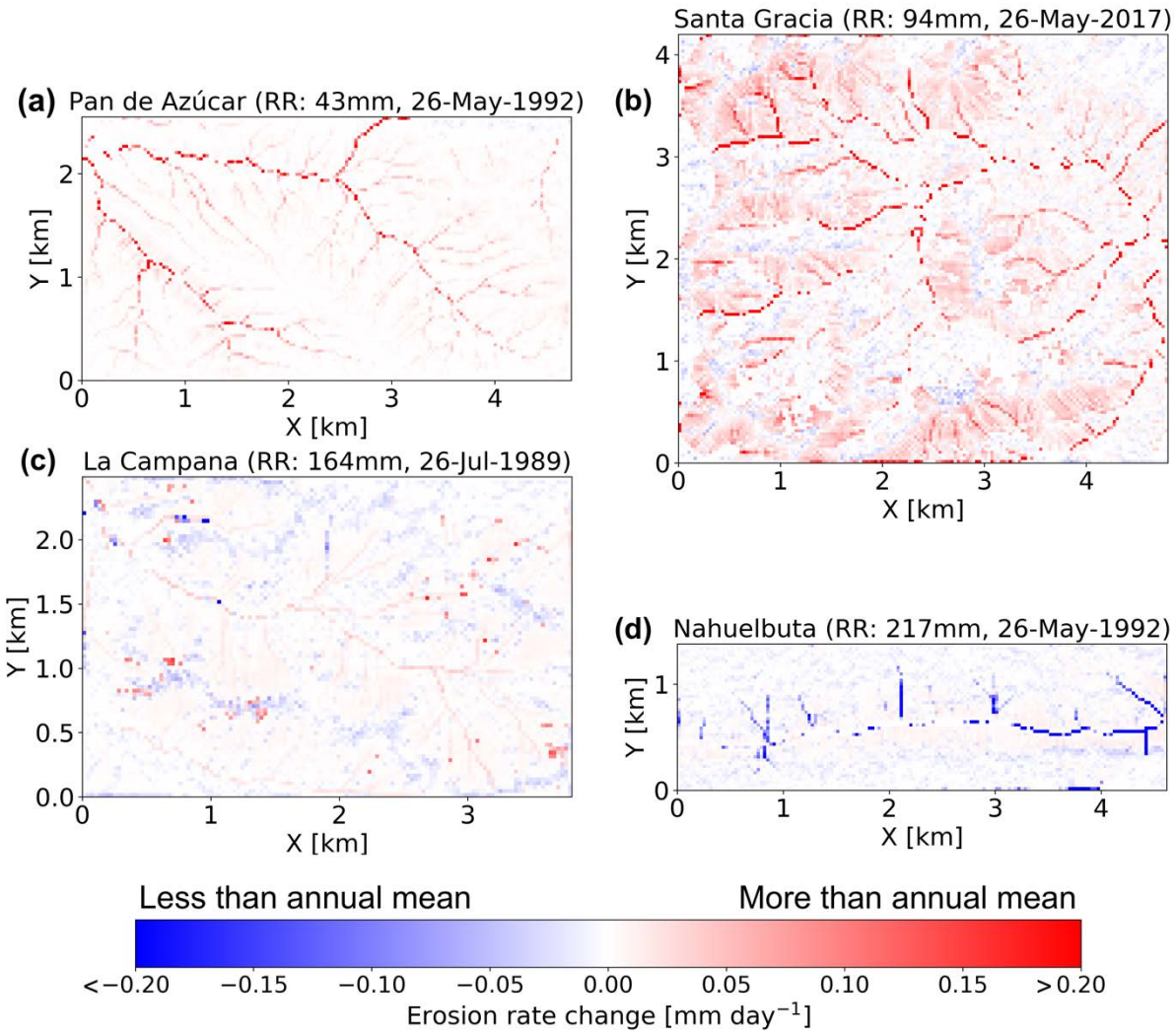

Figure 10. Changes in erosion rates (with respect to annual means per grid cell) occurred during the day with maximum precipitation events for the catchments in (a) arid - barren land (Pan de Azúcar), (b) semi-arid - grassland (Santa Gracia), (c) Mediterranean - shrubland (La Campana), and (d) humid temperate - dense forest (Nahuelbuta).

5.3. Comparison of discharge estimates from LEM and hydrological model

Due to the lack of observations of surface water discharge rates in the selected study areas required to validate LEM (LandLab) output, we compare the LEM output with that of a physically-based hydrological model (SWAT). Both models utilize the same topographical, LULC, and meteorological datasets to minimize the ambiguity in their outputs. To do this, we conducted a correlation of results from the LEM (Landlab) and the hydrological (SWAT) models to evaluate the validity of Landlab at daily time steps. We do this statistically by estimating the Pearson's correlation coefficient (PCC) between the surface water discharge rates normalized by catchment area (Fig. 12), obtained from Landlab and SWAT simulations for precipitation input from 1987 to 2019. The PCC (also known as Pearson' r) is a statistical tool to measure the linear correlation between two datasets with the same population size (Benesty et al., 2009). It is a ratio between the covariance of two variables and the

product of their standard deviations ranging between -1 and 1, with negative values denoting a negative correlation and vice versa for positive values.

We observe a strong positive correlation (Pearson r: >0.8) with low standard error (<0.003) in Landlab and SWAT derived (area normalized) surface water discharge rates in all the catchments, at >95% significance level. This indicates the applicability of Landlab LEM at smaller (daily) time steps to incorporate the significant erosion rates due to extreme precipitation events in long-term landscape evolution. The differences in discharge rates are owed to the difference in implementation of water balance modules (runoff generation and flow routing) in both models.

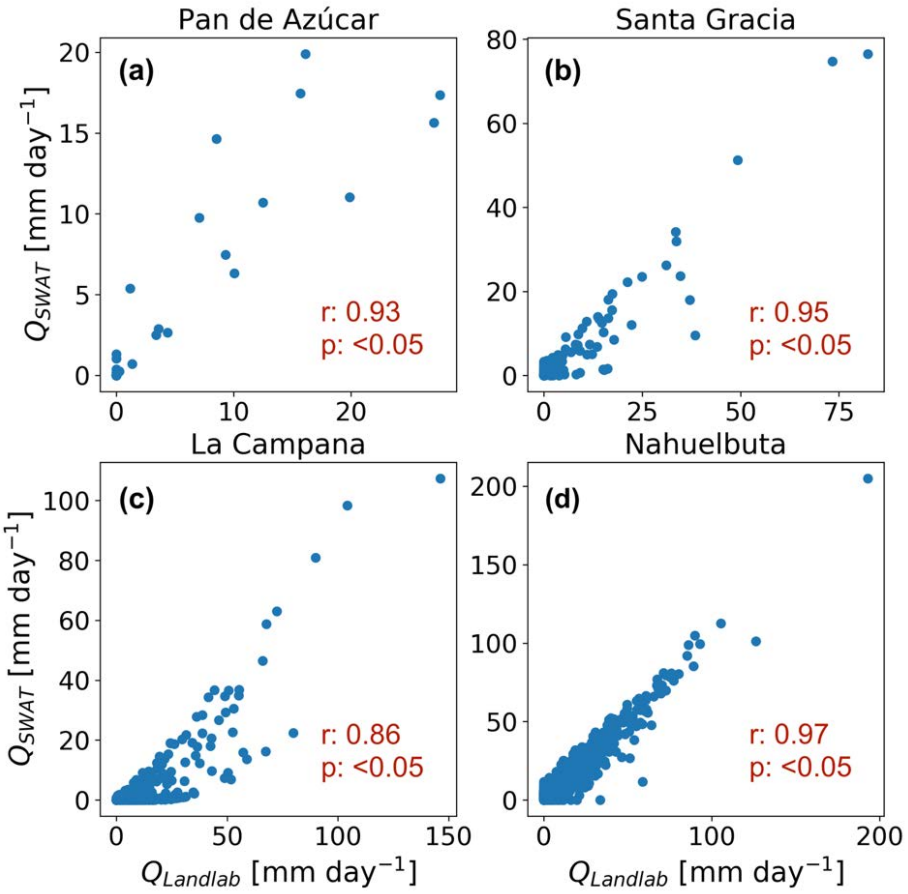

Figure 11. Correlation between surface water discharge rates normalized by catchment area, obtained from landscape evolution model (Landlab) ($Q_{LANDLAB}$) and hydrological model (SWAT) simulations (Q_{SWAT}) for the catchments in (a) arid – barren land (Pan de Azúcar), (b) semi-arid – grassland (Santa Gracia), (c) Mediterranean – shrubland (La Campana), and (d) humid temperate – dense forest (Nahuelbuta).

6 Summary and Conclusions

This study quantified daily precipitation changes in erosion rates for selected catchments in the Chilean Coastal Cordillera. Latitudinally varying land cover distributions were broadly classified as barren, grassland, shrubland, and forest (from north to south). We modified the Landlab LEM to account for PFT-dependent fluvial erosion (based on Manning's roughness coefficients for different PFTs) and vegetation-dependent hillslope diffusion (based on vegetation cover fraction in the entire catchment). We also performed simple hydrological model simulations with the SWAT model, with soil and modeled PET datasets to validate the LEM results. The results (surface water discharge rates normalized by area) from both LEM and hydrological models were correlated using the Pearson correlation coefficient. The main conclusions derived from this study are as follows:

1. Despite experiencing lower precipitation, catchments in the north (i.e., Pan de Azúcar and Santa Gracia) experience a maximum number of days (e.g., nine events in Pan de Azúcar between 1982 and 2019) with extreme precipitation events (See Fig. 5). The majority of these days correspond to low frequency and high magnitude El Nino events (see Table. 2).
2. Concerning the first hypothesis stated in the introduction, we found that the catchment erosion in the grassland with 30% vegetation cover (i.e., Santa Gracia, semi-arid setting) is 9%, 84%, and 93% more sensitive than in barren land (Pan de Azúcar, arid setting), shrubland (La Campana, Mediterranean setting), and dense forest (Nahuelbuta, humid temperate setting), respectively. The sensitivity of catchment erosion is defined as the slope of precipitation and erosion curve (see Fig. 6). This finding confirms the hypothesis. Also, this high sensitivity of northern catchments (Pan de Azúcar and Santa Gracia) is owed to the sparse vegetation and low frequency – high magnitude precipitation events during El Niño years (Table. 2).
3. The amplitude of change in catchment erosion (at daily timescale), with respect to the mean values, is minimum in barren land (arid setting) and increases abruptly in the grassland (semi-arid setting), with moderate change in the shrubland (Mediterranean setting) and dense forest (humid temperate setting). For example, the amplitude of erosion changes ranges from 122 % in the catchment in arid (i.e., Pan de Azúcar) to 278 % in semi-arid (i.e., Santa Gracia) settings and decreases in the Mediterranean (i.e., 140 % in La Campana) and humid temperate (i.e., 134 % in Nahuelbuta) settings. Although the erosion changes in wetter catchments are relatively lower than in drier catchments but are still significant (130 – 140 %) to leave a signal in the landscape evolution.
4. Regarding the second hypothesis, we found a strong positive correlation (Pearson $r > 0.8$ and $r < 0.05$) in surface water discharge rates (normalized by domain area) obtained from LEM (Landlab) and hydrological model (SWAT). This yields the applicability of Landlab-SPACE LEM at shorter time scales (e.g., daily time-step). However, the differences in Landlab and SWAT model results are inevitable due to the difference in implementation of both models' erosion and runoff routines.

Taken together, we conclude that LULC distribution (including vegetation cover and type) poses the first-order control (over precipitation magnitude) on catchment erosion during extreme precipitation events. However, these short-term events have the potential to leave a signature in the landscapes with >100 % amplitude of change (with respect to mean) in catchment erosion in all the LULC and climate settings. These events are often surpassed in long-term landscape evolution models, and hence temporal downscaling introduces a more realistic representation of the landscape's sediment dynamics. Landlab, despite being a complex LEM, efficiently simulated the runoff rates comparable with that of a physically-based hydrological model (SWAT). However, modern topography (in a transient state) is preferred over steady-state conditions in such applications. In that case, some transients in the model results are expected, as the model parameters (rock uplift rate, erodibility, etc.) are usually not the same, which produced the modern-day topography.

Appendix

Table A1. Input parameters with corresponding units for the landscape evolution model

Model Parameters	Values
Grid spacing (dx)	30 [m]
Model runtime (totalT)	1900 [years] (1982 – 2019 repeated over 50 times)
time-step (dt)	1 [day]
Rock uplift rate (U)[1]	1.37×10^{-7} [m day^{-1}] (or 0.05 [mm a^{-1}])
Initial sediment thickness (H_initial)[2]	20 (AZ), 0.45 (SG), 0.6 (LC), 0.7 (NA) [cm]
Bedrock erodibility (Kr)[1]	2×10^{-9} [m^{-1}]
Sediment erodibility (Ks)[1]	2×10^{-8} [m^{-1}]
Reach scale bedrock roughness (H*)[1]	1 [m]
Porosity (φ)[1]	0.2 [-]
Fraction of fine sediments (Ff)[1]	0.2 [-]
Effective terminal settling velocity (Vs)[1]	0.024 [m day^{-1}]
m, n[1]	0.6, 1 [-]
Bedrock erosion threshold stream power (ω_cr)[1]	1.37×10^{-5} [m day^{-1}]
Sed. entr. threshold stream power (ω_cs)[1]	1.37×10^{-6} [m day^{-1}]
Bare soil diffusivity (K_b)[1]	2.74×10^{-5} [m^2 day^{-1}]
Exponential decay coefficient (α)[1]	0.3 [-]
Critical channel formation area (A_{crit})[1]	1×10^{6} [m^2]
Manning's number for barren land[3]	0.01 [-]
Manning's number for grasses[3]	0.35 [-]
Manning's number for shrubs[3]	0.4 [-]
Manning's number for trees[3]	0.4 [-]
Hydraulic conductivity (K)	1×10^{-6} [m s^{-1}]
Soil bulk density (B)[4]	1300 (AZ), 1500 (SG), 1300 (LC), 800 (NA) [kg m^{-3}]
Soil type[4]	sandy loam (AZ, SG, LC); sandy clay loam (NA)
Initial soil moisture (s)[4]	0.058 (AZ), 0.02 (SG), 0.053 (LC), 0.15 (NA) [m^3 m^{-3}]

[1] Sharma et al. (2021), [2] Schaller et al. (2018), [3] Kalyanapu et al. (2010), [4] Bernhard et al. (2018).

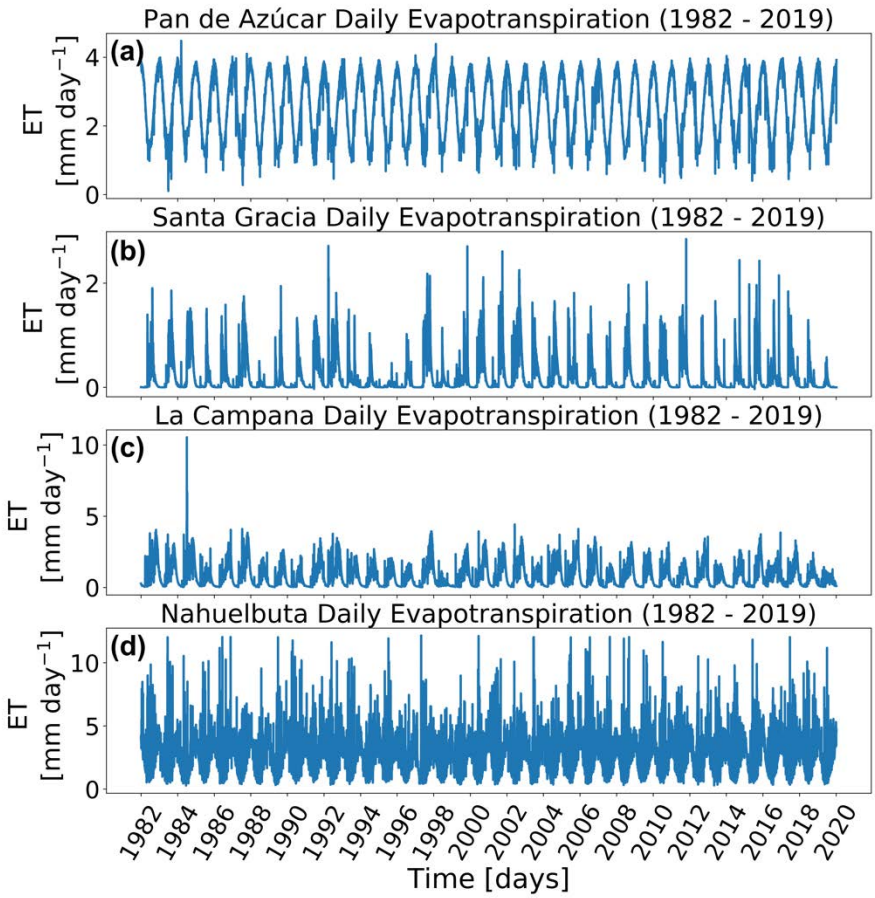

Figure A1. Evapotranspiration rates [mm day^{-1}] for 1982 – 2019 were obtained from Global Land Evaporation Amsterdam Model version-3 (Martens et al., 2017) in (a) arid – barren land (Pan de Azúcar), (b) semi-arid – grassland (Santa Gracia), (c) Mediterranean – shrubland (La Campana), and (d) humid temperate – dense forest (Nahuelbuta).

Acknowledgments

Hemanti Sharma and Todd A. Ehlers acknowledge support from the Open Access Publishing Fund of the University of Tübingen. We also acknowledge support from the Research Training Group 1829 Integrated Hydrosystem Modelling, funded by the German Research Foundation (DFG). In addition, Todd A. Ehlers acknowledges support from the German priority research program “EarthShape: Earth Surface Shaping by Biota” (SPP-1803; EH329/14-2). We thank xxx and yyy for their constructive reviews.

References

Abbaspour, K. and Vaghefi, S.A.: Harmonized World Soil Database in SWAT Format, https://doi.org/10.1594/PANGAEA.901309, 2019.

Abbaspour, K. C., Vaghefi, S.A., Yang, H., and Srinivasan, R.: Global soil, landuse, evapotranspiration, historical and future weather databases for SWAT Applications, Sci. Data, 6, 263, https://doi.org/10.1038/s41597-019-0282-4, 2019.

Arnold, J. G., Srinivasan, R., Muttiah, R. S., and Williams, J. R.: LARGE AREA HYDROLOGIC MODELING AND ASSESSMENT PART I: MODEL DEVELOPMENT1, JAWRA J. Am. Water Resour. Assoc., 34, 73–89, https://doi.org/10.1111/j.1752-1688.1998.tb05961.x, 1998.

Baartman, J. E. M., Temme, A. J. A. M., Veldkamp, T., Jetten, V. G., and Schoorl, J. M.: Exploring the role of rainfall variability and extreme events in long-term landscape development, CATENA, 109, 25–38, https://doi.org/10.1016/j.catena.2013.05.003, 2013.

Bates, P. D. and De Roo, A. P. J.: A simple raster-based model for flood inundation simulation, J. Hydrol., 236, 54–77, https://doi.org/10.1016/S0022-1694(00)00278-X, 2000.

Bates, P. D., Horritt, M. S., and Fewtrell, T. J.: A simple inertial formulation of the shallow water equations for efficient two-dimensional flood inundation modelling, J. Hydrol., 387, 33–45, https://doi.org/10.1016/j.jhydrol.2010.03.027, 2010.

Benesty, J., Chen, J., Huang, Y., and Cohen, I.: Pearson Correlation Coefficient, in: Noise Reduction in Speech Processing, edited by: Cohen, I., Huang, Y., Chen, J., and Benesty, J., Springer Berlin Heidelberg, Berlin, Heidelberg, 1–4, https://doi.org/10.1007/978-3-642-00296-0_5, 2009.

Bernhard, N., Moskwa, L.-M., Schmidt, K., Oeser, R. A., Aburto, F., Bader, M. Y., Baumann, K., von Blanckenburg, F., Boy, J., van den Brink, L., Brucker, E., Büdel, B., Canessa, R., Dippold, M. A., Ehlers, T. A., Fuentes, J. P., Godoy, R., Jung, P., Karsten, U., Köster, M., Kuzyakov, Y., Leinweber, P., Neidhardt, H., Matus, F., Mueller, C. W., Oelmann, Y., Oses, R., Osses, P., Paulino, L., Samolov, E., Schaller, M., Schmid, M., Spielvogel, S., Spohn, M., Stock, S., Stroncik, N., Tielbörger, K., Übernickel, K., Scholten, T., Seguel, O., Wagner, D., and Kühn, P.: Pedogenic and microbial interrelations to regional climate and local topography: New insights from a climate gradient (arid to humid) along the Coastal Cordillera of Chile, CATENA, 170, 335–355, https://doi.org/10.1016/j.catena.2018.06.018, 2018.

Bezak, N., Petan, S., and Mikoš, M.: Spatial and Temporal Variability in Rainfall Erosivity Under Alpine Climate: A Slovenian Case Study Using Optical Disdrometer Data, Front. Environ. Sci., 9, 735492, https://doi.org/10.3389/fenvs.2021.735492, 2021.

Boix-Fayos, C., de Vente, J., Martínez-Mena, M., Barberá, G. G., and Castillo, V.: The impact of land use change and check-dams on catchment sediment yield, Hydrol. Process., 22, 4922–4935, https://doi.org/10.1002/hyp.7115, 2008.

Braun, J. and Willett, S. D.: A very efficient O(n), implicit and parallel method to solve the stream power equation governing fluvial incision and landscape evolution, Geomorphology, 180–181, 170–179, https://doi.org/10.1016/j.geomorph.2012.10.008, 2013.

Brown, C. E.: Coefficient of Variation, in: Applied Multivariate Statistics in Geohydrology and Related Sciences, Springer, Berlin, Heidelberg, 1998.

Brunsden, D. and Thornes, J. B.: Landscape Sensitivity and Change, Trans. Inst. Br. Geogr., 4, 463, https://doi.org/10.2307/622210, 1979.

Cai, W., McPhaden, M. J., Grimm, A. M., Rodrigues, R. R., Taschetto, A. S., Garreaud, R. D., Dewitte, B., Poveda, G., Ham, Y.-G., Santoso, A., Ng, B., Anderson, W., Wang, G., Geng, T., Jo, H.-S., Marengo, J. A., Alves, L. M., Osman, M., Li, S., Wu, L., Karamperidou, C., Takahashi, K., and Vera, C.: Climate impacts of the El Niño–Southern Oscillation on South America, Nat. Rev. Earth Environ., 1, 215–231, https://doi.org/10.1038/s43017-020-0040-3, 2020.

Coppus, R. and Imeson, A. C.: Extreme events controlling erosion and sediment transport in a semi-arid sub-andean valley, Earth Surf. Process. Landf., 27, 1365–1375, https://doi.org/10.1002/esp.435, 2002.

Coulthard, T. J.: Landscape evolution models: a software review, Hydrol. Process., 15, 165–173, https://doi.org/10.1002/hyp.426, 2001.

Coulthard, T. J., Macklin, M. G., and Kirkby, M. J.: A cellular model of Holocene upland river basin and alluvial fan evolution, Earth Surf. Process. Landf., 27, 269–288, https://doi.org/10.1002/esp.318, 2002.

Coulthard, T. J., Neal, J. C., Bates, P. D., Ramirez, J., de Almeida, G. A. M., and Hancock, G. R.: Integrating the LISFLOOD-FP 2D hydrodynamic model with the CAESAR model: implications for modelling landscape evolution: INTEGRATING HYDRODYNAMICS IN LANDSCAPE EVOLUTION MODELS, Earth Surf. Process. Landf., 38, 1897–1906, https://doi.org/10.1002/esp.3478, 2013.

Earth Resources Observation And Science (EROS) Center: Shuttle Radar Topography Mission (SRTM) 1 Arc-Second Global, https://doi.org/10.5066/F7PR7TFT, 2017.

Farhan, Y. and Alnawaiseh, S.: Spatio-Temporal Variation in Rainfall Erosivity over Jordan Using Annual and Seasonal Precipitation, Nat. Resour., 09, 242–267, https://doi.org/10.4236/nr.2018.96016, 2018.

Garatuza-Payán, J., Sánchez-Andrés, R., Sánchez-Carrillo, S., and Navarro, J. M.: Using remote sensing to investigate erosion rate variability in a semiarid watershed, due to changes in vegetation cover, IAHS Publ, 292, 144–151, 2005.

González-Hidalgo, J. C., de Luis, M., and Batalla, R. J.: Effects of the largest daily events on total soil erosion by rainwater. An analysis of the USLE database, Earth Surf. Process. Landf., 34, 2070–2077, https://doi.org/10.1002/esp.1892, 2009.

Gonzalez-Hidalgo, J. C., Batalla, R. J., Cerdà, A., and de Luis, M.: Contribution of the largest events to suspended sediment transport across the USA, Land Degrad. Dev., 21, 83–91, https://doi.org/10.1002/ldr.897, 2010.

Green, W. H. and Ampt, G. A.: Studies on Soil Phyics., J. Agric. Sci., 4, 1–24, https://doi.org/10.1017/S0021859600001441, 1911.

Hobley, D. E. J., Adams, J. M., Nudurupati, S. S., Hutton, E. W. H., Gasparini, N. M., Istanbulluoglu, E., and Tucker, G. E.: Creative computing with Landlab: an open-source toolkit for building, coupling, and exploring two-dimensional numerical models of Earth-surface dynamics, Earth Surf. Dyn., 5, 21–46, https://doi.org/10.5194/esurf-5-21-2017, 2017.

Hooke, J. M. and Mant, J. M.: Geomorphological impacts of a flood event on ephemeral channels in SE Spain, Geomorphology, 34, 163–180, https://doi.org/10.1016/S0169-555X(00)00005-2, 2000.

Istanbulluoglu, E.: Vegetation-modulated landscape evolution: Effects of vegetation on landscape processes, drainage density, and topography, J. Geophys. Res., 110, https://doi.org/10.1029/2004jf000249, 2005.

Johnstone, S. A. and Hilley, G. E.: Lithologic control on the form of soil-mantled hillslopes, Geology, 43, 83–86, https://doi.org/10.1130/G36052.1, 2014.

Kalyanapu, A. J., Burian, S. J., and McPherson, T. N.: Effect of land use-based surface roughness on hydrologic model output, J. Spat. Hydrol., 9, 51–71, 2010.

Kirchner, J. W., Finkel, R. C., Riebe, C. S., Granger, D. E., Clayton, J. L., King, J. G., and Megahan, W. F.: Mountain erosion over 10 yr, 10 k.y., and 10 m.y. time scales, Geology, 29, 591, https://doi.org/10.1130/0091-7613(2001)029<0591:MEOYKY>2.0.CO;2, 2001.

Kojima, S., Soto, I., Quiroz, M., Valencia, P., and Fernandez, I.: Geological and Geochemical Characteristics of the Intrusion-Related Vein-Type Gold Deposits in the El Morado District, Coastal Cordillera, Northern Chile, Resour. Geol., 67, 197–206, https://doi.org/10.1111/rge.12129, 2017.

Lesschen, J. P., Schoorl, J. M., and Cammeraat, L. H.: Modelling runoff and erosion for a semi-arid catchment using a multi-scale approach based on hydrological connectivity, Geomorphology, 109, 174–183, https://doi.org/10.1016/j.geomorph.2009.02.030, 2009.

Leyland, J., Hackney, C. R., Darby, S. E., Parsons, D. R., Best, J. L., Nicholas, A. P., Aalto, R., and Lague, D.: Extreme flood-driven fluvial bank erosion and sediment loads: direct process measurements using integrated Mobile Laser Scanning (MLS) and hydro-acoustic techniques: Direct measurement of flood-driven erosion using MLS and MBES, Earth Surf. Process. Landf., 42, 334–346, https://doi.org/10.1002/esp.4078, 2016.

Martens, B., Miralles, D. G., Lievens, H., van der Schalie, R., de Jeu, R. A. M., Fernández-Prieto, D., Beck, H. E., Dorigo, W. A., and Verhoest, N. E. C.: GLEAM v3: satellite-based land evaporation and root-zone soil moisture, Geosci. Model Dev., 10, 1903–1925, https://doi.org/10.5194/gmd-10-1903-2017, 2017.

Medeiros, P. H. A. and de Araújo, J. C.: Temporal variability of rainfall in a semiarid environment in Brazil and its effect on sediment transport processes, J. Soils Sediments, https://doi.org/10.1007/s11368-013-0809-9, 2013.

Meng, X., Zhu, Y., Yin, M., and Liu, D.: The impact of land use and rainfall patterns on the soil loss of the hillslope, Sci. Rep., 11, 16341, https://doi.org/10.1038/s41598-021-95819-5, 2021.

Meusburger, K., Steel, A., Panagos, P., Montanarella, L., and Alewell, C.: Spatial and temporal variability of rainfall erosivity factor for Switzerland, Hydrol. Earth Syst. Sci., 16, 167–177, https://doi.org/10.5194/hess-16-167-2012, 2012.

Norbiato, D., Borga, M., Degli Esposti, S., Gaume, E., and Anquetin, S.: Flash flood warning based on rainfall thresholds and soil moisture conditions: An assessment for gauged and ungauged basins, J. Hydrol., 362, 274–290, https://doi.org/10.1016/j.jhydrol.2008.08.023, 2008.

Nunes, A. N., de Almeida, A. C., and Coelho, C. O. A.: Impacts of land use and cover type on runoff and soil erosion in a marginal area of Portugal, Appl. Geogr., 31, 687–699, https://doi.org/10.1016/j.apgeog.2010.12.006, 2011.

Oeser, R. A., Stroncik, N., Moskwa, L.-M., Bernhard, N., Schaller, M., Canessa, R., Brink, L. van den, Köster, M., Brucker, E., Stock, S., Fuentes, J. P., Godoy, R., Matus, F. J., Pedraza, R. O., McIntyre, P.

O., Paulino, L., Seguel, O., Bader, M. Y., Boy, J., Dippold, M. A., Ehlers, T. A., Kühn, P., Kuzyakov, Y., Leinweber, P., Scholten, T., Spielvogel, S., Spohn, M., Übernickel, K., Tielbörger, K., Wagner, D., and Blanckenburg, F. von: Chemistry and microbiology of the Critical Zone along a steep climate and vegetation gradient in the Chilean Coastal Cordillera, CATENA, 170, 183–203, https://doi.org/10.1016/j.catena.2018.06.002, 2018.

Priestley, C. H. B. and Taylor, R. J.: On the Assessment of Surface Heat Flux and Evaporation Using Large-Scale Parameters, Mon. Weather Rev., 100, 81–92, https://doi.org/10.1175/1520-0493(1972)100<0081:OTAOSH>2.3.CO;2, 1972.

Rengers, F. K., McGuire, L. A., Kean, J. W., Staley, D. M., and Hobley, D. E. J.: Model simulations of flood and debris flow timing in steep catchments after wildfire: SIMULATIONS OF FLOOD AND DEBRIS FLOW TIMING, Water Resour. Res., 52, 6041–6061, https://doi.org/10.1002/2015WR018176, 2016.

Rossel, K., Aguilar, G., Salazar, E., Martinod, J., Carretier, S., Pinto, L., and Cabré, A.: Chronology of Chilean Frontal Cordillera building from geochronological, stratigraphic and geomorphological data insights from Miocene intramontane-basin deposits, Basin Res., 30, 289–310, https://doi.org/10.1111/bre.12221, 2018.

Santos, M. and Fragoso, M.: Precipitation Thresholds for Triggering Floods in the Corgo Basin, Portugal, Water, 8, 376, https://doi.org/10.3390/w8090376, 2016.

Schaller, M., Ehlers, T. A., Lang, K. A. H., Schmid, M., and Fuentes-Espoz, J. P.: Addressing the contribution of climate and vegetation cover on hillslope denudation, Chilean Coastal Cordillera (26°–38°S), Earth Planet. Sci. Lett., 489, 111–122, https://doi.org/10.1016/j.epsl.2018.02.026, 2018.

Schaller, M., Dal Bo, I., Ehlers, T. A., Klotzsche, A., Drews, R., Fuentes Espoz, J. P., and van der Kruk, J.: Comparison of regolith physical and chemical characteristics with geophysical data along a climate and ecological gradient, Chilean Coastal Cordillera (26 to 38\degree\,S), SOIL, 6, 629–647, https://doi.org/10.5194/soil-6-629-2020, 2020.

Schmid, M., Ehlers, T. A., Werner, C., Hickler, T., and Fuentes-Espoz, J.-P.: Effect of changing vegetation and precipitation on denudation – Part 2: Predicted landscape response to transient climate and vegetation cover over millennial to million-year timescales, Earth Surf. Dyn., 6, 859–881, https://doi.org/10.5194/esurf-6-859-2018, 2018.

Serpa, D., Nunes, J. P., Santos, J., Sampaio, E., Jacinto, R., Veiga, S., Lima, J. C., Moreira, M., Corte-Real, J., Keizer, J. J., and Abrantes, N.: Impacts of climate and land use changes on the hydrological and erosion processes of two contrasting Mediterranean catchments, Sci Total Env., 538, 64–77, https://doi.org/10.1016/j.scitotenv.2015.08.033, 2015.

Sharma, A., Tiwari, K. N., and Bhadoria, P. B. S.: Effect of land use land cover change on soil erosion potential in an agricultural watershed, Environ. Monit. Assess., 173, 789–801, https://doi.org/10.1007/s10661-010-1423-6, 2011.

Sharma, H., Ehlers, T. A., Glotzbach, C., Schmid, M., and Tielbörger, K.: Effect of rock uplift and Milankovitch timescale variations in precipitation and vegetation cover on catchment erosion rates, Earth Surf. Dyn., 9, 1045–1072, https://doi.org/10.5194/esurf-9-1045-2021, 2021.

Shobe, C. M., Tucker, G. E., and Barnhart, K. R.: The SPACE 1.0 model: A Landlab component for 2-D calculation of sediment transport, bedrock erosion, and landscape evolution, Geosci. Model Dev. Discuss., 1–38, https://doi.org/10.5194/gmd-2017-175, 2017.

Snyder, N. P., Whipple, K. X., Tucker, G. E., and Merritts, D. J.: Importance of a stochastic distribution of floods and erosion thresholds in the bedrock river incision problem, J. Geophys. Res. Solid Earth, 108, https://doi.org/10.1029/2001JB001655, 2003.

Stolte, J.: Effects of land use and infiltration behaviour on soil conservation strategies, 2003.

Tucker, G. E. and Hancock, G. R.: Modelling landscape evolution, Earth Surf. Process. Landf., 35, 28–50, https://doi.org/10.1002/esp.1952, 2010.

Übernickel, K., Ehlers, T. A., Ershadi, M. R., Paulino, L., Fuentes Espoz, J.-P., Maldonado, A., Oses-Pedraza, R., and von Blanckenburg, F.: Time series of meteorological station data in the EarthShape study areas of in the Coastal Cordillera, Chile, https://doi.org/10.5880/FIDGEO.2020.043, 2020.

Valdés-Pineda, R., Valdés, J. B., Diaz, H. F., and Pizarro-Tapia, R.: Analysis of spatio-temporal changes in annual and seasonal precipitation variability in South America-Chile and related ocean–atmosphere circulation patterns, Int. J. Climatol., 36, 2979–3001, https://doi.org/10.1002/joc.4532, 2016.

Vanacker, V., von Blanckenburg, F., Govers, G., Molina, A., Poesen, J., Deckers, J., and Kubik, P.: Restoring dense vegetation can slow mountain erosion to near natural benchmark levels, Geology, 35, 303, https://doi.org/10.1130/G23109A.1, 2007.

Walsh, P., Jakeman, A., and Thompson, C.: Modelling headwater channel response and suspended sediment yield to in-channel large wood using the Caesar-Lisflood landscape evolution model, Geomorphology, 363, 107209, https://doi.org/10.1016/j.geomorph.2020.107209, 2020.

Willgoose, G.: Mathematical Modeling of Whole Landscape Evolution, Annu. Rev. Earth Planet. Sci., 33, 443–459, https://doi.org/10.1146/annurev.earth.33.092203.122610, 2005.

Winchell, M., Srinivasan, R., Di Luzio, M., and Arnold, J.: ARCSWAT INTERFACE FOR SWAT2012, 2013.

Zanaga, D., Van De Kerchove, R., De Keersmaecker, W., Souverijns, N., Brockmann, C., Quast, Ralf, Wevers, Jan, Grosu, Alex, Paccini, Audrey, Vergnaud, Sylvain, Cartus, Oliver, Santoro, Maurizio, Fritz, Steffen, Georgieva, Ivelina, Lesiv, Myroslava, Carter, Sarah, Herold, Martin, Li, Linlin, Tsendbazar, Nandin-Erdene, Ramoino, Fabrizio, and Arino, Olivier: ESA WorldCover 10 m 2020 v100 (v100), https://doi.org/10.5281/ZENODO.5571936, 2021.

Zellou, B. and Rahali, H.: Assessment of reduced-complexity landscape evolution model suitability to adequately simulate flood events in complex flow conditions, Nat. Hazards, 86, 1–29, https://doi.org/10.1007/s11069-016-2671-8, 2017.

Ziese, M., Rauthe-Schöch, A., Becker, A., Finger, P., Rustemeier, E., and Schneider, U.: GPCC Full Data Daily Version 2020 at 1.0°: Daily Land-Surface Precipitation from Rain-Gauges built on GTS-based and Historic Data: Gridded Daily Totals (2020), https://doi.org/10.5676/DWD_GPCC/FD_D_V2020_100, 2020.

4 Conclusions

This section summarizes the significant findings of this thesis by revisiting the research questions and their underlying hypotheses stated in the introduction (section 1.2). The research questions were pertaining to evaluating the effects of changing precipitation and vegetation pattern at variable time scales ranging from Millennial (e.g., Milankovitch cycles) to daily, using the complex landscape evolution modeling approach.

4.1 Research questions revisited

Research question 1: How do the rock uplift rates and the periodicity of variations in climate and vegetation cover affect the erosion and sedimentation over millennial (i.e., Milankovitch cycles) timescales?

The above research question aimed to identify which factor, tectonics (i.e., rock uplift rates) or periodicity (e.g., 21kyr, 41kyr, or 100kyr) of change in climate (namely precipitation) and vegetation cover, is more vital in influencing catchment erosion over millennial timescales, in mixed bedrock-alluvial systems. In order to address the above research question, transients in precipitation and vegetation cover were introduced to steady-state topography, using landscape model simulations with model parameters tuned to two locations in the Chilean Coastal Cordillera (see Fig. 1) with a distinct climate and ecological settings. These study areas included Pan de Azucar (arid) with 10% vegetation cover and MAP of 30 mm yr^{-1} and La Campana (Mediterranean) with 70% vegetation cover and MAP of 350 mm yr^{-1}. The following hypotheses were tested in section 3.1 of this thesis (Sharma et al., 2021). The hypotheses with their outcome are as follows:

(i) If vegetation cover and climate vary on Milankovitch timescales, then any increase or decrease in catchment erosion will be more pronounced over longer (e.g., 100 kyr) rather than shorter (e.g., 21 kyr) periodicities due to the longer duration of change imposed.

The amplitude of change in catchment erosion and sedimentation was found to be more pronounced over longer (e.g., 100 kyr) than shorter climate and vegetation periodicity (e.g., 23 kyr) in both arid and Mediterranean settings. This finding confirms the hypothesis. Furthermore, the periodicity effects on erosion and sedimentation are more prominent in the catchment in the Mediterranean setting (with vegetation cover of 70%) than in the arid setting (with vegetation cover of 70%). The above finding indicates a sensitivity of the response to the climate and ecological settings of the area of interest.

(ii) If increasing rates of tectonic uplift (e.g., 0.05 - 0.2 mm yr^{-1}) cause an increase in catchment erosion rates, then any periodic variations in climate and vegetation cover will be muted

(or lower amplitude) at higher uplift rates, as the effect of rock uplift on erosion will outweigh climate and vegetation change effects.

All transient forcings in precipitation and vegetation cover (over Milankovitch timescales) explored in Sharma et al. (2021) resulted in variations in catchment erosion around the mean erosion rates. The mean erosion rates are determined by the rock uplift rates. As rock uplift rates increased from 0.05 to 0.2 mm a^{-1}, the effects of periodic changes in precipitation and vegetation cover on erosion and sedimentation rates were found to be more pronounced. For example, these changes in erosion and sedimentation were around 35 % and 110 %, respectively, of the background rock uplift rate. This finding negates the hypothesis and suggests that regardless of the tectonic setting considered in this study (within the range of rock uplift rates explored here), erosional transients from varying precipitation and vegetation cover occur. However, the detection of these changes requires the measurement of erosion rates integrating over short timescales such that the average (tectonically driven) mean erosion rate is not recovered.

Broadly, the above findings conclude that Milankovitch timescale changes in climate and associated vegetation cover influence catchment-scale erosion and sedimentation. However, these transient changes are superimposed upon tectonically driven rock uplift rates.

Research question 2: How do the seasonal variations in precipitation and vegetation cover affect catchment-scale erosion rates in different climate and ecological settings?

The above research question aimed to identify which factor, precipitation or vegetation cover, poses a first-order control on catchment erosion over seasonal timescales. In order to resolve the above question, a numerical model setup with Landlab (modified to account for spatially and temporally variable vegetation cover) was implemented. The model was simulated to estimate catchment erosion subjected to seasonal variations in precipitation and vegetation cover on modern-day (transient) topography. The model parameters were tuned to four locations with a steep climate and ecological gradient (e.g., arid, semi-arid, Mediterranean, and humid settings) in the Chilean Coastal Cordillera (see Fig. 1). The following hypotheses were tested in section 3.2 of this thesis for the same. The hypotheses with their outcomes are as follows:

(i) If precipitation is the first-order driver of seasonal erosion rates, then the influence of seasonal changes in vegetation cover would be of low significance.

The amplitude of change in catchment erosion (with respect to mean) ranges between 6.5% (in humid-temperate) to 36% (in the Mediterranean setting) when vegetation cover is varied at seasonal timescales, but precipitation rates are kept constant. In contrast, in simulations with seasonally variable precipitation and constant vegetation cover, the amplitude of change in erosion rates is higher and ranges

between 13% (in arid setting) to 91% (in Mediterranean setting). Finally, simulations with coupled precipitation and vegetation cover variations result in variations in catchment erosion of 13% (in arid setting) to 97% (in Mediterranean setting). This implies that precipitation variations more strongly influence seasonal variations in erosion rates. However, seasonal vegetation cover variations' effects on erosion are also significant (between 5-36%). Hence, the above hypothesis is partially confirmed.

(ii) Catchment-scale erosion rates in arid and semi-arid regions are more sensitive to seasonality in precipitation and vegetation than in the Mediterranean and humid-temperate regions.

The simulated catchment erosion subjected to seasonal variations in vegetation and precipitation is most pronounced in semi-arid and Mediterranean settings and then in arid and humid-temperature settings. For example, the sensitivity of erosion rates to changing precipitation and vegetation increases from arid (~13%) to semi-arid (~86%) and Mediterranean settings (~97%) and again decreases in humid-temperate settings (~50-52%) due to the abundance of vegetation cover. Hence, the above hypothesis is partially confirmed for semi-arid and humid temperate settings.

Broadly, the above findings conclude that variations in precipitation pose a first-order control on catchment erosion at seasonal timescales, and the effects of vegetation cover changes are secondary (but still significant). Also, the amplitude of change in catchment erosion is strongly influenced by the climate and ecological setting of the area of interest.

Research question 3: How do the extreme precipitation events affect catchment-scale erosion rates in regions with variable land use and land cover types?

The above research question aimed to identify which factor, precipitation variation or plant functional type (PFT) distribution, poses a first-order control on catchment erosion during extreme precipitation events. In order to resolve the above question, a numerical model setup with Landlab (modified to account for spatially variable vegetation type) was implemented. The model was simulated to estimate catchment erosion subjected to stochastic variations in precipitation (including extreme events) on modern-day (transient) topography. The model parameters (same as section 3.2) for study areas (Fig. 1) were downscaled for daily timesteps. The climate (land cover classification) in study areas is classified as arid (barren land), semi-arid (grassland), Mediterranean (shrubland), and humid temperate (dense forest) environments. The following hypotheses were tested in section 3.2 of this thesis for the same. The hypotheses with their outcomes are as follows:

(i) If land use and land cover (LULC) distribution pose first-order control on catchment erosion, then regions with less resilient vegetation cover (barren or grasses) would

experience more erosion during extreme events, despite the prevalence of high magnitude precipitation events in regions with more resilient vegetation cover (e.g., shrubs and trees).

The Landlab results indicate that the LULC distribution significantly influences catchment erosion during extreme precipitation events

. For example, the catchment erosion in grassland with sparse vegetation cover (i.e., Santa Gracia, semi-arid setting) is 9%, 84%, and 93% more sensitive than in barren land (Pan de Azúcar, arid setting), shrubland (La Campana, Mediterranean setting), and dense forest (Nahuelbuta, humid temperate setting), respectively. The sensitivity of catchment erosion is defined as the slope of precipitation and erosion curve (see Fig. 6 in section 3.3.2). This finding confirms the hypothesis.

(ii) If Landlab (modified to account for PFTs) provides a reliable output at shorter time scales, its results should be comparable with that of a physically-based model.

A strong positive correlation (Pearson $r > 0.8$ and $r < 0.05$) was found in surface water discharge rates (normalized by domain area), obtained from LEM (Landlab-SPACE) and hydrological model (SWAT). This yields the applicability of Landlab-SPACE at shorter time scales (e.g., with daily timestep). However, the differences in Landlab and SWAT model results are inevitable due to the difference in implementation of both models' erosion and runoff routines.

Broadly, the above findings conclude that vegetation cover and type significantly influence catchment erosion during extreme precipitation events. However, these short-term events have the potential to leave a signature in the landscapes with >100 % amplitude of change (with respect to mean) in catchment erosion in all the study areas, especially in arid and semi-arid settings with little or no vegetation cover. Temporal downscaling in the landscape evolution models introduces a more realistic representation of the landscape's sediment dynamics. Despite the numerical complexity of the model, the runoff rates obtained from Landlab were satisfactorily comparable with that of a physically-based hydrological model (SWAT), underlying the applicability of Landlab at short timescales. However, modern topography (in a transient state) is preferred over steady-state conditions in such applications. The major limitations are the long computation time and unavoidable transients in the model output due to a mismatch of model parameters and actual parameters, which lead to the modern topography.

4.2 Outlook

The modeling approaches used in this thesis augment the existing knowledge on the degree of influence of variations in tectonics, climate, and vegetation on catchment erosion at various timescales. However, there exist knowledge gaps to be fulfilled with the robust field, flume, and modeling experiments. One of which includes better parametrization of the models to robustly constrain vegetation-dependent hillslope and fluvial processes. This can be accomplished with future field or flume studies to estimate erosion-related parameters (e.g., erosivity) specific to the climate and ecological conditions of the study areas.

Also, most landscape evolution models are designed to simulate steady-state conditions. However, ideal steady-state topographies are non-existent. This poses a problem in simulations with a short timescale (with present-day topography in a transient state). This problem can potentially be handled by calibrating the model equations (geomorphic transport laws) to modern topography, preferably using stochastic (e.g., Bayesian) techniques (e.g., Stephenson et al., 2006; Avdeev et al., 2011).

This thesis investigated catchment erosion for spatially uniform precipitation rates due to smaller catchment sizes (i.e., <100 km^2). However, in larger catchments (or river basins), higher spatial heterogeneity in precipitation alters erosion and deposition patterns, eventually resulting in more developed gullies (Peleg et al., 2021) and rainfall to runoff conversion (Emmanuel et al., 2015). This problem may be resolved by coupling the existing landscape evolution models with dynamically estimated precipitation rates based on the topography.

A significant portion of the water cycle in the river catchments is available in the form of groundwater. Especially at smaller timescales (seasonal or daily), sub-surface processes like soil-water infiltration, baseflow, and groundwater return flow into the streams play a crucial role in determining the surface runoff. Surface runoff and the volume of water available in the streams are the critical factors influencing fluvial processes. This can be accomplished by designing a model framework that efficiently integrates a simple hydrogeological model into a two-dimensional landscape evolution model for more realistic simulations of the surface processes. The integrated model needs to be optimized to simulate efficient computation time.

5 Appendix

This section contains the paths to the simulations and datasets available on the ESD Fileserver and the source of Landlab and ArcSWAT.

Manuscript 1: Sharma et al. (2021)

Folder in ESD Fileserver containing model simulation scripts:
/esd/esd01/data/hsharma/model_runs/SPACE/Paper_1/Simulations

Folder in ESD Fileserver containing plotting scripts:
/esd/esd01/data/hsharma/model_runs/SPACE/Paper_1/Plots

Manuscript 2: Sharma et al. *(in preparation)*

Folder in ESD Fileserver containing model simulation scripts:
/esd/esd01/data/hsharma/model_runs/SPACE/Paper_2/Simulations

Folder in ESD Fileserver containing plotting scripts:
/esd/esd01/data/hsharma/model_runs/SPACE/Paper_2/Plots

Manuscript 3: Sharma et al. *(in preparation)*

Folder in ESD Fileserver containing model simulation scripts:
/esd/esd01/data/hsharma/model_runs/SPACE/Paper_3/Simulations

Folder in ESD Fileserver containing plotting scripts:
/esd/esd01/data/hsharma/model_runs/SPACE/Paper_3/Plots

Landlab: The source code of the version of Landlab, used in this thesis, on ESD Fileserver:
/esd/esd01/data/hsharma/landlab.tar.gz

SWAT: The plugin for ArcSWAT 2012 version can be downloaded from the following link:

https://swat.tamu.edu/software/arcswat/

References

Acosta, V. T., Schildgen, T. F., Clarke, B. A., Scherler, D., Bookhagen, B., Wittmann, H., von Blanckenburg, F., and Strecker, M. R.: Effect of vegetation cover on millennial-scale landscape denudation rates in East Africa, Lithosphere, 7, 408–420, https://doi.org/10.1130/l402.1, 2015.

Adams, B. A., Whipple, K. X., Forte, A. M., Heimsath, A. M., and Hodges, K. V.: Climate controls on erosion in tectonically active landscapes, Sci. Adv., 6, eaaz3166, https://doi.org/10.1126/sciadv.aaz3166, 2020.

Ahnert, F.: Some comments on the quantitative formulation of geomorphological processes in a theoretical model, EARTH Surf. Process., 2, 191–201, https://doi.org/10.1002/esp.3290020211, 1976.

Amundson, R., Heimsath, A., Owen, J., Yoo, K., and Dietrich, W. E.: Hillslope soils and vegetation, Geomorphology, 234, 122–132, https://doi.org/10.1016/j.geomorph.2014.12.031, 2015.

Arnold, J. G., Srinivasan, R., Muttiah, R. S., and Williams, J. R.: LARGE AREA HYDROLOGIC MODELING AND ASSESSMENT PART I: MODEL DEVELOPMENT1, JAWRA J. Am. Water Resour. Assoc., 34, 73–89, https://doi.org/10.1111/j.1752-1688.1998.tb05961.x, 1998.

Avdeev, B., Niemi, N. A., and Clark, M. K.: Doing more with less: Bayesian estimation of erosion models with detrital thermochronometric data, Earth Planet. Sci. Lett., 305, 385–395, https://doi.org/10.1016/j.epsl.2011.03.020, 2011.

Barnhart, K. R., Glade, R. C., Shobe, C. M., and Tucker, G. E.: Terrainbento 1.0: a Python package for multi-model analysis in long-term drainage basin evolution, Geosci. Model Dev., 12, 1267–1297, https://doi.org/10.5194/gmd-12-1267-2019, 2019.

Barnhart, K. R., Hutton, E. W. H., Tucker, G. E., Gasparini, N. M., Istanbulluoglu, E., Hobley, D. E. J., Lyons, N. J., Mouchene, M., Nudurupati, S. S., Adams, J. M., and Bandaragoda, C.: Short communication: Landlab v2.0: a software package for Earth surface dynamics, Earth Surf. Dyn., 8, 379–397, https://doi.org/10.5194/esurf-8-379-2020, 2020.

Bernhard, N., Moskwa, L.-M., Schmidt, K., Oeser, R. A., Aburto, F., Bader, M. Y., Baumann, K., von Blanckenburg, F., Boy, J., van den Brink, L., Brucker, E., Büdel, B., Canessa, R., Dippold, M. A., Ehlers, T. A., Fuentes, J. P., Godoy, R., Jung, P., Karsten, U., Köster, M., Kuzyakov, Y., Leinweber, P., Neidhardt, H., Matus, F., Mueller, C. W., Oelmann, Y., Oses, R., Osses, P., Paulino, L., Samolov, E., Schaller, M., Schmid, M., Spielvogel, S., Spohn, M., Stock, S., Stroncik, N., Tielbörger, K., Übernickel, K., Scholten, T., Seguel, O., Wagner, D., and Kühn, P.: Pedogenic and microbial interrelations to regional climate and local topography: New insights from a climate gradient (arid to humid) along the Coastal Cordillera of Chile, CATENA, 170, 335–355, https://doi.org/10.1016/j.catena.2018.06.018, 2018.

Boix-Fayos, C., de Vente, J., Martínez-Mena, M., Barberá, G. G., and Castillo, V.: The impact of land use change and check-dams on catchment sediment yield, Hydrol. Process., 22, 4922–4935, https://doi.org/10.1002/hyp.7115, 2008.

Bonnet, S. and Crave, A.: Landscape response to climate change: Insights from experimental modeling and implications for tectonic versus climatic uplift of topography, Geology, 31, 123–126, https://doi.org/10.1130/0091-7613(2003)031<0123:Lrtcci>2.0.Co;2, 2003.

Burbank, D. W., Leland, J., Fielding, E., Anderson, R. S., Brozovic, N., Reid, M. R., and Duncan, C.: Bedrock incision, rock uplift and threshold hillslopes in the northwestern Himalayas, Nature, 379, 505–510, https://doi.org/10.1038/379505a0, 1996.

Cerdà, A.: The influence of aspect and vegetation on seasonal changes in erosion under rainfall simulation on a clay soil in Spain, Can. J. Soil Sci., 78, 321–330, https://doi.org/10.4141/S97-060, 1998.

Collins, D. B. G.: Modeling the effects of vegetation-erosion coupling on landscape evolution, J. Geophys. Res., 109, https://doi.org/10.1029/2003jf000028, 2004.

Coulthard, T. J.: Landscape evolution models: a software review, Hydrol. Process., 15, 165–173, https://doi.org/10.1002/hyp.426, 2001.

Davy, P. and Lague, D.: Fluvial erosion/transport equation of landscape evolution models revisited, J. Geophys. Res., 114, https://doi.org/10.1029/2008jf001146, 2009.

Didan, Kamel: MOD13Q1 MODIS/Terra Vegetation Indices 16-Day L3 Global 250m SIN Grid V006, https://doi.org/10.5067/MODIS/MOD13Q1.006, 2015.

Egholm, D. L., Knudsen, M. F., and Sandiford, M.: Lifespan of mountain ranges scaled by feedbacks between landsliding and erosion by rivers, Nature, 498, 475–478, https://doi.org/10.1038/nature12218, 2013.

Emmanuel, I., Andrieu, H., Leblois, E., Janey, N., and Payrastre, O.: Influence of rainfall spatial variability on rainfall–runoff modelling: Benefit of a simulation approach?, Hydrol. Appl. Weather Radar, 531, 337–348, https://doi.org/10.1016/j.jhydrol.2015.04.058, 2015.

Gabet, E. J., Pratt-Sitaula, B. A., and Burbank, D. W.: Climatic controls on hillslope angle and relief in the Himalayas, Geology, 32, 629, https://doi.org/10.1130/G20641.1, 2004.

Gao, P., Jiang, G., Wei, Y., Mu, X., Wang, F., Zhao, G., and Sun, W.: Streamflow regimes of the Yanhe River under climate and land use change, Loess Plateau, China: STREAMFLOW REGIMES OF THE YANHE RIVER UNDER CLIMATE AND LUCC, Hydrol. Process., 29, 2402–2413, https://doi.org/10.1002/hyp.10309, 2015.

Gilbert, G. K.: Report on the geology of the Henry Mountains, Washington, D.C., https://doi.org/10.3133/70039916, 1877.

Glodny, J., Gräfe, K., Echtler, H., and Rosenau, M.: Mesozoic to Quaternary continental margin dynamics in South-Central Chile (36–42°S): the apatite and zircon fission track perspective, Int. J. Earth Sci., 97, 1271–1291, https://doi.org/10.1007/s00531-007-0203-1, 2008.

Green, W. H. and Ampt, G. A.: Studies on Soil Phyics., J. Agric. Sci., 4, 1–24, https://doi.org/10.1017/S0021859600001441, 1911.

Hobley, D. E. J., Adams, J. M., Nudurupati, S. S., Hutton, E. W. H., Gasparini, N. M., Istanbulluoglu, E., and Tucker, G. E.: Creative computing with Landlab: an open-source toolkit for building, coupling, and exploring two-dimensional numerical models of Earth-surface dynamics, Earth Surf. Dyn., 5, 21–46, https://doi.org/10.5194/esurf-5-21-2017, 2017.

Horritt, M. S. and Bates, P. D.: Evaluation of 1D and 2D numerical models for predicting river flood inundation, J. Hydrol., 268, 87–99, https://doi.org/10.1016/S0022-1694(02)00121-X, 2002.

Huxman, T. E., Smith, M. D., Fay, P. A., Knapp, A. K., Shaw, M. R., Loik, M. E., Smith, S. D., Tissue, D. T., Zak, J. C., Weltzin, J. F., Pockman, W. T., Sala, O. E., Haddad, B. M., Harte, J., Koch, G. W.,

Schwinning, S., Small, E. E., and Williams, D. G.: Convergence across biomes to a common rain-use efficiency, Nature, 429, 651–654, https://doi.org/10.1038/nature02561, 2004.

Istanbulluoglu, E.: Vegetation-modulated landscape evolution: Effects of vegetation on landscape processes, drainage density, and topography, J. Geophys. Res., 110, https://doi.org/10.1029/2004jf000249, 2005.

Istanbulluoglu, E. and Bras, R. L.: On the dynamics of soil moisture, vegetation, and erosion: Implications of climate variability and change, Water Resour. Res., 42, 2006.

Johnstone, S. A. and Hilley, G. E.: Lithologic control on the form of soil-mantled hillslopes, Geology, 43, 83–86, https://doi.org/10.1130/G36052.1, 2014.

Julien, P. Y., Saghafian, B., and Ogden, F. L.: RASTER-BASED HYDROLOGIC MODELING OF SPATIALLY-VARIED SURFACE RUNOFF1, JAWRA J. Am. Water Resour. Assoc., 31, 523–536, https://doi.org/10.1111/j.1752-1688.1995.tb04039.x, 1995.

Kalyanapu, A. J., Burian, S. J., and McPherson, T. N.: Effect of land use-based surface roughness on hydrologic model output, J. Spat. Hydrol., 9, 51–71, 2010.

Kirby, E. and Whipple, K.: Quantifying differential rock-uplift rates via stream profile analysis, Geology, 29, 415, https://doi.org/10.1130/0091-7613(2001)029<0415:QDRURV>2.0.CO;2, 2001.

Kirby, E. and Whipple, K. X.: Expression of active tectonics in erosional landscapes, J. Struct. Geol., 44, 54–75, https://doi.org/10.1016/j.jsg.2012.07.009, 2012.

Lague, D.: Reduction of long-term bedrock incision efficiency by short-term alluvial cover intermittency, J. Geophys. Res. Earth Surf., 115, https://doi.org/10.1029/2008jf001210, 2010.

Langbein, W. B. and Schumm, S. A.: Yield of sediment in relation to mean annual precipitation, Eos Trans. Am. Geophys. Union, 39, 1076–1084, https://doi.org/10.1029/TR039i006p01076, 1958.

Melnick, D.: Rise of the central Andean coast by earthquakes straddling the Moho, Nat. Geosci., 9, 401–407, https://doi.org/10.1038/ngeo2683, 2016.

Melnick, D., Bookhagen, B., Strecker, M. R., and Echtler, H. P.: Segmentation of megathrust rupture zones from fore-arc deformation patterns over hundreds to millions of years, Arauco peninsula, Chile: EARTHQUAKE SEGMENTATION AT ARAUCO, J. Geophys. Res. Solid Earth, 114, https://doi.org/10.1029/2008JB005788, 2009.

Meng, X., Zhu, Y., Yin, M., and Liu, D.: The impact of land use and rainfall patterns on the soil loss of the hillslope, Sci. Rep., 11, 16341, https://doi.org/10.1038/s41598-021-95819-5, 2021.

Montgomery, D. R. and Brandon, M. T.: Topographic controls on erosion rates in tectonically active mountain ranges, Earth Planet. Sci. Lett., 201, 481–489, https://doi.org/10.1016/S0012-821X(02)00725-2, 2002.

Oeser, R. A., Stroncik, N., Moskwa, L.-M., Bernhard, N., Schaller, M., Canessa, R., Brink, L. van den, Köster, M., Brucker, E., Stock, S., Fuentes, J. P., Godoy, R., Matus, F. J., Pedraza, R. O., McIntyre, P. O., Paulino, L., Seguel, O., Bader, M. Y., Boy, J., Dippold, M. A., Ehlers, T. A., Kühn, P., Kuzyakov, Y., Leinweber, P., Scholten, T., Spielvogel, S., Spohn, M., Übernickel, K., Tielbörger, K., Wagner, D., and Blanckenburg, F. von: Chemistry and microbiology of the Critical Zone along a steep climate and vegetation gradient in the Chilean Coastal Cordillera, CATENA, 170, 183–203, https://doi.org/10.1016/j.catena.2018.06.002, 2018.

Peleg, N., Skinner, C., Ramirez, J. A., and Molnar, P.: Rainfall spatial-heterogeneity accelerates landscape evolution processes, Geomorphology, 390, 107863, https://doi.org/10.1016/j.geomorph.2021.107863, 2021.

Rengers, F. K., McGuire, L. A., Kean, J. W., Staley, D. M., and Hobley, D. E. J.: Model simulations of flood and debris flow timing in steep catchments after wildfire: SIMULATIONS OF FLOOD AND DEBRIS FLOW TIMING, Water Resour. Res., 52, 6041–6061, https://doi.org/10.1002/2015WR018176, 2016.

Sala, O. E., Parton, W. J., Joyce, L. A., and Lauenroth, W. K.: Primary Production of the Central Grassland Region of the United States, Ecology, 69, 40–45, https://doi.org/10.2307/1943158, 1988.

Schaller, M., Dal Bo, I., Ehlers, T. A., Klotzsche, A., Drews, R., Fuentes Espoz, J. P., and van der Kruk, J.: Comparison of regolith physical and chemical characteristics with geophysical data along a climate and ecological gradient, Chilean Coastal Cordillera (26 to 38\degree\,S), SOIL, 6, 629–647, https://doi.org/10.5194/soil-6-629-2020, 2020.

Schmid, M., Ehlers, T. A., Werner, C., Hickler, T., and Fuentes-Espoz, J.-P.: Effect of changing vegetation and precipitation on denudation – Part 2: Predicted landscape response to transient climate and vegetation cover over millennial to million-year timescales, Earth Surf. Dyn., 6, 859–881, https://doi.org/10.5194/esurf-6-859-2018, 2018.

Sharma, H., Ehlers, T. A., Glotzbach, C., Schmid, M., and Tielbörger, K.: Effect of rock uplift and Milankovitch timescale variations in precipitation and vegetation cover on catchment erosion rates, Earth Surf. Dyn., 9, 1045–1072, https://doi.org/10.5194/esurf-9-1045-2021, 2021.

Shobe, C. M., Tucker, G. E., and Barnhart, K. R.: The SPACE 1.0 model: A Landlab component for 2-D calculation of sediment transport, bedrock erosion, and landscape evolution, Geosci. Model Dev. Discuss., 1–38, https://doi.org/10.5194/gmd-2017-175, 2017.

Starke, J., Ehlers, T. A., and Schaller, M.: Latitudinal effect of vegetation on erosion rates identified along western South America, Science, 367, 1358–1361, https://doi.org/10.1126/science.aaz0840, 2020.

Stephenson, J., Gallagher, K., and Holmes, C.: A Bayesian approach to calibrating apatite fission track annealing models for laboratory and geological timescales, Geochim. Cosmochim. Acta, 70, 5183–5200, https://doi.org/10.1016/j.gca.2006.07.027, 2006.

Tucker, G. E. and Hancock, G. R.: Modelling landscape evolution, Earth Surf. Process. Landf., 35, 28–50, https://doi.org/10.1002/esp.1952, 2010.

Tucker, G. E., Lancaster, S. T., Gasparini, N. M., Bras, R. L., and Rybarczyk, S. M.: An object-oriented framework for distributed hydrologic and geomorphic modeling using triangulated irregular networks, Comput. Geosci., 27, 959–973, https://doi.org/10.1016/S0098-3004(00)00134-5, 2001.

Turowski, J. M., Lague, D., Crave, A., and Hovius, N.: Experimental channel response to tectonic uplift, J. Geophys. Res. Earth Surf., 111, n/a-n/a, https://doi.org/10.1029/2005jf000306, 2006.

Wang, L., Zheng, F., Liu, G., Zhang, X. J., Wilson, G. V., Shi, H., and Liu, X.: Seasonal changes of soil erosion and its spatial distribution on a long gentle hillslope in the Chinese Mollisol region, Int. Soil Water Conserv. Res., 9, 394–404, https://doi.org/10.1016/j.iswcr.2021.02.001, 2021.

Wang, S., Fu, B., Piao, S., Lü, Y., Ciais, P., Feng, X., and Wang, Y.: Reduced sediment transport in the Yellow River due to anthropogenic changes, Nat. Geosci., 9, 38–41, https://doi.org/10.1038/ngeo2602, 2016.

Wei, W., Chen, L., Zhang, H., and Chen, J.: Effect of rainfall variation and landscape change on runoff and sediment yield from a loess hilly catchment in China, Environ. Earth Sci., 73, 1005–1016, https://doi.org/10.1007/s12665-014-3451-y, 2015.

Whipple, K. X. and Tucker, G. E.: Dynamics of the stream-power river incision model: Implications for height limits of mountain ranges, landscape response timescales, and research needs, J. Geophys. Res. Solid Earth, 104, 17661–17674, https://doi.org/10.1029/1999jb900120, 1999.

Whipple, K. X., Kirby, E., and Brocklehurst, S. H.: Geomorphic limits to climate-induced increases in topographic relief, Nature, 401, 39–43, https://doi.org/10.1038/43375, 1999.

Willgoose, G.: Mathematical Modeling of Whole Landscape Evolution, Annu. Rev. Earth Planet. Sci., 33, 443–459, https://doi.org/10.1146/annurev.earth.33.092203.122610, 2005.

Winchell, M., Srinivasan, R., Di Luzio, M., and Arnold, J.: ARCSWAT INTERFACE FOR SWAT2012, 2013.

Zhang, L., Parker, G., Stark, C. P., Inoue, T., Viparelli, E., Fu, X., and Izumi, N.: Macro-roughness model of bedrock–alluvial river morphodynamics, Earth Surf. Dyn., 3, 113–138, https://doi.org/10.5194/esurf-3-113-2015, 2015.

Zhang, W., An, S., Xu, Z., Cui, J., and Xu, Q.: The impact of vegetation and soil on runoff regulation in headwater streams on the east Qinghai–Tibet Plateau, China, Catena, 87, 182–189, https://doi.org/10.1016/j.catena.2011.05.020, 2011.

Zhang, X., Yu, G. Q., Li, Z. B., and Li, P.: Experimental Study on Slope Runoff, Erosion and Sediment under Different Vegetation Types, Water Resour. Manag., 28, 2415–2433, https://doi.org/10.1007/s11269-014-0603-5, 2014.

Zhang, Y., Xiao, X., Guanter, L., Zhou, S., Ciais, P., Joiner, J., Sitch, S., Wu, X., Nabel, J., Dong, J., Kato, E., Jain, A. K., Wiltshire, A., and Stocker, B. D.: Precipitation and carbon-water coupling jointly control the interannual variability of global land gross primary production, Sci. Rep., 6, 39748, https://doi.org/10.1038/srep39748, 2016.